

**University of New Mexico
UNM Digital Repository**

Optical Science and Engineering ETDs

Engineering ETDs

2-2-2016

Simulation of strongly injection-locked semiconductor ring lasers

Fei-Hung Chu

Follow this and additional works at: https://digitalrepository.unm.edu/ose_etds

Recommended Citation

Chu, Fei-Hung. "Simulation of strongly injection-locked semiconductor ring lasers." (2016). https://digitalrepository.unm.edu/ose_etds/4

This Dissertation is brought to you for free and open access by the Engineering ETDs at UNM Digital Repository. It has been accepted for inclusion in Optical Science and Engineering ETDs by an authorized administrator of UNM Digital Repository. For more information, please contact disc@unm.edu.

Fei-Hung Chu

Candidate

Optical Science and Engineering

Department

The dissertation is approved, and it is acceptable in quality and form for publication on microfilm:

Approved by the Dissertation Committee:

Dr. Marek Osiński, Chairperson

Dr. Ganesh Balakrishnan

Dr. Gennady Smolyakov

Dr. Nader Naderi

**SIMULATION OF STRONGLY INJECTION-LOCKED
SEMICONDUCTOR RING LASERS**

BY

FEI-HUNG CHU

B.S., Mechanical Engineering, National Taiwan University, 2001
M.S., Electrical Engineering, University of Pittsburgh, 2008

DISSERTATION

Submitted in Partial Fulfillment of the
Requirements for the Degree of

**Doctor of Philosophy
Optical Science and Engineering**

The University of New Mexico
Albuquerque, New Mexico

December 2015

ACKNOWLEDGMENTS

I would like to thank my advisor and dissertation chair, Dr. Marek Osiński, for his guidance and encouragement throughout my six years of PhD study, and also for his invaluable advices in preparing this dissertation. My gratitude is extended to my dissertation committee members, Dr. Ganesh Balakrishnan and Dr. Gennady Smolyakov from CHTM, and Dr. Nader Naderi from AFRL for their support and valuable comments. Many thanks to my colleague, Dr. Hemashilpa Kalagara, for her help and discussions.

I will always be indebted to my parents, who have been unconditionally supportive along the way. Finally and most importantly, my wife, Yi-Han Chang, and my daughters, Kimberly and Heidi Chu, are where my motivation and inspiration come from.

SIMULATION OF STRONGLY INJECTION-LOCKED SEMICONDUCTOR RING LASERS

by

FEI-HUNG CHU

M.S., Electrical Engineering, University of Pittsburgh, 2008
PhD., Optical Science and Engineering, University of New Mexico, 2015

ABSTRACT

To overcome the limited modulation bandwidth of directly modulated semiconductors, a novel scheme for modulation bandwidth enhancement and tailoring is presented. This scheme involves a single-frequency master laser monolithically integrated with strongly injection-locked whistle-geometry semiconductor ring lasers. Improved high-speed performance of the novel scheme is confirmed through numerical modeling, showing greatly enhanced resonance frequency of up to \sim 160 GHz. Approaches to further improve the modulation response of strongly injection-locked ring lasers, including cascaded injection-locking and Q-modulated injection-locking are also presented.

TABLE OF CONTENTS

ACKNOWLEDGMENTS	iii
ABSTRACT.....	iv
TABLE OF CONTENTS.....	v
CHAPTER 1 INTRODUCTION	1
CHAPTER 2 BACKGROUND	4
2.1 DIRECT MODULATION VS. EXTERNAL MODULATION OF SEMICONDUCTOR LASERS.....	4
2.2 ENHANCEMENT OF MODULATION BANDWIDTH IN INJECTION-LOCKED SEMICONDUCTOR LASERS	5
2.3 INJECTION-LOCKED VCSELS VS. MICRORING LASERS	13
CHAPTER 3 PROPERTIES OF WHISTLE-GEOMETRY RING LASERS	18
3.1 INTRODUCTION	18
3.2 RECIPROCITY PRINCIPLE IN WRL STRUCTURES.....	21
3.3 MODULATION RESPONSE OF FREE-RUNNING WRLS	27
3.4 MONOLITHICALLY INTEGRATED ULTRAFAST DBR/USRL SYSTEM	32
CHAPTER 4 HIGH-SPEED MODULATION ANALYSIS OF STRONGLY INJECTION-LOCKED SEMICONDUCTOR RING LASERS	34
4.1 INTRODUCTION	34
4.2 THEORETICAL MODEL.....	37
4.3 NUMERICAL SIMULATION	43
4.4 EFFECT OF LIGHT BACKSCATTERING	56
4.5 LARGE SIGNAL EFFECT	67
4.5 CONCLUSION.....	78
CHAPTER 5 ANALYSIS OF HIGH-FREQUENCY MODULATION RESPONSE OF STRONGLY INJECTION-LOCKED CASCADED SEMICONDUCTOR RING LASERS	80
5.1 RATE EQUATIONS FOR CASCADED SCHEME.....	81
5.2 SIMULATION RESULTS	85
5.3 CONCLUSION.....	97
CHAPTER 6 FREQUENCY CHIRP IN STRONGLY INJECTION-LOCKED SEMICONDUCTOR RING LASERS.....	98
6.1 INTRODUCTION	98

6.2 FREQUENCY CHIRP OF SEMICONDUCTOR LASERS UNDER STRONG INJECTION LOCKING	99
6.3 NUMERICAL SIMULATION OF FREQUENCY CHIRP BASED ON RATE EQUATIONS.....	100
6.4 CONCLUSION.....	109
CHAPTER 7 Q-MODULATED STRONGLY-INJECTION-LOCKED WHISTLE-GEOMETRY RING LASERS	110
7.1 INTRODUCTION	110
7.2 Q-MODULATED WRLS	112
7.3 SIMULATION RESULTS	116
7.4 CONCLUSION.....	119
CHAPTER 8 SUMMARY AND FUTURE WORK	120
8.1 SUMMARY	120
8.2 FUTURE WORK.....	122
REFERENCES	123
LIST OF PUBLICATIONS	135

CHAPTER 1

INTRODUCTION

With the rapid increase of data transmission rate in optical communication system and emergence of radio-frequency and microwave photonics, where signals modulated at very high-speed are transmitted over optical fibers, compact and ultra-fast optical transmitters are more demanded than ever. While external modulation can achieve high-speed performance, the design complexity of external modulators and requirement for heterogeneous integration with semiconductor lasers make it less attractive than direct modulation.

However, the modulation bandwidth of directly modulated lasers under free-running condition is rather limited, typically around 10 GHz, even though with certain designs 30 GHz of modulation bandwidth is possible [Matsui 1997], [Kjebon 1997]. Besides low modulation bandwidth, directly modulated lasers also suffer from frequency chirp, i.e. frequency shift due to the modulation of injection current, which results in pulse broadening over long optical fibers and limits the bit rate-distance product [Agrawal 2010].

Injection locking is an efficient and robust technique to improve the dynamic and spectral performance of a directly modulated semiconductor laser that was demonstrated for the very first time in 1976 using edge-emitting lasers [Lang 1976], and in 1994 for vertical-cavity surface-emitting lasers (VCSELs) [Brown De Colstoun 1994]. By injecting light from the master laser into the slave laser, one can obtain increase in

resonance frequency and modulation bandwidth [Henry 1985], [Simpson 1995], [Murakami 2009], [Meng 1998a], reduction in nonlinear distortions [Meng 1998b], [Meng 1999], single-mode performance and side-mode suppression [Iwashita 1982], reduced relative intensity noise [Schunk 1986], [Espana-Boquera 1996], [Liu 1997a], [Yabre 2000], reduced frequency chirp [Toba 1984], [Lin 1984], [Olsson 1985], [Mohrdiek 1994], lower RF link loss [Sung 2008], and nearly single-sideband modulation [Sung 2007]. For instance, the largest reported bandwidth of directly modulated free-running edge-emitting Fabry-Perot and distributed-feedback (DFB) lasers is 30 GHz [Matsui 1997], [Kjebon 1997], whereas in optically injection locked VCSELs and DFB lasers, the highest 3-dB modulation bandwidth of ~80 GHz was observed [Lau 2008]. Owing to these advantages, optical injection locking has several applications, such as optical frequency reference generation [Goldberg 1985], phased array radars [Seeds 1988], phase modulation [Kobayashi 1982], optical signal processing [Yamashita 2000], *etc.*

The utilization of injection-locking to increase the modulation bandwidth of directly-modulated semiconductor lasers in optical communication systems and rf photonic links [Lau 2009], [Tartarini 2007] has been demonstrated, both theoretically and experimentally, to increase the modulation bandwidth and, at the same time, reduce the frequency chirp of directly modulated lasers. With injection locking, as will be explained in Chapter 2, the increase in modulation bandwidth is proportional to the detuning between the master and the slave laser, and the tuning range is, in turn, proportional to the coupling rate from the master to the slave laser, thus strong coupling is desired. Nevertheless, with typical semiconductor laser designs, including vertical-cavity surface-

emitting lasers (VCSELs) and edge-emitting lasers, injection locking cannot be achieved monolithically and requires complex optical path design to eliminate back reflection, and therefore they are not practical in real-world applications.

Injection locking of semiconductor lasers with the master and the slave monolithically integrated on the same substrate can be conveniently achieved with the whistle-geometry ring laser (WRL) proposed in Chapter 3, which ensures strong injection by its small round-trip time and low reflectivity, and unidirectional propagation by the non-identical photon lifetime for the two counterpropagating modes. Enhancement of high-speed modulation response will be demonstrated numerically for the case of a single WRL in Chapter 4. The rate-equation-based simulation shows that the modulation bandwidth for strong injection locking can be enhanced to as high as 160 GHz, while for weak injection it is only 35 GHz.

Cascaded injection locking scheme, which has been shown to enhance the modulation response [Zhao 2007], is also considered in Chapter 5 and strongly injection-locked cascaded WRLs have been designed to mitigate the low-frequency roll-off issue occurring in injection-locked lasers. The frequency chirp analysis then follows in Chapter 6 and demonstrates significant reduction of frequency chirp in terms of chirp-to-power ratios (CPRs) for injection-locking of both single and cascade WRL schemes.

Another approach to improve the modulation response of strongly injection-locked semiconductor lasers is by cavity Q modulation. A novel design based on WRLs is explored in Chapter 7. And finally, a summary is given in Chapter 8 with possible directions for future investigation.

CHAPTER 2

BACKGROUND

2.1 DIRECT MODULATION VS. EXTERNAL MODULATION OF SEMICONDUCTOR LASERS

The continuing increase of transmission rates at all levels of telecommunication networks and fiber-based RF photonic systems raises demand for very high-speed, low-cost optical transmitters. Much effort has been put into developing wide-bandwidth lasers and modulators over the past ten years. To date, the largest reported bandwidth of directly modulated free-running semiconductor lasers at 1.55 μm is 30 GHz, as measured in a Fabry-Perot edge-emitting buried-heterostructure multiple-quantum-well (MQW) laser [Matsui 1997] and in a DFB laser [Kjebon 1997]. On the other hand, external modulators operating at speeds of 40 Gb/s are currently available commercially [Covega 2008] and modulators operating at speeds in the 100-GHz range are under development [Chang 2002]. The widest reported 3-dB modulation bandwidth for Ti:LiNbO₃ electro-optic (EO) modulators is 70 GHz, with the maximum measured frequency of 110 GHz [Noguchi 1998]. The drawback of the Ti:LiNbO₃ modulators, however, is their poor sensitivity, as represented by their unattractively high half-wave voltage V_π . Very high modulation frequency and broad-band performance of the Ti:LiNbO₃ modulators come at the expense of too high V_π , which makes them less attractive for system applications [Cox 2006]. A very impressive 145 GHz modulation bandwidth has been demonstrated for a PMMA/DR1 polymer EO modulator at 1310 nm [Lee 2002]. However, the technology of polymer

modulators is still very immature, with most of the development effort being focused on the polymer material itself. In general, the polymers with larger EO effect are the least stable against temperature and optical power, which casts doubt on long-term stability of polymer materials [Cox 2006]. In addition, the frequency response of any EO modulator is typically determined by the electrode RF propagation loss and the phase mismatch between the optical beam and modulation microwave [Chung 1991], [Gopalakrishnan 1994], [Chang 2002], which makes overall design and fabrication of these devices complex and costly. Therefore, low-cost small-size directly modulated laser sources with very high modulation bandwidths exceeding 100 GHz are still highly desirable for the rapidly growing applications of RF optical fiber links, and could revolutionize the future of optical telecommunication.

2.2 ENHANCEMENT OF MODULATION BANDWIDTH IN INJECTION-LOCKED SEMICONDUCTOR LASERS

Since their inception, semiconductor lasers have been key components for many applications in optical fiber communication because of their excellent spectral and beam properties and capability to be directly modulated at very high rates. However, their frequency response has limited the commercial use of directly modulated lasers to digital transmission not exceeding 10 Gb/s. The modulation response of a diode laser is determined by the rate at which the electrons and holes recombine in the active region (spontaneous carrier lifetime τ_{sp}), and the rate at which photons can escape from the laser

cavity (photon lifetime τ_p). The modulation bandwidth is limited by the relaxation oscillation frequency f_{RO} of the laser given by [Lau 1985]

$$2\pi f_{\text{RO}} = \sqrt{g_N \gamma_p P_0} \quad (2-1)$$

where g_N is the differential optical gain, P_0 is the average photon number in the laser cavity, and γ_p is the photon decay rate given by the reciprocal of τ_p . Eq. (2-1) suggests that the relaxation oscillation frequency can be increased by proper design of laser parameters to get either higher photon density or shorter photon lifetime. Increased injection currents for higher P_0 values and shorter laser cavities for smaller τ_p are ordinarily employed for that purpose in diode lasers. Both approaches, however, involve higher injection current densities, which could result in optical damage to the laser facets and excessive heating. Safe levels of injection current therefore limit the modulation bandwidth in semiconductor lasers. To date, the highest reported experimental relaxation oscillation frequency for a solitary edge-emitting laser is ~ 24.5 GHz [Matsui 1997], and ~ 15 GHz for a vertical-cavity surface emitting laser (VCSEL) [Lear 1997].

Optical injection locking has been shown to be an extremely effective method to improve microwave performance and linearity of diode lasers and to reach beyond the record values of f_{RO} achieved for free-running devices. Injection locking was first demonstrated in 1976 using edge-emitting lasers [Kobayashi 1976], and in 1996 for VCSELs [Li 1996]. The technique uses output of one laser (master) to optically lock another laser (slave), which can still be directly modulated. Significant increase in the resonance frequency and modulation bandwidth, with reduction in nonlinear distortions [Meng 1999] and frequency chirp [Mohrdiek 1994] has been achieved by injecting

external light into diode lasers. So far, improved microwave performance has been observed in edge-emitting lasers with Fabry-Perot cavity [Simpson 1995], [Simpson 1997], [Jin 2006], distributed feedback (DFB) lasers [Meng 1998], [Hwang 2004], [Sung 2004], [Lau 2008b], and VCSELs [Chrostowski 2002], [Chrostowski 2003], [Okajima 2003], [Chang 2003], [Zhao 2004], [Zhao 2006], [Chrostowski 2006a], [Chrostowski 2006b], [Wong 2006], [Lau 2008b]. The highest experimentally observed f_{RO} in excess of 100 GHz was reported for injection-locked DFB lasers and VCSELs, with a record 3-dB bandwidth of 80 GHz being achieved in injection-locked VCSELs [Lau 2008b].

Many aspects of the injection-locking experimental results have been reproduced in analytical studies [Luo 1991], [Simpson 1996], [Nizette 2002], [Nizette 2003], [Lau 2007], [Lau 2008a] and numerical simulations using rate equation models [Luo 1990], [Luo 1992a], [Luo 1992b], [Liu 1997], [Jones 2000], [Chen 2000], [Murakami 2003], [Wieczorek 2006]. Dynamic behavior of diode lasers is described by a system of coupled nonlinear differential equations for the optical field and carrier density in the laser cavity. While for a free-running laser these equations exhibit only damped oscillations with corresponding relaxation oscillation frequency and damping rate, external optical injection increases the number of degrees of freedom by one, which leads to a much greater variety of dynamic behavior. In particular, perturbation analysis of rate equations [Simpson 1996], [Simpson 1997] revealed that the enhanced resonance frequency (the peak frequency in the modulation spectrum) was identical to the difference between the injected light frequency and a shifted cavity resonance, which agreed well with experimental observations. The physical mechanism behind this effect was further clarified in [Murakami 2003], [Wieczorek 2006]. Under strong optical injection, a

beating between the injected light frequency and the cavity resonant frequency dominates the dynamic behavior.

Fig. 2-1 presents a simple illustration of cavity effects and emission frequency in an injection-locked single-mode semiconductor laser. The optical gain spectrum and longitudinal mode spacing are assumed to be sufficiently broad to cover the frequency range of interest. A positive detuning $\Delta\omega_{inj} = \omega_{inj} - \omega_0$ is assumed between the resonant angular frequency ω_0 of a solitary (free-running) laser and the angular frequency ω_{inj} of the injected field (Fig. 2-1a). When the laser is in steady state and locked (Fig. 2-1b), it emits all its power at the injected frequency ω_{inj} . The cavity resonance, however, must shift to lower frequency by $\Delta\omega(N)$, because the refractive index of the active medium increases with the carrier density decrease, and the carrier density N is reduced below its uninjected threshold value due to optical injection. The shift in the carrier-dependent cavity resonance $\Delta\omega$ is given by [Lang 1982], [Mogensen 1985]:

$$\Delta\omega(N) = \frac{\alpha}{2} v_{g,eff} \Delta G(N) = \frac{\alpha}{2} v_{g,eff} G_N \Delta N, \quad (\Delta N = N - N_{th}), \quad (2-2)$$

with α - the linewidth broadening factor, $v_{g,eff}$ - the effective group velocity, N_{th} - the threshold carrier density, and G - the modal gain, assumed to vary linearly with the carrier density $G(N) = G_N(N-N_0)$, where G_N is the differential modal gain and N_0 is the transparency carrier density. In steady state, the gain is too small to support the shifted-frequency mode, and lasing can occur only at the locked frequency ω_{inj} , provided $\omega_{inj} - \omega_{shift}$ remains within the stable locking range. In the transient process, however, the gain may become sufficient to sustain a mode at the shifted cavity resonance ω_{shift} . Thus,

under modulation conditions, the slave laser output may exhibit a damped oscillation at the beat frequency $\omega_{\text{inj}} - \omega_{\text{shift}}$ due to interference between those two fields. According to Eq. (2-2), the resonant frequency produced by this transient interference is given by

$$\omega_{\text{res}} = \Delta\omega_{\text{inj}} - \Delta\omega(N) = \Delta\omega_{\text{inj}} - \frac{\alpha}{2} v_{g,\text{eff}} G_N \Delta N . \quad (2-3)$$

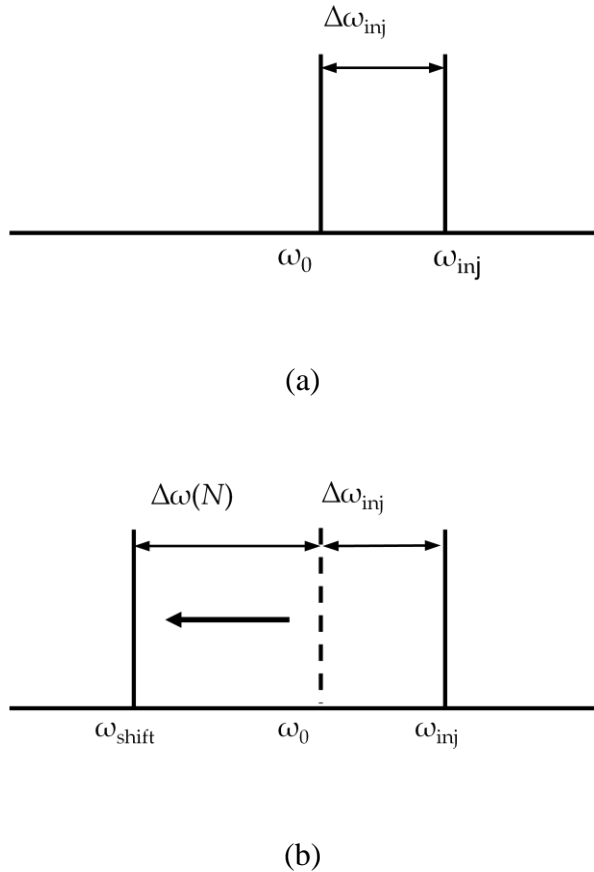


Fig. 2-1. Schematic illustration of the effects of optical injection on resonant condition in a semiconductor laser. (a) Spectrum without injection. ω_0 is the angular frequency of the solitary laser, ω_{inj} is the frequency of the master, and $\Delta\omega_{\text{inj}}$ is the frequency detuning. (b) Cavity resonant condition under injection locking. ω_{shift} is the cavity resonance frequency shifted towards lower frequency from ω_0 by $\Delta\omega(N)$ due to light injection.

The most comprehensive study of the modification of dynamical properties of a semiconductor laser by a strong injected signal was reported in [Wieczorek 2006]. Bifurcation theory and continuation techniques were used to explore a wide range of experimental situations involving different injection conditions and types of lasers. The following system of coupled rate equations for injection-locked diode lasers was found to reproduce adequately many aspects of modulation-bandwidth enhancement found experimentally in injection-locked VCSELs:

$$\frac{dE}{dt} = \frac{1}{2} \Gamma v_{g,\text{eff}} g_N (N - N_{\text{th}}) E + \kappa E_{\text{inj}} \cos \varphi , \quad (2-4)$$

$$\frac{d\varphi}{dt} = 2\pi\Delta - \frac{\alpha}{2} \Gamma v_{g,\text{eff}} g_N (N - N_{\text{th}}) - \kappa \frac{E_{\text{inj}}}{E} \sin \varphi , \quad (2-5)$$

$$\frac{dN}{dt} = \frac{j_{\text{mod}}}{ed} - \gamma_N N - \frac{\epsilon_0 n_{g,\text{eff}} c}{2h\nu} [g_{\text{th}} + g_N (N - N_{\text{th}})] E^2 , \quad (2-6)$$

where E is the intracavity electric field amplitude, φ is the phase difference between the injected and intracavity fields, Γ is the optical confinement factor, κ is the coupling rate coefficient, E_{inj} is the amplitude of the injected field incident upon the slave cavity, Δ is the detuning between injected and free-running laser frequencies, j_{mod} is the modulated pumping current density, e is the electron charge, d is the active region thickness, γ_N is the electron population decay rate, ϵ_0 is the permittivity of vacuum, $n_{g,\text{eff}}$ is the effective group index, h is Planck's constant, ν is the frequency of the intracavity field, and g_{th} is the threshold gain. Injection of a coherent field, with amplitude E_{inj} and frequency ν_{inj} , introduces driving terms in the laser field equations, as shown in Eqs. (2-4), (2-5) [Spencer 1972]. The threshold gain and carrier density in a free-running laser are

$$g_{\text{th}} = \frac{n_{g,\text{eff}} \gamma_p}{c\Gamma} ; \quad N_{\text{th}} = N_0 + \frac{n_{g,\text{eff}} \gamma_p}{c\Gamma g_N} . \quad (2-7)$$

For sinusoidal modulation, the pumping current density j_{mod} in Eq. (2-6) can be written as

$$j_{\text{mod}} = j_0 [1 + \delta \sin(2\pi f t)] , \quad (2-8)$$

where j_0 is the pre-bias current density, δ is the modulation depth, and f is the modulation frequency. Eqs. (2-4)-(2-6) assume single-mode operation, typical for VCSELs or DFB lasers.

No theoretical limitation has been found for further increase in the relaxation oscillation frequency f_{RO} . It should be noted, however, that a higher f_{RO} does not necessarily imply a broader modulation bandwidth. A large relaxation oscillation damping rate γ_{RO} can undermine the ability of the laser to respond to fast modulation. Hence, a combination of high f_{RO} and low γ_{RO} is required for a broad modulation bandwidth. In practice, directly modulated lasers often suffer from high distortions near the resonance frequency f_{RO} , which makes them useful only at RF frequencies much lower than f_{RO} [Lau 1984]. A common practice to increase f_{RO} is to pump the laser high above threshold. However, f_{RO} and γ_{RO} are linked in a free-running laser, so any increase in f_{RO} is accompanied by a greater increase in γ_{RO} . One very important finding of [Wieczorek 2006] is that coherent optical injection can be used to break that link. For some combinations of injection strength and detuning, f_{RO} can be made to increase, while γ_{RO} can remain constant or even slightly decrease (Fig. 2-2).

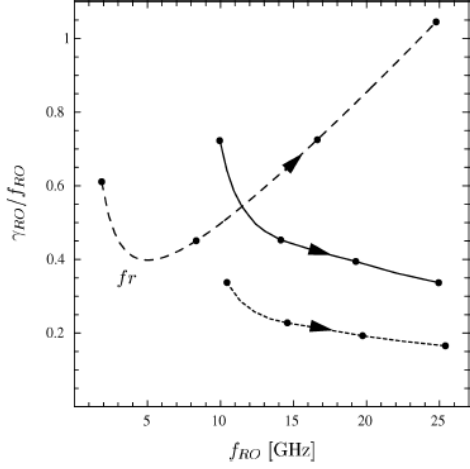


Fig. 2-2. Intrinsic link between f_{RO} and γ_{RO} in a free-running semiconductor laser with $\alpha = 2$ (dashed curve). The arrow indicates increasing pumping current. Solid and dotted lines illustrate various ways to adjust the relation between f_{RO} and γ_{RO} in the same laser pumped at twice the threshold current, by choosing different combinations of injection strength and detuning. The arrows indicate increasing detuning [Wieczorek 2006]. The solid and dotted lines correspond to v_{inj} taken 4 and 2 GHz below the stable locking range boundary, respectively.

Another factor limiting modulation bandwidth in injection-locked lasers, evident in all strong-injection-locking experiments, is a sharp roll-off of their modulation response that occurs at low modulation frequencies, before the modulation response gets enhanced by the resonance frequency. The cause of this “sagging” low-frequency response has recently been identified [Lau 2008a] as decoupling of the carrier injection rate from the relaxation oscillation dynamics under strong injection conditions. The cut-off frequency of the low-frequency roll-off can be approximated as [Lau 2008a]:

$$\omega_p \approx \left[1 + \omega_{res}^{-2} \alpha \gamma_p \kappa \sqrt{\frac{S_{master}}{S_0}} \sin(-\varphi_0) \right] g_N S_0, \quad (2-9)$$

where φ_0 is the injection-locked phase difference between the injected and intracavity fields, S_0 is the photon number in the slave cavity, and S_{master} is the number of photons incident from the master laser. The sine term approaches unity as the positive detuning increases. However, the resonance frequency ω_{res} goes up, forcing ω_p to smaller values. Two design parameters can be used to maximize ω_p : 1) higher differential gain g_N , and 2) increased optical power in the slave cavity. We note that a larger α parameter, a higher coupling efficiency (increased coupling rate coefficient κ), and increased power from the master laser S_{master} would all result in an increased ω_{res} according to Eqs. (2-3)-(2-5), hence they would be ineffective in increasing ω_p . The most straightforward method to maximize ω_p is to increase internal optical power of the slave laser. By increasing the slave laser bias current from $1.3 \times I_{\text{th}}$ to $5 \times I_{\text{th}}$, a very significant improvement in 3-dB bandwidth from ~ 1 GHz to a record ~ 80 GHz (corresponding to $\omega_{\text{res}} = 68$ GHz) has been demonstrated in injection-locked VCSELs [Lau 2008b].

2.3 INJECTION-LOCKED VCSELS VS. MICRORING LASERS

As described in Section 2.2, injection locking has been actively researched for its potential to improve ultrahigh frequency performance of semiconductor lasers for both digital and analog applications, with VCSELs demonstrating the record high values for enhanced modulation bandwidth. VCSELs were considered to be particularly attractive as injection-locked transmitters because of: 1) short cavity length, leading to a high coupling efficiency, 2) single-mode operation, and 3) low power, resulting in increased injection ratio $P_{\text{master}}/P_{\text{slave}}$ (P_{master} is the incident optical power and P_{slave} is the VCSEL

output power) when a master laser with relatively high power is used. The coupling rate coefficient κ , as given by [Schunk 1986] for standard Fabry-Perot lasers, is:

$$\kappa = c\sqrt{1-R}/(2n_{g,\text{eff}}L) , \quad (2-10)$$

where R is the reflectivity of the laser mirror through which the light is injected and L is the cavity length. Thus, a short cavity length results in a higher coupling efficiency.

However, in order to keep the lasing threshold at a reasonably low level, VCSELs require very high mirror reflectivity R , which according to Eq. (2-10) would bring κ down to a very small value. The value of $\kappa \approx 1 \times 10^{12} \text{ s}^{-1}$, estimated using Eq. (2-10), was reported for VCSELs used in [Chrostowski 2006b].

While the parameter $P_{\text{master}}/P_{\text{slave}}$, defined in [Chrostowski 2006b] as the ratio of the optical power incident on the VCSEL and the output power of the free-running VCSEL, is easy to determine experimentally, it is the ratio of injected power and internal power in the active region of the slave laser that determines its behavior. For example, the stable locking range is given by [Henry 1985]

$$-\frac{c}{2n_{g,\text{eff}}L}\sqrt{\frac{S_{\text{inj}}}{S}}\sqrt{1+\alpha^2} < \Delta\omega_{\text{inj}} < \frac{c}{2n_{g,\text{eff}}L}\sqrt{\frac{S_{\text{inj}}}{S}} , \quad (2-11)$$

where S_{inj} is the number of photons injected from the master laser and S is the number of photons inside the slave laser cavity. Eq. (2-11) can also be rewritten in terms of the incident power P_{master} and the coupling rate coefficient κ as

$$-\kappa\sqrt{\frac{P_{\text{master}}}{P}}\sqrt{1+\alpha^2} < \Delta\omega_{\text{inj}} < \kappa\sqrt{\frac{P_{\text{master}}}{P}} , \quad (2-11a)$$

where P is the slave laser internal power. Both the wavelength detuning range $\Delta\omega_{\text{inj}}$ for stable injection locking (> 2 nm) and enhanced resonant frequency ω_{res} (up to ~ 107 GHz) have been reported to increase with the injection ratio, with no upper limit observed within the instrumentation limit. This is in good agreement with Eq. (2-3), where both terms on the right-hand side can be made to increase with increased injection rate.

The steady-state analysis of Eqs. (2-4)-(2-6) [Murakami 2003] revealed that two parameters are of key importance for achieving highly enhanced modulation bandwidth (for a given internal power of the slave laser) – the cavity roundtrip time $\tau_{\text{rt}} = 2n_{g,\text{eff}}L/c$ and the reflectivity R of the cavity mirror used for injection. Under steady-state injection-locking conditions, the right-hand side of Eq. (2-3) can be written as

$$\omega_{\text{res}} = -\kappa \frac{E_{\text{inj}}}{E_0} \sin \varphi_0 = -\frac{c\sqrt{1-R}}{2n_{g,\text{eff}}L} \frac{E_{\text{inj}}}{E_0} \sin \varphi_0 , \quad (2-12)$$

with the phase difference φ_0 between the injected and intracavity fields given by

$$\varphi_0 = \sin^{-1} \left\{ -\frac{\Delta\omega_{\text{inj}}}{\kappa\sqrt{1+\alpha^2}} \frac{E_0}{E_{\text{inj}}} \right\} - \tan^{-1} \alpha . \quad (2-13)$$

As the frequency detuning moves to the positive edge of the locking range in Eq.(2-11), φ_0 approaches $-\pi/2$, thereby increasing ω_{res} [Mogensen 1985], [Murakami 2003]. The smallest possible values for both τ_{rt} and R (maximizing the coupling rate coefficient κ) would be ideal for reaching the ultimate limits of modulation bandwidth enhancement in injection-locked lasers. The inherent design trade-off between these parameters, however, makes further optimization of both edge-emitting lasers and VCSELs for enhanced high-speed performance very problematic. While injection-locked VCSELs benefit greatly

from very short cavities and, hence, very small τ_{rt} , their high-speed performance, at the same time, is compromised by very high mirror reflectivity of a typical VCSEL, resulting in coupling rate coefficients similar to edge emitters. Further improvement of modulation bandwidth in injection-locked VCSELs is expected to come solely from higher power master lasers used for optical injection [Lau 2008b]. For this reason, more complicated cascaded schemes have been attempted, with demonstrated improvement in modulation bandwidth as compared to solitary injection-locked VCSELs [Zhao 2007]. The cascaded optical injection locking is a very promising technique that has scaling-up potential to eventually reach very wide modulation bandwidth over 100 GHz by cascading more slave lasers in a daisy chain structure, as long as the master laser has enough power to stably lock the slave laser with the largest detuning value [Zhao 2007]. This, however, can hardly be realized with VCSELs, notable for their very high mirror reflectivity. In addition, stand-alone VCSELs pose a very serious alignment problem in injection-locking experiments and, at the same time, are not suitable for monolithic integration when injection locking is the requirement. We believe VCSELs are very hard to be optimized for any further improvement in their speed.

To overcome these limitations of VCSELs, we propose a novel injection locking scheme involving distributed Bragg reflector (DBR) master lasers monolithically integrated with unidirectional microring slave lasers. Unidirectional semiconductor ring lasers (USRRLs) are ideal for this particular application, as they can be designed for minimal back reflections (eliminating the need for optical isolators protecting the master laser from optical feedback), while simultaneously allowing for complete coupling of the DBR laser output into the ring, supporting the favored propagation direction. By the very

nature of USRL, low reflectivity for incident light does not at all compromise the quality of the ring cavity, and does not affect the threshold condition for the wave propagating in the favored direction. This makes USRLs free from the design constraints that edge-emitting lasers and VCSELs suffer from. In contrast to VCSELs, the USRL geometry allows for easy cascading of individual ring lasers integrated on the same chip. While there are no published data on high speed modulation of microring lasers, we note that the cavity length of the MQW lasers with 3-dB modulation bandwidth of 30 GHz was 120 μm [Matsui 1997], which is equivalent to microring lasers with the diameter of 36 μm . Hence, it is very reasonable to expect at least comparable modulation rates from microring lasers.

CHAPTER 3

PROPERTIES OF WHISTLE-GEOMETRY RING LASERS

3.1 INTRODUCTION

Semiconductor ring lasers offer several advantages over conventional edge emitting lasers and VCSELs [Mezosi 2014], including monolithic integration with other photonic circuits, good control of cavity length, high output efficiency in unidirectional mode, single mode operation without grating, and wafer scale testing. The smallest size 1.55- μm InGaAsP/InP ring lasers fabricated to date have the diameter of only 10 μm [Park 2005]. The free spectral range for such a laser $\text{FSR} = \lambda_0^2/(n_{g,\text{eff}}L) \approx 21.84 \text{ nm}$ ($n_{g,\text{eff}} = 3.5$) will provide sufficiently high intermodal gain discrimination to support single longitudinal mode operation under direct modulation. Recent numerical calculations [Stamatakis 2006] indicate that single longitudinal mode operation for a 60- μm diameter 1.55- μm InGaAsP/InP microring laser operating cw should hold up to current values of $\sim 2.2I_{\text{th}}$. The corresponding range for stable single longitudinal mode operation is expected to be even wider in a smaller 10- μm diameter 1.55- μm InP/InGaAsP ring laser, providing higher intermodal gain discrimination.

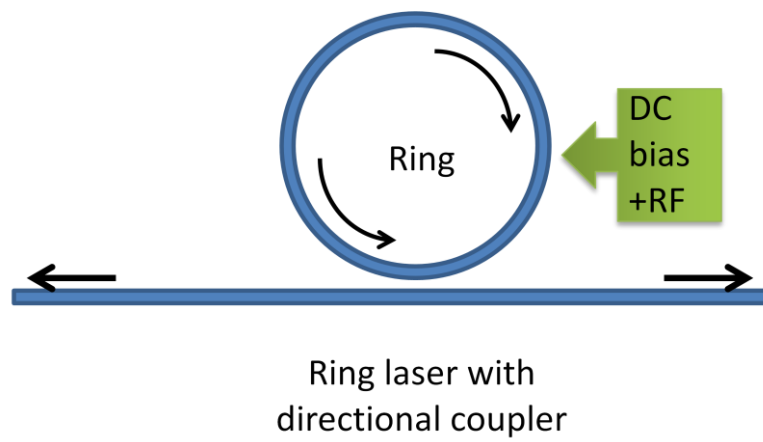
Several configurations have been adopted to couple optical output from a ring laser, including whistle-geometry (often referred to as Y-junction) coupler, directional coupler, and multimode interferometer (MMI) coupler. Ring lasers with the output coupler in the configuration of whistle-geometry have received much less attention than other configurations. Compared to the other two options, whistle geometry couplers, though easier to fabricate, result in more radiation loss and backreflections at the

coupling junction [Krauss 1995] and hence higher threshold and lower external quantum efficiency. However, as will be shown in the next section, its asymmetry also results in unequal photon lifetime for the two counter-propagating modes, which promotes unidirectional operation not attainable in other configurations. Unidirectionality can be further enhanced with an embedded S-section as described in [Hohimer 1992b].

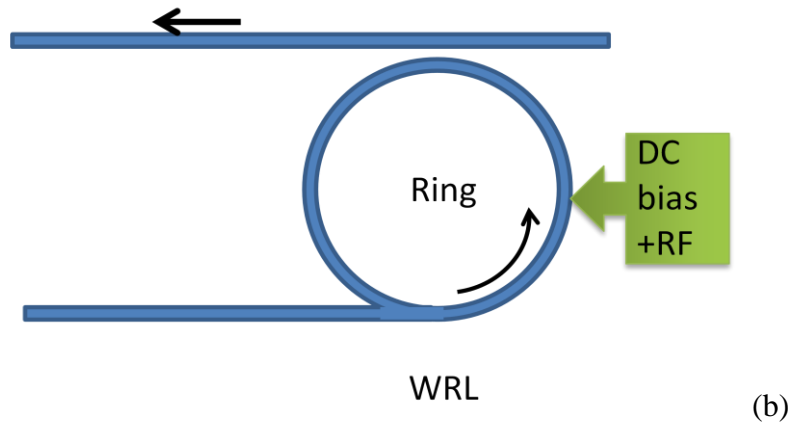
In most cases among the reported whistle geometry ring lasers, the straight section (output waveguide) is not electrically isolated from the ring resonator and hence is an integral part of the laser cavity [Hohimer 1992a], [Han 1992]. Small WRLs with a radii less than 40 μm were reported in [Han 1992], where InGaAs/AlGaAs/GaAs quantum well deeply-etched whistle-geometry ring lasers ($\lambda=1007 \text{ nm}$) with an output waveguide of around 500 μm result in threshold current densities of 2.9 kA/cm^2 for 11 μm outer radius and 2.563 kA/cm^2 for 21 μm outer radius.

When injection-locking is considered, with the configuration shown in Figure 3-1a, coupling from the master to the slave laser is limited by the directional coupler, and there is no direction preference in the ring cavity, which results in back reflection into the master laser. These limitations are also why most of the reported optical injection experiments on ring and/or microring lasers focus on switching of lasing direction by injection signals [Wang 2008], [Yuan 2007], [Yuan 2008a], [Yuan 2008b].

On the other hand, whistle geometry configuration greatly increases the coupling from the master to the slave ring laser, and its intrinsic unidirectionality due to unequal photon lifetime between the counter-propagating modes minimizes the back reflection.



(a)



(b)

Fig. 3-1. (a) Schematic diagram of semiconductor ring laser with directional coupler. (b) Schematic diagram of whistle geometry ring laser.

3.2 RECIPROCITY PRINCIPLE IN WRL STRUCTURES

A key feature of the WRL is the asymmetry between the two counterpropagating modes, with the structure of Fig. 3-1b strongly favoring the counterclockwise (CCW) mode over the clockwise (CW) mode even in absence of any injected light. This results in different lifetimes for the two counterpropagating modes, which might be misconstrued as a violation of the Helmholtz reciprocity principle and the time-reversal symmetry of Maxwell's equations. According to the Helmholtz reciprocity principle, a ray of light and its reverse ray encounter matched optical events, such as reflections, refractions, and absorption in a passive medium, or at an interface. While this principle does not apply to moving, nonlinear, or magnetic media, it is expected to apply to the structure of Fig. 3-1b when properly interpreted. The important realization is that the reciprocity principle applies to the complete solution of the Maxwell's equations when a mode conversion takes place, but not to each mode separately. In the structure of Fig. 3-1b, the mode conversion occurs due to bending losses (which are symmetric and apply equally to both counterpropagating modes), scattering at the junction with the straight waveguide (which may or may not affect both modes equally), and the outcoupling into the straight waveguide (which affects only the CW mode and is the primary reason for the asymmetry between the two counterpropagating modes). Thus, the losses experienced by the counterpropagating modes (and therefore their lifetimes) can be different without violating the reciprocity principle. In addition, the lasing medium of the whistle geometry structure is nonlinear, as the gain is saturated, although this effect is expected to be much less important than the WRL geometry itself.

In order to verify that our interpretation of how the reciprocity principle applies to the WRL structure is correct, we have performed three-dimensional (3-D) finite-difference time-domain (FDTD) simulations using the commercial FDTD tool FullWAVE, distributed by RSoft-Synopsys. The FDTD simulations automatically preserve reciprocity, as they represent complete solutions of the Maxwell's equations without any decomposition into individual modes. No gain or absorption was introduced in the simulations. The wavelength of the launched light was taken as 1.55 μm . The ring diameter was 20 μm , and the single-transverse-mode ridge-waveguide width was 1.4 μm . The ridge waveguide height was 3.497 μm , with the MQW active region \sim 1.65 μm above the bottom of the ridge. The effective refractive index in the ridge waveguide was calculated to be 3.319, and the refractive index of the surrounding medium was taken as 1.535, which corresponds to benzocyclobutene (BCB).

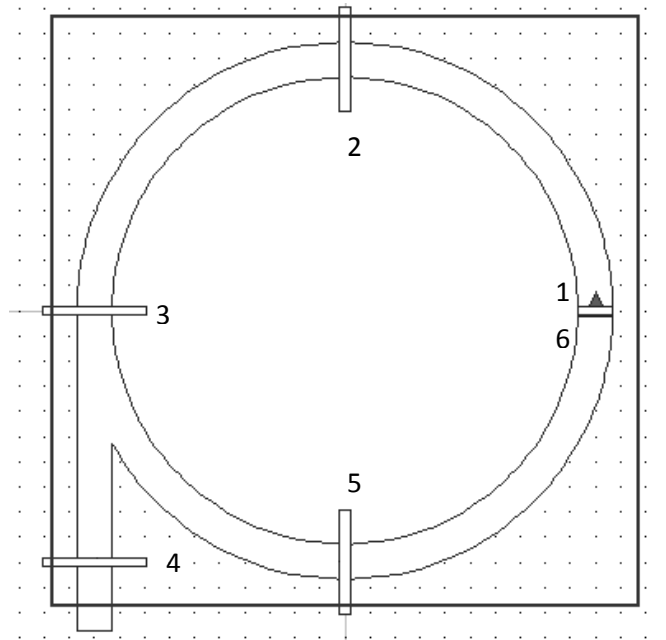


Fig. 3-2 The WRL structure with six monitors at various locations.

Fig. 3-2 shows the positions of six monitors used in the simulations. The monitors, which record the local average power in the mode and provide snapshots of the propagating fields, are represented by rectangular markers. The launching point for both CW and CCW modes is between two closely spaced monitors 1 and 6 at the right hand side of the ring, of which one is used to record the initial intensity, while the other records the intensity after a complete propagation circle. As an example, the launch monitor 1 for the CCW mode is marked with a black triangle in Fig. 3-2.

In Figs. 3-3 and 3-4, we demonstrate the asymmetry between the CCW and CW modes in the WRL structure. We ran two FDTD simulations by launching the fundamental bent-waveguide mode in either CW or CCW direction and monitoring its propagation. The fundamental bent-waveguide mode was calculated using the FemSIM finite-element module from RSoft-Synopsys, and launched continuously at the right-hand side of the ring, as indicated in Fig. 3-2. The XZ plane in Figs. 3-3 and 3-4 is parallel to the epitaxial layers, while the Y axis is parallel to the epitaxial growth direction. In the first case (see Fig. 3-3), the mode was launched in the CCW direction and most of the light ended up leaving the ring resonator by entering the straight section. In contrast, when the mode was launched in the CW direction, it remained well confined to the ring, as shown in Fig. 3-4, and practically no light entered the straight waveguide. These results are in full agreement with the expected asymmetric behavior of a WRL structure. Since the full-roundtrip losses for the modes propagating in the CCW and CW directions are significantly different, the corresponding photon lifetimes will also be different, as assumed in our rate equation model presented throughout this work. This result in no way violates the reciprocity principle, as it is applied only to a subset of the complete solution.

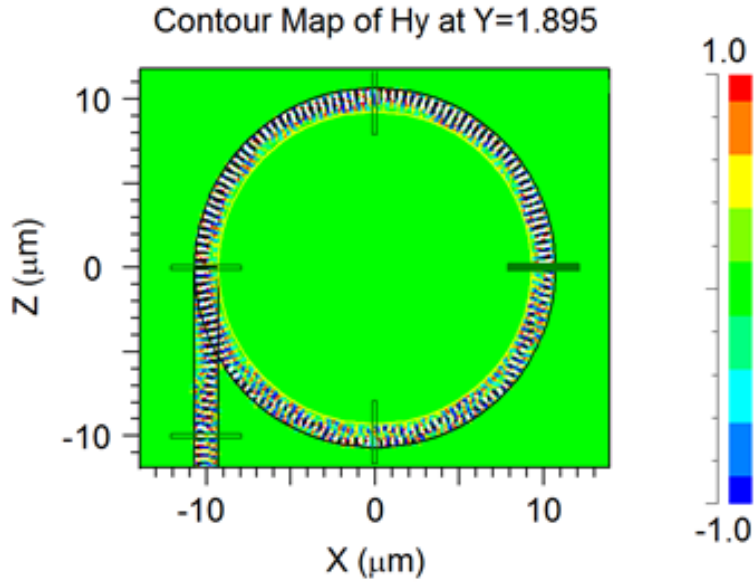


Fig. 3-3. 3-D simulation result for the WRL structure, showing the H_y -component distribution for the fundamental E_{10}^x mode of the bent waveguide when the mode is launched at the right side of the ring in the CCW direction. The color code indicates the values of the H_y component.

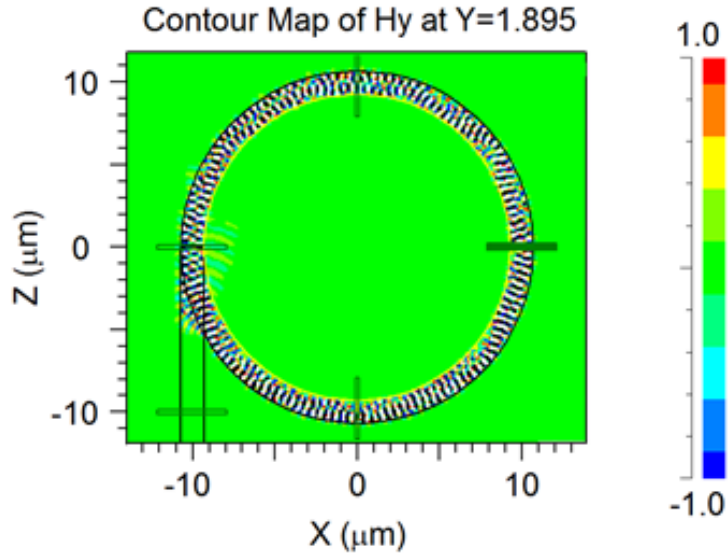


Fig. 3-4. 3-D simulation result for the WRL structure, showing the H_y -component distribution for the fundamental E_{10}^x mode of the bent waveguide when the mode is launched at the right side of the ring in the CW direction. The color code indicates the values of the H_y component.

The average power values recorded by the monitors for the modes launched in the CW and CCW directions are compared in Fig. 3-5. Note that the steady-state solution is established after the initial transient for each monitor. As expected, after the first quarter circle of propagation, there is no difference between the CCW reading on monitor 2 and the CW reading on monitor 5. In addition, these readings are indistinguishable from the CCW1 and CW6 readings taken within $0.1 \mu\text{m}$ from the launching point. This indicates that the bending losses in the cavity for the fundamental E_{10}^x mode are negligible. The CW mode undergoes some scattering/conversion at the junction with the straight waveguide, therefore the CW reading at monitor 3 is lower than the CCW reading. There is a dramatic difference in reading on monitor 4, with a large portion of the CCW mode (73% of the initially launched power) being by design redirected into the straight waveguide, while practically no CW power is detected in the straight waveguide, with the CW4 reading of only 5×10^{-4} . This structure-induced asymmetry between the two counterpropagating modes persists in two subsequent readings at three quarters of a circle and at a completion of a full circle, where the average power in the CCW mode is about 3.3 times lower than in the CW mode. Hence, there is a factor of 3.3 difference in the losses experienced by the CCW and CW modes. This translates in the photon lifetime in the CCW mode being about 3.3 times shorter than in the CW mode.

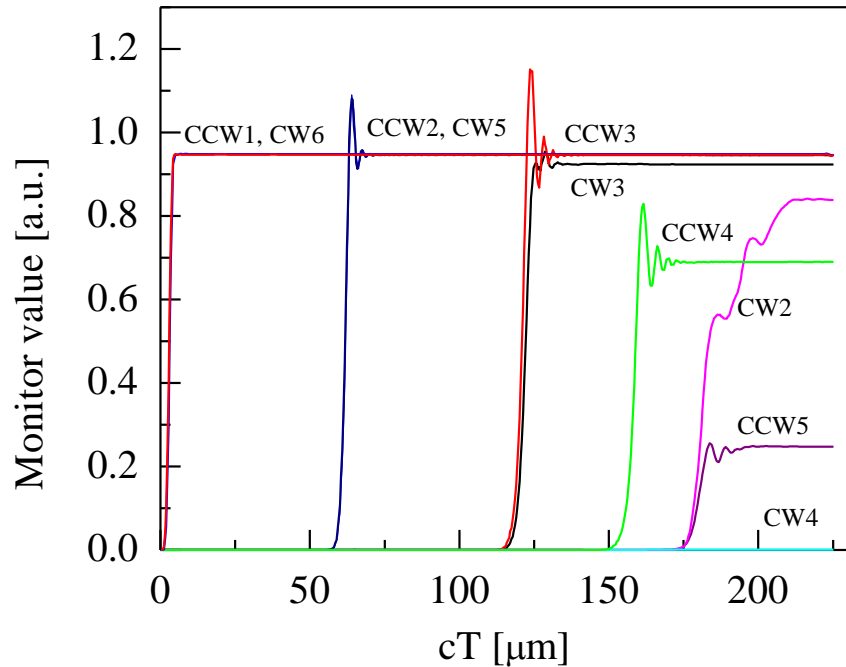


Fig. 3-5. Three-dimensional simulation results for the WRL structure, showing the comparison of average power values on monitors at various locations on the WRL structure, normalized to launched power. The CCW2 and CW5 monitor readings, after the first quarter-circle propagation, are indistinguishable from each other and from the initial launch readings CCW1 and CW6. The CW4 monitor reading is nearly zero.

3.3 MODULATION RESPONSE OF FREE-RUNNING WRLS

The modulation response can be obtained numerically using the following rate equations:

$$\frac{dS_{ccw}}{dt} = \left[G_{ccw} - \frac{1}{\tau_p^{ccw}} \right] S_{ccw} + R_{sp}, \quad (3-1)$$

$$\frac{d\theta_{ccw}}{dt} = \frac{\alpha}{2} \left[G_{ccw} - \frac{1}{\tau_p^{ccw}} \right], \quad (3-2)$$

$$\frac{dS_{cw}}{dt} = \left[G_{cw} - \frac{1}{\tau_p^{cw}} \right] S_{cw} + R_{sp}, \quad (3-3)$$

$$\frac{d\theta_{cw}}{dt} = \frac{\alpha}{2} \left[G_{cw} - \frac{1}{\tau_p^{cw}} \right]. \quad (3-4)$$

$$\frac{dN_r}{dt} = \eta_i \frac{I_r}{q} - \frac{N_r}{\tau_c} - G_{cw} S_{cw} - G_{ccw} S_{ccw}. \quad (3-5)$$

where the subscripts and/or superscripts *cw* and *ccw* denote the mode (CW or CCW) to which the corresponding parameters belong. S , θ , and N represent the photon number, optical phase, and the total carrier number, respectively, in the ring laser cavity, within which a uniform carrier density is assumed, and τ_p the photon lifetime, R_{sp} the spontaneous emission rate, η_i the current injection efficiency, α the linewidth broadening factor, I_r the injection current, q the electron charge and τ_c the carrier lifetime of the ring laser. The modal gain of the ring laser taking into account the nonlinear gain saturation effects is given by:

$$G_{cw} = \frac{G_{0r}(N_r - N_{0r})}{1 + \varepsilon_s S_{cw}/V_r + \varepsilon_c S_{ccw}/V_r}, \text{ and} \quad (3-6)$$

$$G_{ccw} = \frac{G_{0r}(N_r - N_{0r})}{1 + \varepsilon_s S_{ccw1,2}/V_r + \varepsilon_c S_{cw}/V_r}, \quad (3-7)$$

with G_{0r} the differential modal gain, defined as

$$G_{0r} = \frac{\Gamma a v_g}{V_r}, \quad (3-8)$$

where N_{0r} is the carrier number at transparency, Γ is the optical confinement factor, a is the differential gain, v_g is the group velocity, V_r is the volume of the active region, and ε_s and ε_c are the self- and cross-gain saturation coefficients respectively.

Sinusoidal modulation is assumed throughout the simulation and the small-signal modulation is applied through the injection current of the ring laser:

$$I_r = I_{0r}[1 + \delta \sin(2\pi f t)], \quad (3-9)$$

where I_{0r} is the bias injection current, f is the modulation frequency, and δ is the modulation depth. A modulation depth of 1% is assumed.

Both configurations in Fig. 3-1 are simulated. For the symmetric structure shown in Fig. 3-1a, the photon lifetimes for the two counter-propagating modes are assumed to be equal, $\tau_p^{cw} = \tau_p^{ccw}$, while for the whistle geometry configuration shown in Fig. 3-1b, $\tau_p^{cw} \neq \tau_p^{ccw}$. Fig. 3-6a shows the calculated light-current characteristic for the free-running symmetric ring laser in terms of photon numbers in the CW and CCW modes versus applied injection current. Without external optical injection into the CCW mode,

symmetry in the photon lifetimes for the CW and CCW modes in the weak-injection scheme results in bidirectional operation of the ring laser, with identical light-current characteristics for the CW and CCW modes. The clamping behavior of the carrier number above threshold is also illustrated in Fig. 3-6a. The observed slight increase in the carrier number above threshold is explained by the effect of gain saturation. Fig. 3-6b shows the calculated light-current characteristic for the free-running whistle-geometry ring laser. As expected, strong asymmetry in the photon lifetimes for the CW and CCW modes results in very stable unidirectional (CCW) operation of the WRL.

The normalized frequency response curves for both cases are shown in Fig. 3-7. The whistle-geometry ring laser shows slightly higher resonance frequency and larger bandwidth because under the same bias condition, the photon number in the CCW mode of the WRL is slightly higher than the total photon number in the CW and CCW modes of the symmetric ring laser.

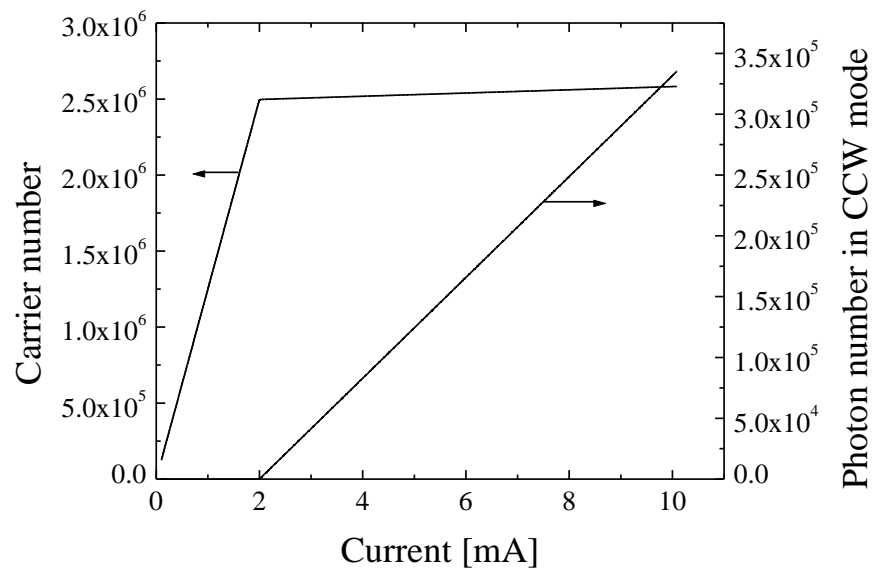
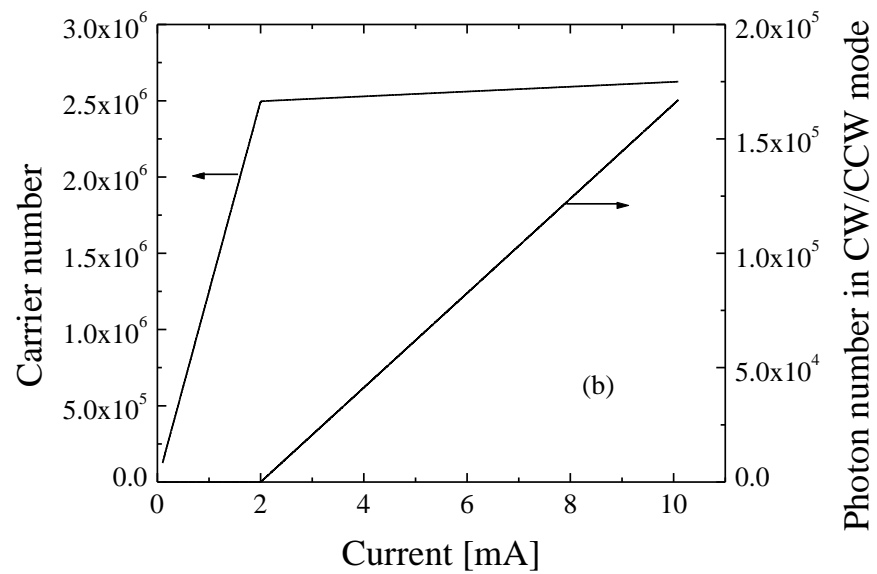


Fig. 3-6. (a) Photon number and carrier number versus injection current for the symmetric ring laser Fig. 3-1a, and (b) photon number in the CW/CCW mode and carrier number versus injection current for the free-running ring whistle-geometry ring laser of Fig. 3-1b.

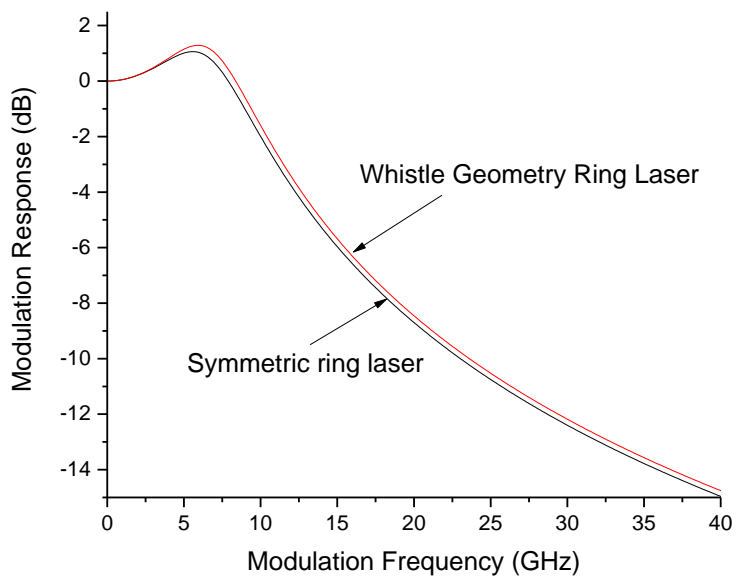


Fig. 3-7. Modulation response curves for ring lasers in WRL and directional coupler configurations.

3.4 MONOLITHICALLY INTEGRATED ULTRAFAST DBR/USRL SYSTEM

As shown in Fig. 3-7, the proposed scheme for optical injection locking incorporates a high-power DBR master laser monolithically integrated with a unidirectional microring slave laser. A single-transverse-mode ridge waveguide structure will be the basis for both the 1.55- μm InGaAs/AlGaInAs MQW DBR and ring lasers. An identical waveguide structure (“injecting” waveguide WG-1 in Fig. 3-7) will be used to transmit the output from the master DBR laser and inject it into the USRL. An “injecting” waveguide WG-1 is used to transmit the output from the master DBR laser and inject it into the USRL.

The basic DBR structure comprises deep-etched Bragg reflectors as indicated in the inset of the Fig. 3-7 which requires no regrowth over patterned substrates and allows definition of the DBR structure, the USRL, the photodetector, and all the waveguides and couplers in a single deep-etching step, thus reducing the technological complexity. To maximize the output directed towards the USRL, the back mirror of the DBR laser will have a much higher reflectivity than the front mirror. An integrated photodetector located at the backside of the DBR laser is used to monitor the emission from the master laser. A waveguide directional coupler WG-2 is used to collect the output of the ring laser as well as to monitor any counterpropagating waves. The same waveguide can also be used to collect the output of the DBR laser when the ring laser is not operating. The input facet of the photodiode and output facet of the waveguide WG-2 are at Brewster’s angle to minimize optical reflections.

Furthermore, the optoelectronic integrated circuit (OEIC) illustrated in Fig. 3-7 can be easily extended to a monolithically integrated cascaded scheme, in which the output from the ring laser is carried by WG-2 to another unidirectional microring laser. Multiple stages of cascading can be implemented by taking this approach.

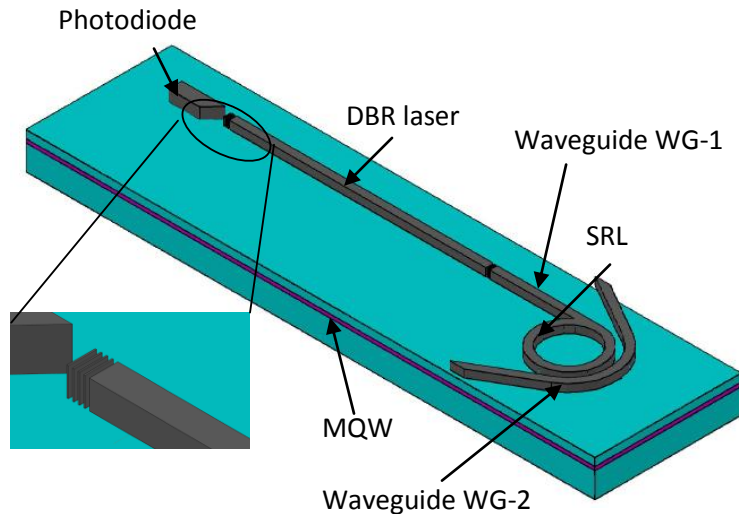


Fig. 3-7. Sketch of a ridge-waveguide configuration to be used in the DBR laser/USRL OEICs (not to scale), including a DBR laser, a ring laser, passive waveguides WG-1 and WG-2, and an integrated photodiode. All these components will have separate electrodes. MQW stands for multiple-quantum-well active region.

CHAPTER 4

HIGH-SPEED MODULATION ANALYSIS OF STRONGLY INJECTION-LOCKED SEMICONDUCTOR RING LASERS

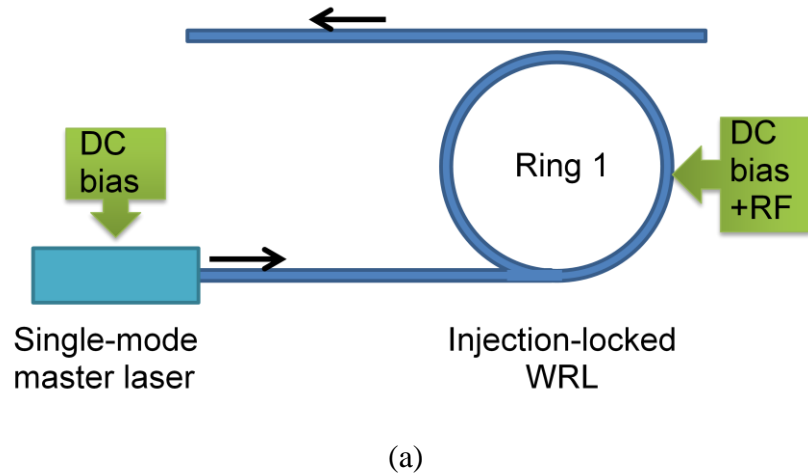
A novel scheme for modulation bandwidth enhancement is presented, involving distributed Bragg reflector master laser monolithically integrated with strongly injection-locked whistle-geometry microring laser. Enhanced high-speed performance of the novel scheme is confirmed through numerical modeling by comparing it with an earlier scheme, where optical injection was provided by a waveguide directional coupler adjacent to the ring laser.

4.1 INTRODUCTION

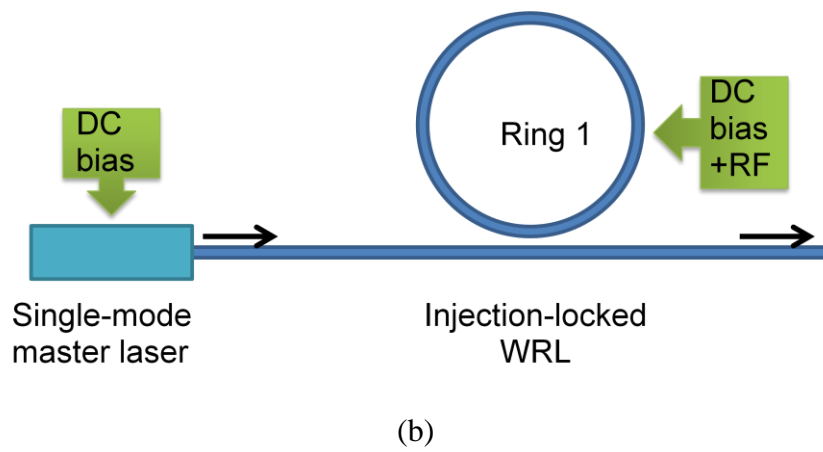
To overcome the limitations of VCSELs discussed in Chapter 2, we propose a novel injection-locking scheme (Fig. 4-1a) involving a distributed Bragg reflector (DBR) master laser monolithically integrated with a unidirectional whistle-geometry microring laser. The new concept of the whistle-geometry semiconductor ring laser (WRL) is especially attractive for this particular application, as it can be designed for minimal back reflections (eliminating, potentially, the need for an optical isolator protecting the master laser from optical feedback), while simultaneously allowing for complete coupling of the DBR laser output into the ring, supporting the favored propagation direction. By the very nature of WRL, low reflectivity for incident light does not at all compromise the quality of the ring cavity, and does not affect the threshold condition for the wave propagating in the favored direction. This makes WRLs free from the design constraints that edge-

emitting lasers and VCSELs suffer from. Injection locking of semiconductor ring lasers for high-speed modulation enhancement has been theoretically investigated in [Chrostowski 2008]. Their design (Fig. 4-1b), however, allowed for only weak optical injection provided by a waveguide directional coupler adjacent to the ring laser. In addition to dramatically increased injection coupling rate, the new scheme for direct optical injection benefits from strong asymmetry in the photon lifetimes for the clockwise and counterclockwise modes, thus further promoting stable unidirectional operation of the ring laser.

In this chapter, we report on the numerical modeling results for optically injection-locked microring lasers monolithically integrated with single-mode master DBR lasers and make comparison between the two schemes for optical injection.



(a)



(b)

Fig. 4-1. (a) Schematic diagram of an optically injection-locked (strong injection) whistle-geometry semiconductor ring laser monolithically integrated with single-mode master DBR laser. (b) Schematic diagram of an optically injection-locked (weak injection) ring laser monolithically integrated with single-mode master DBR laser.

4.2 THEORETICAL MODEL

The dynamics of an optically injection-locked microring laser monolithically integrated with single-mode master DBR laser was modeled by a system of rate equations written in terms of the photon numbers, phases, and total carrier numbers in the master DBR and microring follower lasers [Chrostowski 2008]. The master laser is modeled as a single-mode laser described by the photon number S_m and optical phase θ_m , related to the master laser field as $E_m = \sqrt{S_m} \exp i\theta_m(t)$:

$$\frac{dS_m}{dt} = \left[G_{0m} (N_m - N_{0m}) - \frac{1}{\tau_p^m} \right] S_m + R_{sp} \quad (4-1)$$

$$\frac{d\theta_m}{dt} = \frac{\alpha}{2} \left[G_{0m} (N_m - N_{0m}) - \frac{1}{\tau_p^m} \right]. \quad (4-2)$$

The total carrier number in the master DBR laser is described by N_m , and a uniform carrier density is assumed in the laser cavity

$$\frac{dN_m}{dt} = \eta_i \frac{I_m}{q} - \frac{N_m}{\tau_c} - G_{0m} (N_m - N_{0m}) S_m. \quad (4-3)$$

In Eqs. (4-1) - (4-3), G_{0m} is the differential modal gain given by

$$G_{0m} = \frac{\Gamma a v_g}{V_m}, \quad (4-4)$$

where Γ is the optical confinement factor, a is the differential gain, v_g is the group velocity, and V_m is the master laser active region volume. Other parameters in Eqs. (4-1) - (4-3) are the linewidth broadening factor α , transparency carrier number N_{0m} , carrier lifetime τ_c , photon lifetime τ_p^m , spontaneous emission rate R_{sp} , and internal quantum

efficiency η_i .

The ring laser is modeled by two counterpropagating modes with photon numbers S_{cw} , S_{ccw} and optical phases θ_{cw} , θ_{ccw} for the clockwise (CW) and counterclockwise (CCW) modes, respectively. The master laser light is injected into the CCW mode:

$$\frac{dS_{\text{ccw}}}{dt} = \left[G_{\text{ccw}} - \frac{1}{\tau_p^{\text{ccw}}} \right] S_{\text{ccw}} + R_{\text{sp}} + 2\kappa_c \sqrt{S_m S_{\text{ccw}}} \cos(\theta_{\text{ccw}} - \theta_m) , \quad (4-5)$$

$$\frac{d\theta_{\text{ccw}}}{dt} = \frac{\alpha}{2} \left[G_{\text{ccw}} - \frac{1}{\tau_p^{\text{ccw}}} \right] - (\omega_0 - \omega_{\text{th}}) - \kappa_c \sqrt{\frac{S_m}{S_{\text{ccw}}}} \sin(\theta_{\text{ccw}} - \theta_m) , \quad (4-6)$$

$$\frac{dS_{\text{cw}}}{dt} = \left[G_{\text{cw}} - \frac{1}{\tau_p^{\text{cw}}} \right] S_{\text{cw}} + R_{\text{sp}} , \quad (4-7)$$

$$\frac{d\theta_{\text{cw}}}{dt} = \frac{\alpha}{2} \left[G_{\text{cw}} - \frac{1}{\tau_p^{\text{cw}}} \right] - (\omega_0 - \omega_{\text{th}}) . \quad (4-8)$$

The carrier number in the ring laser is described by N_r , and a uniform carrier density is assumed in the ring laser cavity:

$$\frac{dN_r}{dt} = \eta_i \frac{I_r}{q} - \frac{N_r}{\tau_c} - G_{\text{cw}} S_{\text{cw}} - G_{\text{ccw}} S_{\text{ccw}} . \quad (4-9)$$

As distinct from [Chrostowski 2008], we allow for unequal photon lifetimes τ_p^{cw} and τ_p^{ccw} for the CW and CCW modes, respectively. Nonlinear gain saturation effects are taken into account in Eqs. (4-5) – (4-9) by coefficients ε_s and ε_c for the self- and cross-gain saturation in the expressions for the modal gain, with $\varepsilon_c = 2\varepsilon_s$ [Yuan 2007]

$$G_{\text{cw}} = \frac{G_{0r}(N_r - N_{0r})}{1 + \varepsilon_s S_{\text{cw}} / V_r + \varepsilon_c S_{\text{ccw}} / V_r} \quad \text{and} \quad (4-10)$$

$$G_{\text{ccw}} = \frac{G_{0r}(N_r - N_{0r})}{1 + \varepsilon_s S_{\text{ccw}} / V_r + \varepsilon_c S_{\text{cw}} / V_r},$$

with N_{0r} being the transparency carrier number, and the differential modal gain given by

$$G_{0r} = \frac{\Gamma a v_g}{V_r}, \quad (4-11)$$

where V_r is the ring laser active region volume. Other parameters in Eqs. (4-5) – (4-9) are the injection coupling rate κ_c , the mode frequency of the ring cavity ω_0 , and the free-running mode frequency of the ring cavity at threshold ω_{th} . We neglect the drift of the resonant cavity frequency above threshold in the analysis of the free-running ring laser operation by setting $\omega_0 - \omega_{th}$ equal to zero in both Eq. (4-6) and Eq. (4-8). Under stable injection-locking conditions, $\omega_0 - \omega_{th}$ in Eq. (4-8) is set equal to zero for the CW mode that stays below threshold, whereas ω_0 in Eq. (4-6) is locked to the frequency of the master laser. Hence, $\omega_0 - \omega_{th}$ in Eq. (4-6) effectively represents the angular frequency detuning between the master laser and the ring laser.

It should be pointed out that we neglect in the model all mechanisms that could possibly lead to feedback from the ring laser to the master laser. Zero reflection is assumed from the interface between the injecting waveguide and the ring laser in both injection-locking schemes of Fig. 4-1. Because of the ring laser unidirectionality imposed by optical injection-locking (Fig. 4-1b) and further promoted by the strong asymmetry in

optical losses for the CW and CCW modes in the WRL injection-locking scheme of Fig. 4-1a, there is no stimulated emission from the CW mode of the ring laser that might reach the master laser, and we neglect any feedback resulting from spontaneous emission into the CW mode. Linear coupling between the two counterpropagating modes due to backscattering is also neglected. To some extent, however, optical feedback effects from backscattering or back reflections can be expected in practice due to imperfections resulting from the fabrication process. If necessary, these could be taken care of by using on-chip optical isolators [Yu 2009], [Yu 2010].

Table 4-1 shows the list of parameters used in the simulation. The value for the linewidth broadening parameter α was taken from [Celebi 2006]. A typical value of $\varepsilon_s = 2.7 \times 10^{-18} \text{ cm}^3$ reported in literature [Kawaguchi 1994] was used for the gain self-saturation coefficient. Modal effective index n_{eff} , group velocity v_g , and optical confinement factor Γ were calculated for a deeply etched ridge-waveguide laser structure, assuming a 1.55- μm InGaAs/AlGaInAs MQW epitaxial structure of [Wong 2005] with 7 rather than 6 QWs. Active region volumes V_m and V_r were estimated based on the assumed master laser cavity length $L_m = 200 \mu\text{m}$, ring laser effective cavity length $L_r = 62.83 \mu\text{m}$ (20- μm diameter), the combined thickness of 49 nm of 7 QWs, and the width of the active region determined by the width of the ridge waveguide of 1.4 μm . The power reflectivity of the back DBR mirror of the master laser was assumed to be 100%, whereas that of the front DBR mirror was calculated at 1.55 μm wavelength to be ~82.5% for the front mirror consisting of two quarter-wave layers of benzocyclobutene (BCB) and one quarter-wave layer of semiconductor (refractive index equal to n_{eff}) in between, separating the identical ridge-waveguide structures of the master laser and the

TABLE 4-1
PARAMETERS USED IN SIMULATION

Parameters	Symbol	Value	Units
Material Parameters			
Linewidth broadening factor	α	2	
Carrier lifetime	τ_c	0.4	ns
Spontaneous emission rate	R_{sp}	85	ns ⁻¹
Differential gain	a	1×10^{-15}	cm ²
Transparency carrier density	N_0/V	$\sim 0.485 \times 10^{18}$	cm ⁻³
Internal quantum efficiency	η_i	0.5	
Master Laser			
Cavity length	L_m	200	μm
Reflectivity of injecting mirror	R_m	0.825	
Active volume	V_m	1.372×10^{-11}	cm ³
Optical confinement factor	Γ_m	0.09	
Transparency carrier number	N_{0m}	6.65×10^6	
Modal effective index	n_{eff}	3.279	
Group velocity	v_{gm}	8.76×10^9	cm/s
Photon lifetime	τ_p^m	22.74	ps
Ring Lasers			
Injection coupling rate	κ_c	$6.09 \times 10^{11} (1.36 \times 10^{11})^*$	s ⁻¹
Ring diameter	D	20	μm
Effective cavity length	$L_{rl,2}$	62.83	μm
Active volume	$V_{rl,2}$	4.31×10^{-12}	cm ³
Optical confinement factor	$\Gamma_{1,2}$	0.09	
Transparency carrier number	$N_{0rl,2}$	2.089×10^6	
Modal effective index	$n_{eff1,2}$	3.279	
Group velocity	$v_{g1,2}$	8.76×10^9	cm/s
Photon lifetime in the CCW mode	τ_p^{ccwl}	13.4	ps
Photon lifetime in the CW mode	τ_p^{cw1}	0.69 (13.4)	ps
Nonlinear gain self-saturation	ϵ_s	2.7×10^{-18}	cm ³
Nonlinear gain cross-saturation	ϵ_c	5.4×10^{-18}	cm ³

*Shown in parentheses are the values for the weak-injection scheme when different from those for the strong-injection scheme.

injecting waveguide. The photon lifetime τ_p^m for the master laser was calculated using the following expression that holds for a Fabry-Perot cavity with $R_1 = 100\%$ and $R_2 = R_m$ and neglects internal losses [Chrostowski 2008]

$$\tau_p^m = -\frac{n_{\text{eff}} L}{2c \ln \sqrt{R_m}} , \quad (4-12)$$

where $L = 2L_m$, and $R_m = 0.825$. Neglecting the bending losses, the same expression is applicable to ring lasers of Fig. 3-1 with $L = L_r$ and R_m replaced with $R_r = 1 - T_r$, where T_r represents the power transmission coefficient at the output of the directional coupler. The photon lifetimes τ_p^{cw} and τ_p^{ccw} for the CW and CCW modes of the ring laser in Fig. 1b and for the CCW mode in the ring laser of Fig. 1a were calculated for $T_r = 0.05$ (assumed 5% coupling efficiency of the ridge-waveguide directional coupler used to extract light from the ring laser). For the CW mode of the strongly injection-locked ring laser (Fig. 4-1a), the photon lifetime τ_p^{cw} was assumed to be equal to one roundtrip in the ring laser cavity $\tau_p^{\text{cw}} = n_{\text{eff}} L_r / c$. The coupling rate for injection from the master laser into the ring laser was calculated for the strong-injection scheme of Fig. 4-1a as

$$\kappa_c = \frac{c \sqrt{1 - R_m}}{\pi n_{\text{eff}} d} , \quad (4-13)$$

where d is the ring laser diameter and R_m is the power reflectivity of the front DBR mirror of the master laser (with zero reflection assumed for the interface between the injecting waveguide and the ring laser). For the weak-injection scheme of Fig. 4-1b, Eq. (4-13) was modified to account for additional optical loss associated with the waveguide directional coupler used for injection:

$$\kappa_c = \frac{c\sqrt{(1-R_m)T_r}}{\pi n_{\text{eff}} d} . \quad (4-14)$$

Identical transparency carrier density was assumed for the master laser and the follower ring laser, that is $N_{0m}/V_m = N_{0r}/V_r$. A realistic value for the transparency carrier number N_{0r} , and hence for N_{0m} , was obtained in the following way. We used a reported value of 2.28 kA/cm² for threshold current density [Park 2005] for a very similar InGaAsP/InP 20-μm-diameter microring laser with deeply etched 0.8-μm-wide ridge-waveguide structure, which translates into a predicted threshold current of ~2 mA for the simulated 20-μm-diameter microring laser with deeply etched 1.4-μm-wide ridge-waveguide structure. Therefore, the transparency carrier number N_{0r} was adjusted in numerical simulations to obtain 2 mA threshold current for the ring laser.

4.3 NUMERICAL SIMULATION

For the purpose of comparison, simulations of steady-state characteristics and high-frequency modulation response of the ring laser have been carried out for the two injection-locking schemes of Fig. 4-1 under the same bias conditions. Master laser bias of 12 mA (Fig. 4-2) and ring laser bias of 6 mA at $3I_{\text{th}}$ were consistently chosen throughout the simulations.

We first present the numerical modeling results for the weak-injection scheme of Fig. 4-1b. Simulations of the free-running ring laser were performed by solving Eqs. (4-5) – (4-9) with $S_m = 0$. Fig. 4-3 illustrates the effect of optical injection by showing evolution of the photon number in the CCW mode and carrier number in the ring laser

with increasing injection coupling rate κ_c for zero frequency detuning between the master and ring lasers. One immediate effect of optical injection is the imposed unidirectional operation of the ring laser, which can be seen as doubling of the photon number in the CCW mode (at the expense of the CW mode) occurring at extremely, and arbitrarily, low level of optical injection. Less obvious effect of optical injection is the noticeable immediate decrease in the carrier number accompanying the transition from bidirectional to unidirectional operation of the ring laser, which is explained by the assumed asymmetry of the self-gain and cross-gain saturation coefficients in Eq. (4-10). With the injection coupling rate further increasing, the carrier number is rapidly depleted, while significant intensity builds up in the CCW mode of the injection-locked ring laser.

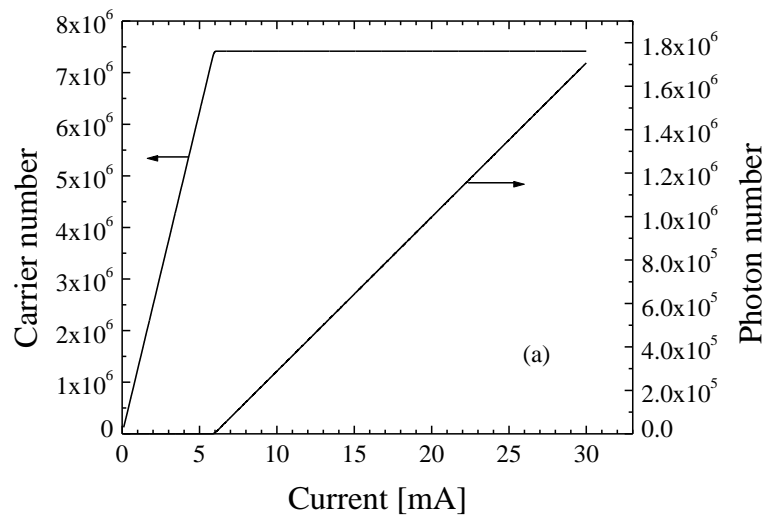


Fig. 4-2. Photon number and carrier number versus injection current for the master DBR laser.

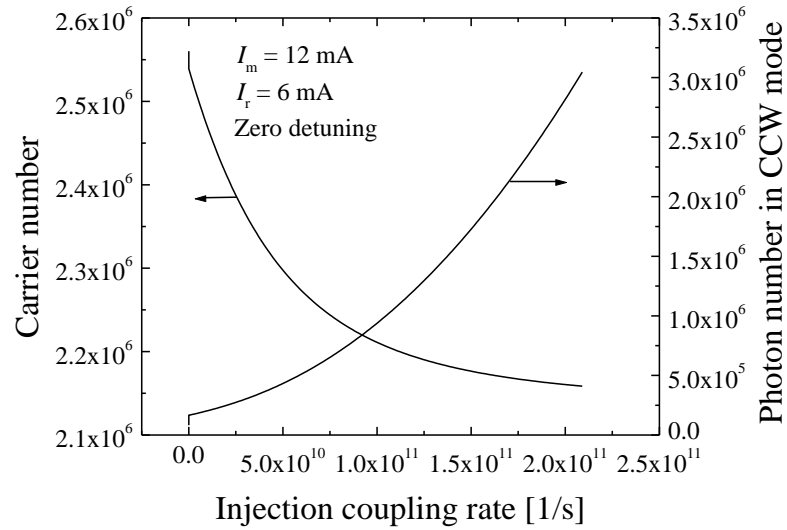


Fig. 4-3. Carrier number and photon number in the CCW mode of the injection-locked ring laser as a function of injection coupling rate calculated for the weak-injection scheme of Fig. 4-1b under steady-state conditions.

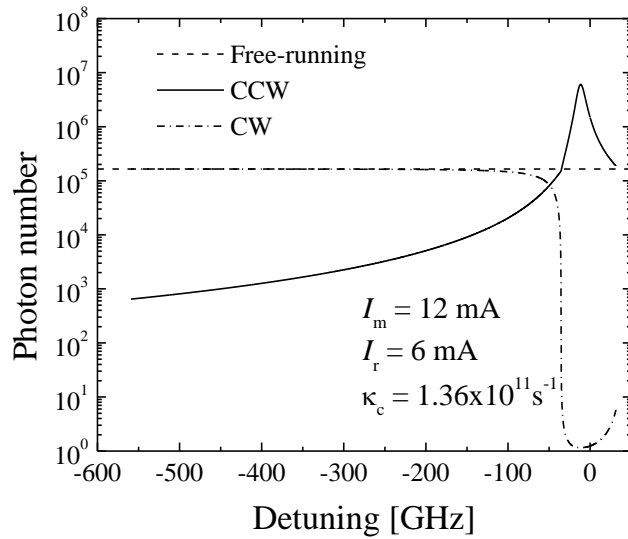


Fig. 4-4. Photon numbers in the CW and CCW modes of the injection-locked ring laser versus frequency detuning calculated for the weak-injection scheme of Fig. 4-1b under steady-state conditions.

The stable injection-locking range obtained for the ring laser in the weak-injection scheme is shown in Fig. 4-4 in terms of the photon numbers in the CW and CCW modes of the ring laser versus the frequency detuning between the master laser and the CCW mode of the ring laser. The maximum of intensity is reached in the CCW mode for ~ 11.5 GHz negative frequency detuning, which corresponds to zero optical phase offset $\theta_{ccw} - \theta_m$ between the master laser and the CCW mode of the ring laser (Fig. 4-5). On the positive detuning side, the stable continuous laser output is observed up to ~ 31.4 GHz, with onset of oscillations beyond this positive detuning edge. Close to the positive detuning edge, the phase offset $\theta_{ccw} - \theta_m$ approaches $-\pi/2$ but stays above that value. On the negative detuning side, however, the steady-state phase offset $\theta_{ccw} - \theta_m$ approaches and goes slightly above $\pi/2$ around 35 GHz negative detuning, which corresponds to destructive interference between the internal field in the CCW mode of the ring laser and the injected field, and should lead to suppression of the CCW mode according to Eq. (4-5). Although the unidirectional operation is no longer maintained beyond ~ 35 GHz negative detuning, the CW mode does not take over immediately, due to lower modal gain for that mode according to Eq. (4-10). Fig. 4-6 illustrates the corresponding behavior of the carrier number in the weakly injection-locked ring laser of Fig. 4-1b. Note that the carrier number for the free-running ring laser in this case corresponds to bidirectional operation, with identical intensities in the CW and CCW modes.

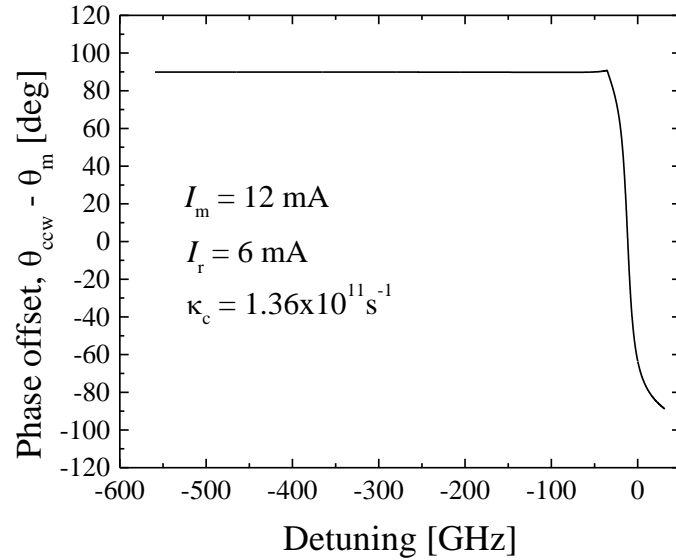


Fig. 4-5. Optical phase offset between the master laser and the CCW mode of the injection-locked ring laser versus frequency detuning calculated for the weak-injection scheme of Fig. 4-1b under steady-state conditions.

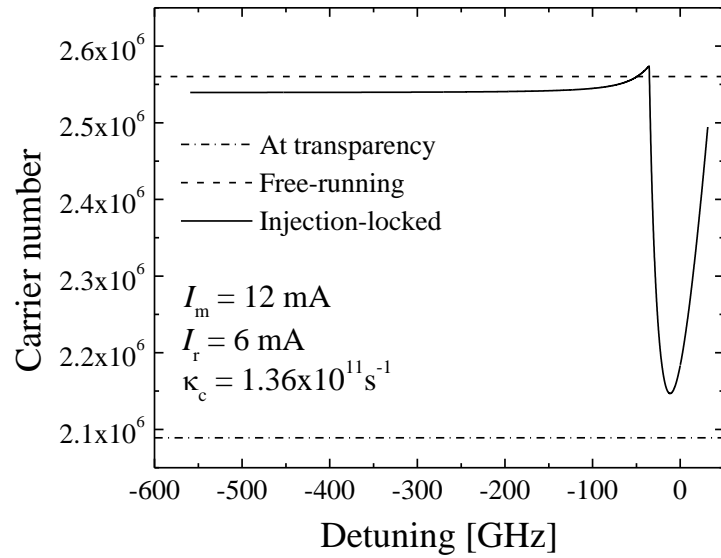


Fig. 4-6. Carrier number in the injection-locked ring laser versus frequency detuning calculated for the weak-injection scheme of Fig. 4-1b under steady-state conditions.

The phase of the CCW mode stays locked to the master laser (Fig. 4-5), and a stable continuous laser output is observed well beyond \sim 35 GHz negative detuning (Fig. 4-4). For high-frequency modulation response simulations, however, we consider only the frequency detuning range from -35 GHz to 31.4 GHz, where the unidirectionality of the ring laser operation is maintained, to avoid optical feedback from the CW mode to the master laser. In the modulation response simulations, a small-signal modulation was applied to the ring laser injection current I_r of Eq. (4-9) in the form

$$I_r = I_{0r} [1 + \delta \sin(2\pi f t)], \quad (4-15)$$

where I_{0r} is the injection current at a constant ring laser bias, f is the modulation frequency, and δ is the modulation depth. 1% modulation depth for the injection current ($\delta = 0.01$) was assumed throughout the simulations. The calculated results for modulation response are presented in terms of the corresponding modulation depth in the photon number in the CCW mode of the ring laser versus modulation frequency. Fig. 4-7 shows modulation frequency response of the free-running ring laser and that of the injection-locked ring laser calculated for several positive and negative values of frequency detuning between the master laser and the ring laser. For comparison, modulation frequency response in each case is normalized to the low frequency response of the free-running laser. The 3-dB modulation bandwidth of the free-running ring laser is \sim 11 GHz with the resonance frequency of \sim 5.6 GHz. There is a significant increase in the resonance frequency of the injection-locked ring laser proportional to the frequency detuning, provided the frequency detuning approaches the edges of the stable injection-locking range, which corresponds to moderate optical power inside the ring cavity. Very

high power inside the ring cavity leads to severely damped modulation response and to very low intensity modulation depth, inferior to that of the free-running laser over the entire modulation frequency range. Although the zero-detuning condition seems attractive for broad-band applications due to its relatively flat frequency modulation response, there is an unavoidable loss in intensity modulation depth associated with injection locking. On the other hand, the drawback associated with the detuning edges is the large pre-resonance sag observed in the modulation response, limiting the usefulness of the system to narrow-band applications.

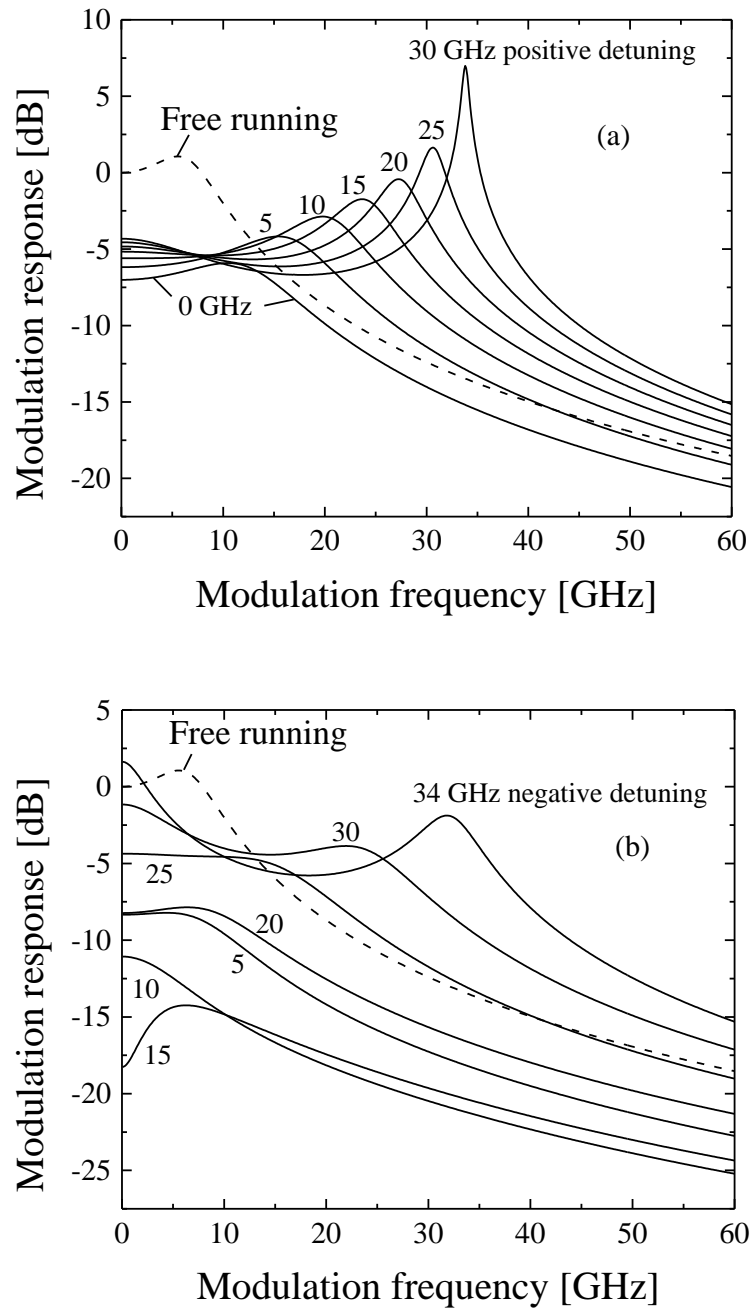


Fig. 4-7. Modulation frequency response of the free-running ring laser (dashed curves) and that of the injection-locked ring laser (weak-injection scheme of Fig. 4-1b) calculated for several values of (a) positive frequency detuning and (b) negative frequency detuning. Modulation frequency response is normalized to low-frequency response of the free-running ring laser. $I_m = 12 \text{ mA}$, $I_r = 6 \text{ mA}$.

We consider now the strong-injection scheme of Fig. 4-1a, involving a WRL. The much higher injection coupling rate in WRL configuration results in a much wider range for stable injection-locking of the ring laser, as shown in Fig. 4-8 in terms of the photon number in the CCW mode of the WRL versus the frequency detuning between the master laser and the WRL. Photon number in the WRL returns to its “free-running” value at the edges of the stable injection-locking range and falls slightly below it due to destructive interference with the injected light. Similarly to the previous case, the CCW mode of the WRL stays locked to the master laser even when the steady-state phase offset goes slightly out of $[-\pi/2; \pi/2]$ range at the edges of the stable locking range (Fig. 4-9). Carrier number in the ring laser goes over its “free-running” value at the edges of the stable injection-locking range (Fig. 4-10) to compensate for the effective increase in threshold for the CCW mode. As distinct from the weak-injection case, this increase in the carrier number is not sufficient for the CW mode to reach its threshold, and the unidirectional operation of the WRL is maintained over the entire stable injection-locking range. Both the maximum of the photon number in the CCW mode of the ring laser (Fig. 4-8) and the minimum of the carrier number (Fig. 4-10) are reached at the negative frequency detuning of ~ 11.9 GHz, which corresponds to zero phase offset between the master laser and the ring laser (Fig. 4-9), *i.e.* to the strongest injection-locking conditions.

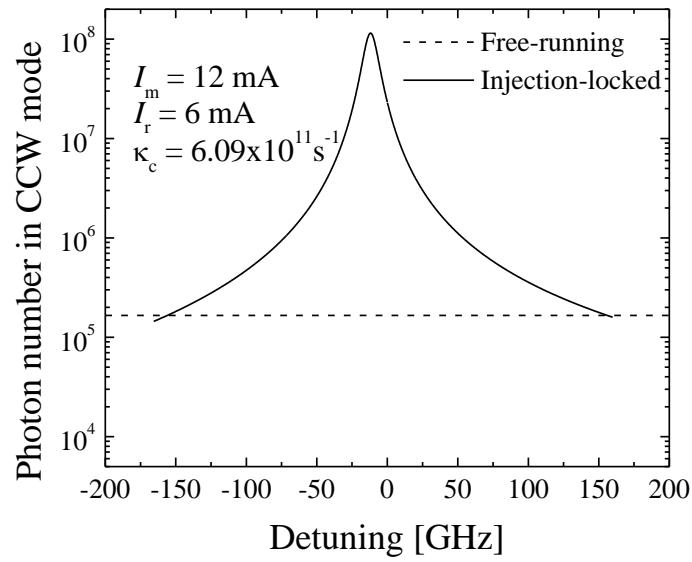


Fig. 4-8. Photon number in the CCW mode of the injection-locked whistle ring laser versus frequency detuning calculated for the strong-injection scheme of Fig. 4-1a under steady-state conditions.

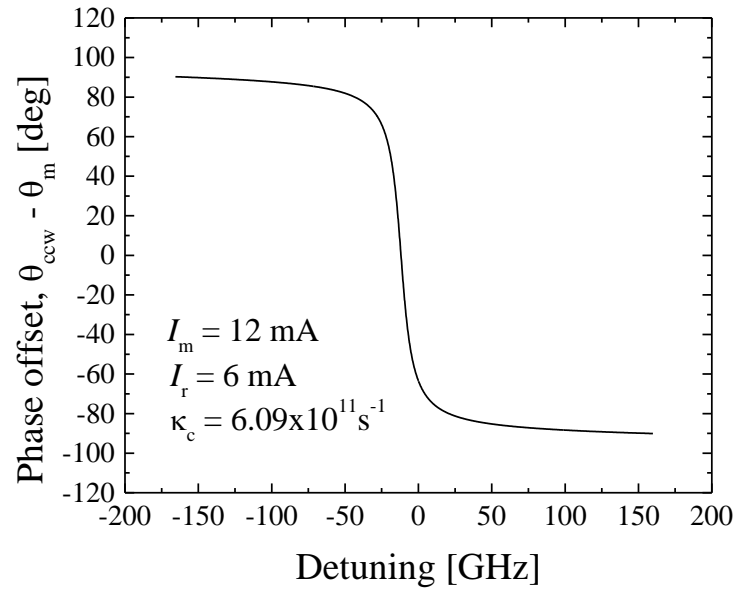


Fig. 4-9. Optical phase offset between the master laser and the CCW mode of the injection-locked whistle ring laser versus frequency detuning calculated for the strong-injection scheme of Fig. 4-1a under steady-state conditions.

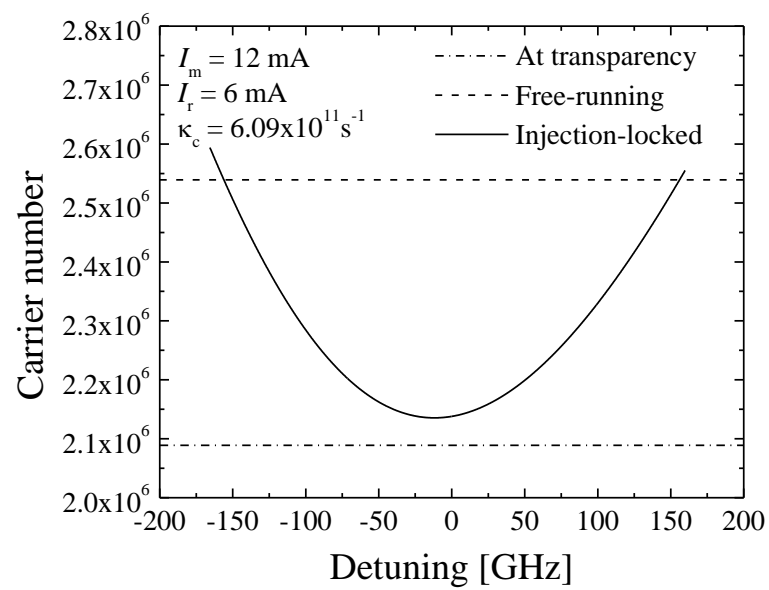


Fig. 4-10. Carrier number in the injection-locked whistle ring laser versus frequency detuning calculated for the strong-injection scheme of Fig. 4-1a under steady-state conditions.

The high-frequency modulation response simulations were performed under the same bias conditions that were used for the weak-injection scheme. Fig. 4-11 shows modulation frequency response of the injection-locked WRL calculated for several positive and negative values of frequency detuning in comparison with the free-running WRL modulation response. The 3-dB modulation bandwidth of the free-running WRL in the strong-injection scheme is ~11.5 GHz, with the resonance frequency of ~5.9 GHz. Great resonance frequency enhancement (up to ~160 GHz) of the injection-locked WRL can be achieved as the frequency detuning approaches the edges of the stable injection-locking range. The modulation response, however, shows the large and growing pre-resonance sag, typical of all optical injection-locked systems. On the other hand, high-frequency modulation at small frequency detuning is not of practical interest due to extremely low intensity modulation depth, inferior to that of the free-running WRL over the entire modulation frequency range.

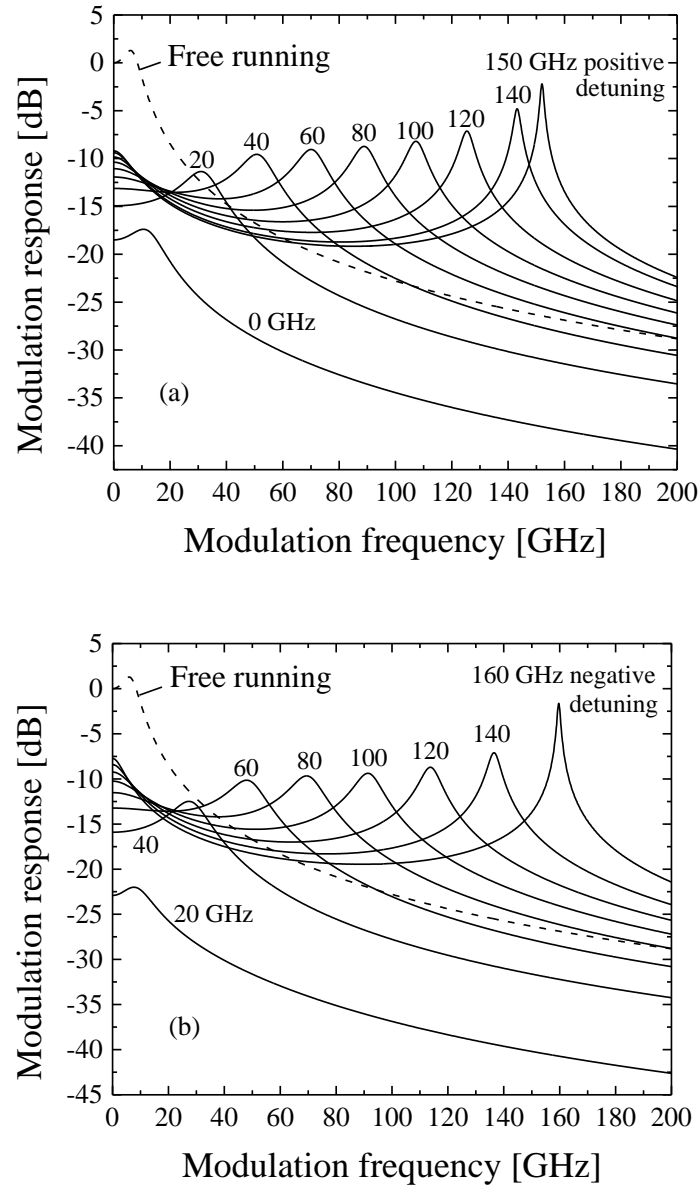


Fig. 4-11. Modulation frequency response of the free-running whistle ring laser (dashed curves) and that of the injection-locked whistle ring laser (strong-injection scheme of Fig. 4-1a) calculated for several values of (a) positive frequency detuning and (b) negative frequency detuning. Modulation frequency response is normalized to low-frequency response of the free-running ring laser. $I_m = 12 \text{ mA}$, $I_r = 6 \text{ mA}$.

4.4 EFFECT OF LIGHT BACKSCATTERING

Greatly enhanced high-speed modulation performance has been predicted in the previous sections for a novel injection-locking scheme involving a DBR or DFB master laser monolithically integrated with a unidirectional semiconductor microring laser. The analysis, however, did not take into account the linear coupling between the two counterpropagating modes due to light backscattering. In this section, the effect of light backscattering between the two counterpropagating modes on high-speed modulation performance of strongly injection-locked unidirectional semiconductor microring lasers is investigated.

The effect of linear coupling between the two counterpropagatin modes due to backscattering can be taken into account by modifying the rate equations for the ring lasers, Eqs (4-5)-(4-8), as:

$$\frac{dS_{ccw}}{dt} = \left[G_{ccw} - \frac{1}{\tau_p^{ccw}} \right] S_{ccw} + R_{sp} + 2\kappa_c \sqrt{S_m S_{ccw}} \cos(\theta_{ccw} - \theta_m) + 2\kappa_s \sqrt{S_{cw} S_{ccw}} \cos(\theta_{ccw} - \theta_{cw} - \theta_s), \quad (4-16)$$

$$\frac{d\theta_{ccw}}{dt} = \frac{\alpha}{2} \left[G_{ccw} - \frac{1}{\tau_p^{ccw}} \right] - (\omega_0 - \omega_{th}) - \kappa_c \sqrt{\frac{S_m}{S_{ccw}}} \sin(\theta_{ccw} - \theta_m) - \kappa_s \sqrt{\frac{S_{cw}}{S_{ccw}}} \sin(\theta_{ccw} - \theta_{cw} - \theta_s), \quad (4-17)$$

$$\frac{dS_{cw}}{dt} = \left[G_{cw} - \frac{1}{\tau_p^{cw}} \right] S_{cw} + R_{sp} + 2\kappa_s \sqrt{S_{ccw} S_{cw}} \cos(\theta_{cw} - \theta_{ccw} - \theta_s), \quad (4-18)$$

$$\frac{d\theta_{cw}}{dt} = \frac{\alpha}{2} \left[G_{cw} - \frac{1}{\tau_p^{cw}} \right] - (\omega_0 - \omega_{th}) - \kappa_s \sqrt{\frac{S_{ccw}}{S_{cw}}} \sin(\theta_{cw} - \theta_{ccw} - \theta_s), \quad (4-19)$$

$$\frac{dN_r}{dt} = \eta_i \frac{I_r}{q} - \frac{N_r}{\tau_c} - G_{cw} S_{cw} - G_{ccw} S_{ccw}, \quad (4-20)$$

where linear coupling between the two counterpropagating modes due to light backscattering is taken into account through the coupling rate $\kappa_s \exp(i\theta_s)$. In the following analysis θ_s was set equal to zero, and the coupling rate due to light backscattering was assumed to be a real number. Simulations were carried out for the same configuration and under the same bias conditions that were assumed in the previous section for the master and the ring lasers.

Consider now a single scattering event over the cavity roundtrip, in which case the backscattering rate κ_s is related to the amplitude scattering coefficient S as

$$\kappa_s = \frac{cS}{\pi n_{\text{eff}} d} , \quad (4-21)$$

where c is the speed of light, n_{eff} is the modal effective index, and d is the ring laser diameter. Fig. 4-12 shows the calculated dependence of κ_s versus S for the particular configuration of the WRL, where the dashed line corresponding to the value of injection coupling rate κ_c is shown for comparison. The results of the following analysis are presented as a function of the scattering coefficient S .

Since the detuning between frequency of the injected light and that of the cavity mode controls the enhanced resonance frequency in the modulation response of injection-locked semiconductor lasers, we performed our analysis for several values of positive frequency detuning $\Delta\omega$ of interest ($\Delta\omega$ of 50 GHz, 80 GHz, 120 GHz, and 150 GHz). We remind the reader here that approaching the boundary of the stable injection-locking range corresponds to progressively weaker locking conditions (see Figs. 4-8 and 4-9).

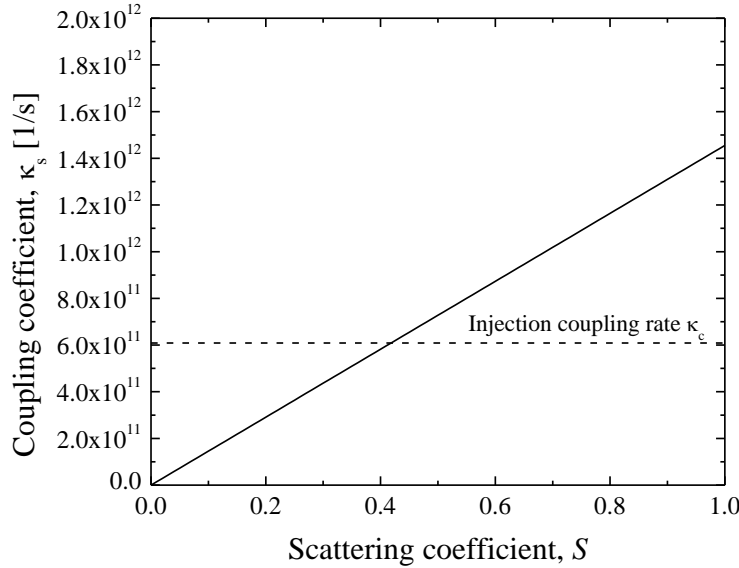


Fig. 4-12. The coupling coefficient due to scattering κ_s as a function of the amplitude scattering coefficient S calculated for the particular configuration of the WRL. The dashed line corresponding to the value of injection coupling rate k_c is shown for comparison.

We first consider the case of $\Delta\omega = 50$ GHz, corresponding to a relatively strong injection locking. For very small values of scattering coefficient $S < 3 \times 10^{-6}$, light backscattering contributes to intensity noise in both CW and CCW modes proportional to S . For S exceeding $S \sim 3 \times 10^{-6}$, the CW mode gets locked by the CCW mode (Fig. 4-13) leading to stable intensity output with no noise present in both counterpropagating modes. Further increase in S leads to weakening and eventual loss of injection locking between the master laser and the CCW mode of the ring laser at $S \sim 0.03281$, with the phase offset $\theta_{ccw} - \theta_m$ approaching $\pi/2$ (Fig. 4-14). For $S > 0.03281$, no steady state solution was found, with intensity pulsation being observed in both CW and CCW modes.

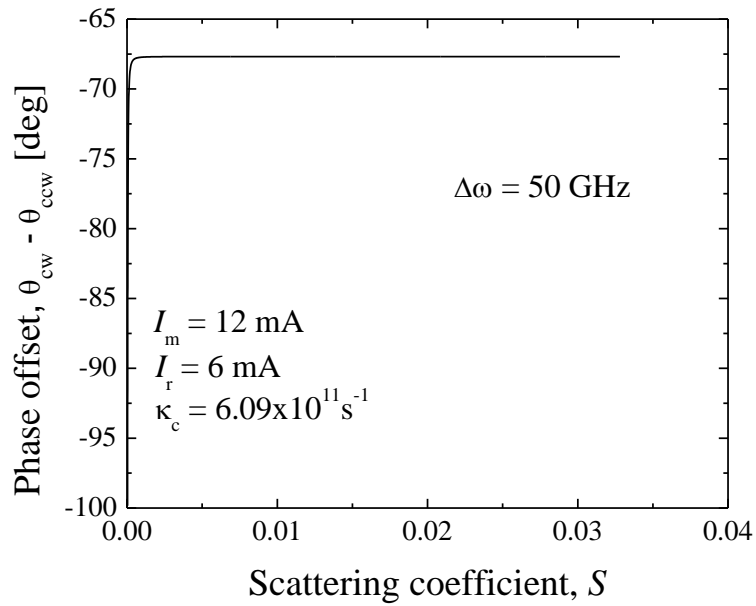


Fig. 4-13. Optical phase offset between the CCW and CW modes of the injection-locked ring laser versus scattering coefficient S under steady-state conditions. $I_m = 12$ mA, $I_r = 6$ mA, $\Delta\omega = 50$ GHz.

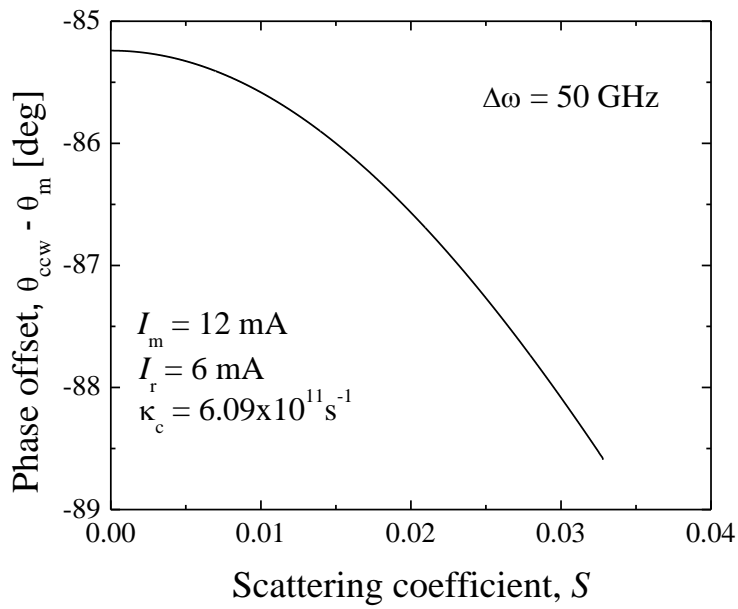


Fig. 4-14. Optical phase offset between the master laser and the CCW mode of the injection-locked ring laser versus scattering coefficient S under steady-state conditions. $I_m = 12$ mA, $I_r = 6$ mA, $\Delta\omega = 50$ GHz.

Evolution of the photon number in CW and CCW modes of the injection-locked ring laser and of their intensity ratio $S_{\text{CW}}/S_{\text{CCW}}$ with increasing scattering coefficient S is shown in Figs. 4-15 and 4-16, respectively. We note that the total number of photons in the ring laser $S_{\text{CW}} + S_{\text{CCW}}$ is not conserved, as the CW mode is much more lossy than the CCW mode and larger scattering coefficient S means more photons from the CCW mode being scattered into CW mode and lost, thus effectively shortening the photon lifetime for the lasing CCW mode, while the CW mode stays below threshold. Fig. 4-17 illustrates the corresponding behavior of the carrier number in the injection-locked ring laser, as the intensity in the lasing CCW mode goes down with enhanced light scattering.

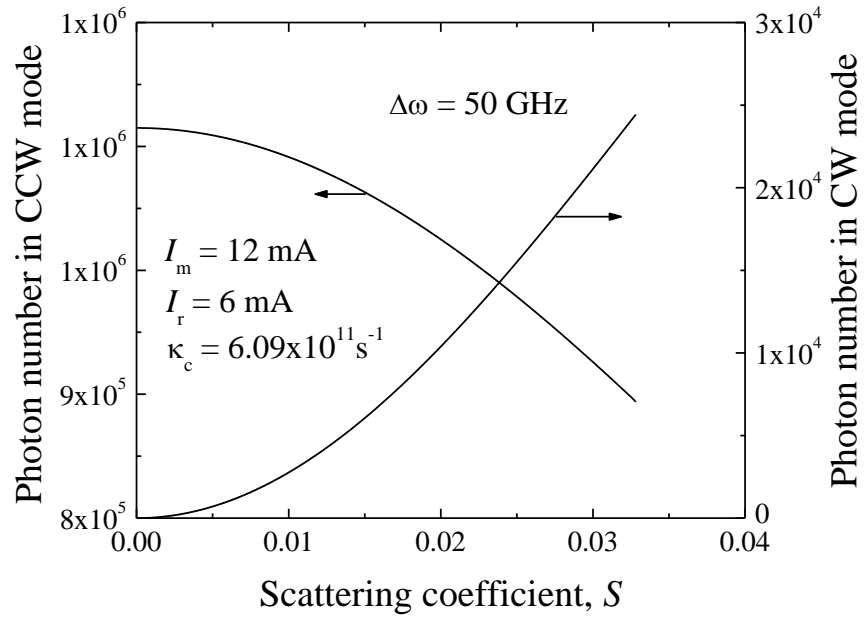


Fig. 4-15. Photon numbers in the CW and CCW modes of the injection-locked ring laser versus scattering coefficient S . $I_m = 12 \text{ mA}$, $I_r = 6 \text{ mA}$, $\Delta\omega = 50 \text{ GHz}$.

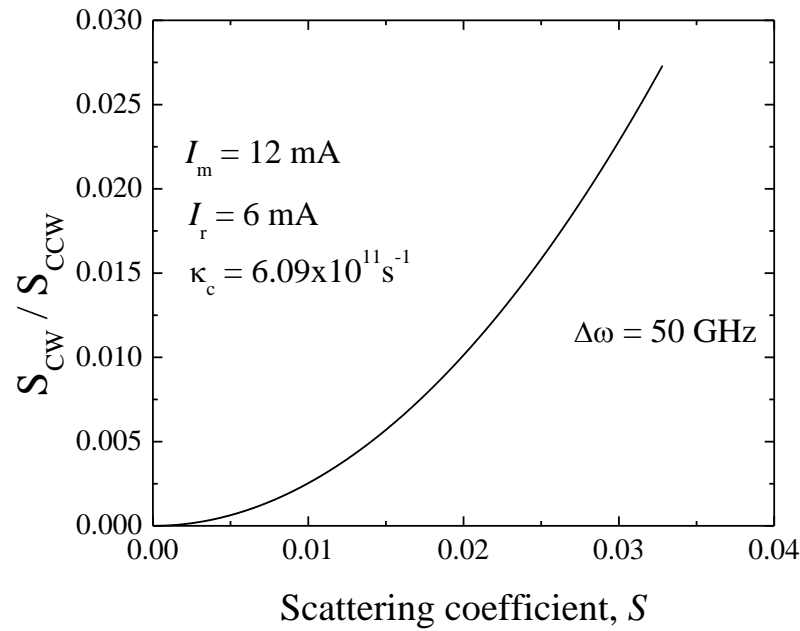


Fig. 4-16. Intensity ratio for the CW and CCW modes of the injection-locked ring laser versus scattering coefficient S . $I_m = 12 \text{ mA}$, $I_r = 6 \text{ mA}$, $\Delta\omega = 50 \text{ GHz}$.

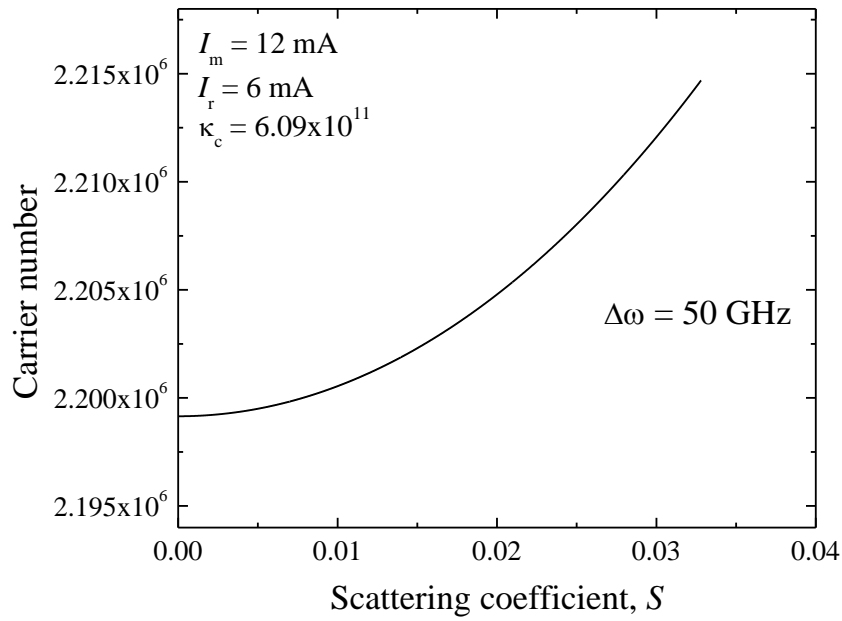


Fig. 4-17. Carrier number in the injection-locked ring laser versus scattering coefficient S . $I_m = 12 \text{ mA}$, $I_r = 6 \text{ mA}$, $\Delta\omega = 50 \text{ GHz}$.

Our analysis of the injection-locked ring laser so far reveals that under relatively strong locking conditions of $\Delta\omega = 50$ GHz the strongly injection-locked WRL would tolerate as much as $\sim 3.28\%$ of light backscattering between the CCW and CW modes preserving the injection locking between the master laser and the CCW mode of the ring laser.

Figs. 4-18 to 4-22 show the results of similar analysis performed for the positive frequency detuning $\Delta\omega = 150$ GHz, corresponding to much weaker locking conditions near the boundary of the stable injection-locking range, with much lower intensity circulating in the CCW mode of the ring laser (see Fig. 4-8). As compared to the case of $\Delta\omega = 50$ GHz, it takes a larger value of scattering coefficient $S \sim 1.21 \times 10^{-4}$, in this situation, for the CW mode to get locked by the CCW mode (Fig. 4-18) and a smaller value of $S \sim 0.01216$ for the injection locking between the master laser and the CCW mode of the ring laser to be eventually lost (Fig. 4-19). Therefore, under relatively weak locking conditions of $\Delta\omega = 150$ GHz the strongly injection-locked WRL would tolerate only as much as $\sim 1.2\%$ of light backscattering between the CCW and CW modes preserving the injection locking between the master laser and the CCW mode of the ring laser. By including the results of similar analysis performed for $\Delta\omega = 80$ GHz and $\Delta\omega = 120$ GHz, we show in Fig. 4-23 the effect of light backscattering on stable injection-locking range attainable in the injection-locked WRL.

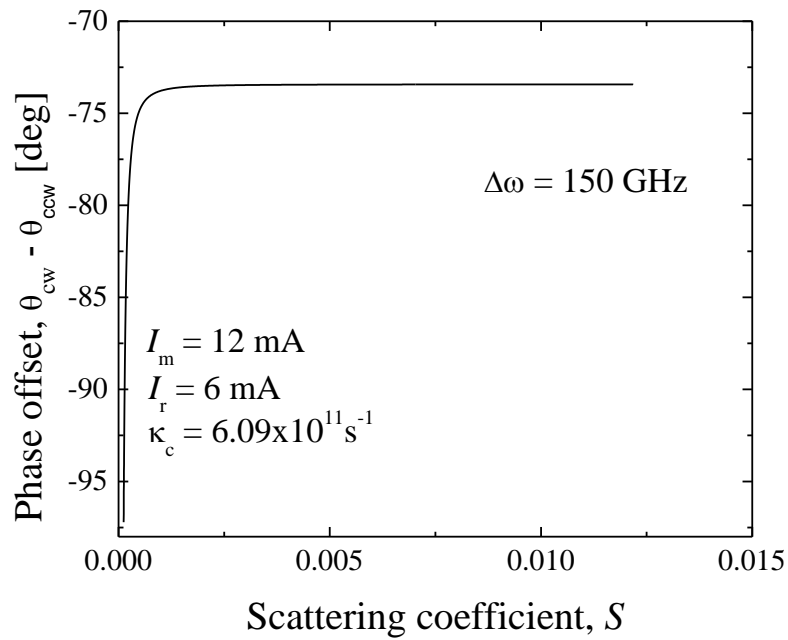


Fig. 4-18. Optical phase offset between the CCW and CW modes of the injection-locked ring laser versus scattering coefficient S under steady-state conditions. $I_m = 12$ mA, $I_r = 6$ mA, $\Delta\omega = 150$ GHz.

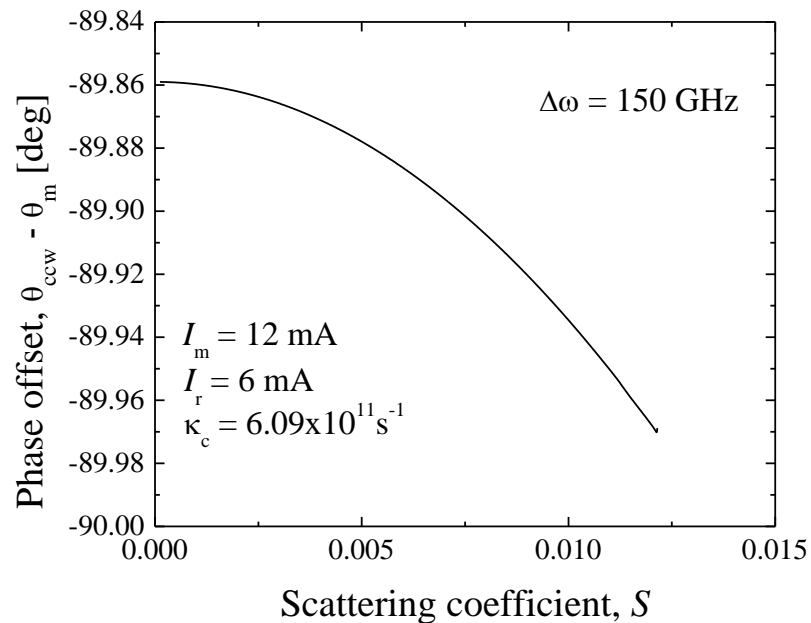


Fig. 4-19. Optical phase offset between the master laser and the CCW mode of the injection-locked ring laser versus scattering coefficient S under steady-state conditions. $I_m = 12$ mA, $I_r = 6$ mA, $\Delta\omega = 150$ GHz.

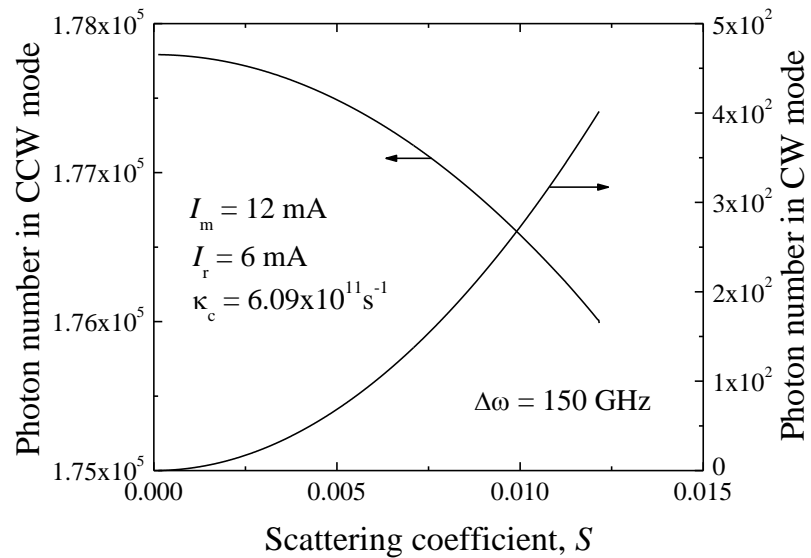


Fig. 4-20. Photon numbers in the CW and CCW modes of the injection-locked ring laser versus scattering coefficient S . $I_m = 12 \text{ mA}$, $I_r = 6 \text{ mA}$, $\Delta\omega = 150 \text{ GHz}$.

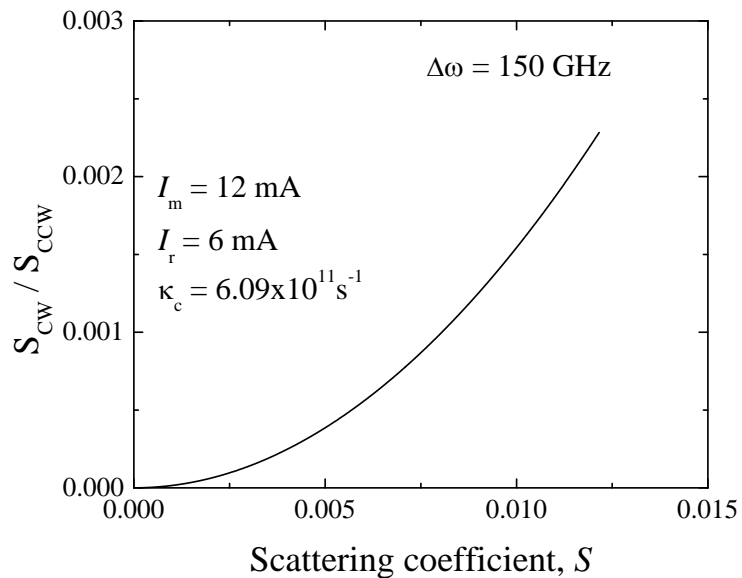


Fig. 4-21. Intensity ratio for the CW and CCW modes of the injection-locked ring laser versus scattering coefficient S . $I_m = 12 \text{ mA}$, $I_r = 6 \text{ mA}$, $\Delta\omega = 150 \text{ GHz}$.

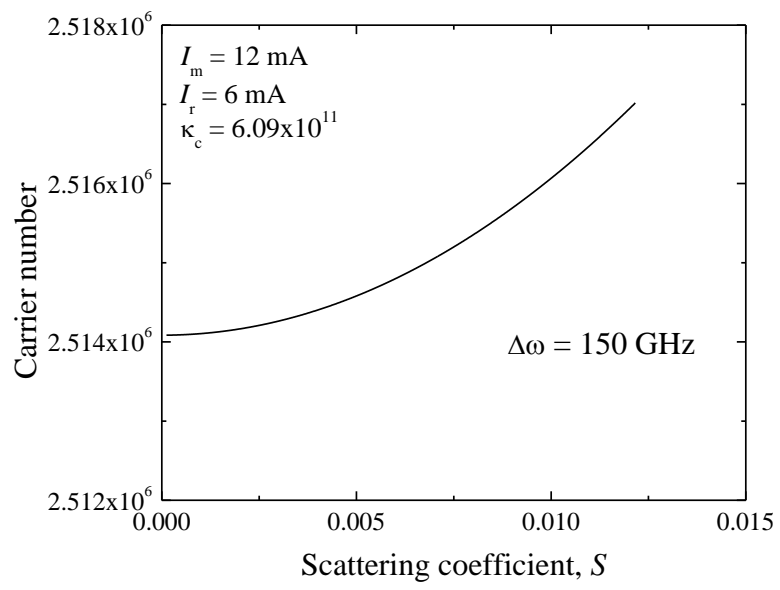


Fig. 4-22. Carrier number in the injection-locked ring laser versus scattering coefficient S . $I_m = 12 \text{ mA}$, $I_r = 6 \text{ mA}$, $\Delta\omega = 150 \text{ GHz}$.

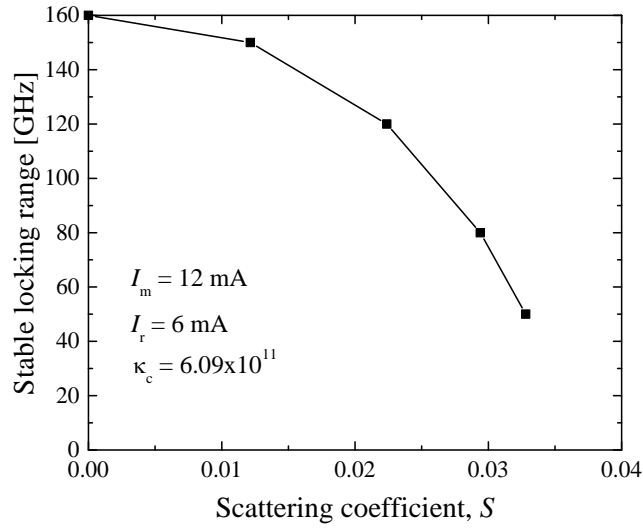


Fig. 4-23. Stable injection-locking range (on the positive frequency detuning side) in the injection-locked ring laser versus scattering coefficient S . $I_m = 12 \text{ mA}$, $I_r = 6 \text{ mA}$, $\Delta\omega = 150 \text{ GHz}$.

In calculating the modulation response, the same bias condition as used in the previous section was assumed throughout the simulations. The calculated results for modulation response are presented in terms of the corresponding modulation depth in the photon number in the CCW mode of the ring laser versus modulation frequency. The modulation frequency response of Fig. 4-24 was calculated for a fixed positive frequency detuning $\Delta\omega = 120$ GHz and several values of scattering coefficient S . Increasing scattering coefficient S makes the resonance in the modulation response more pronounced, which can be explained by the frequency detuning $\Delta\omega$ approaching the boundary of the stable injection-locking range that changes with S as shown in Fig. 4-23.

The effect is similar to the one shown in Fig. 4-11a.

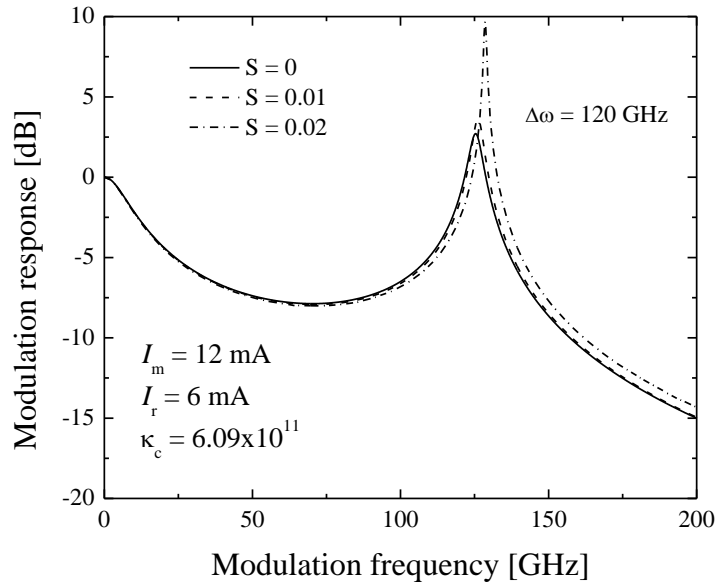


Fig. 4-24. Modulation frequency response of the injection-locked ring laser calculated for several values of scattering coefficient S . Modulation frequency response is normalized to its low-frequency value. $I_m = 12$ mA, $I_r = 6$ mA, $\Delta\omega = 120$ GHz.

4.5 LARGE SIGNAL EFFECT

In transmission of data over analog intensity modulation-direct detection (IM-DD) microwave photonic links, it is important to understand the effect of large signal modulation of semiconductor lasers [Peral 2000] as it makes the photonic link more robust against coherent feedback compared to small signal modulation [Wang 1995]. In this section, large sinusoidal modulation is explored by increasing the modulation depth (δ in Eq. (4-15)) while all other parameters are kept the same.

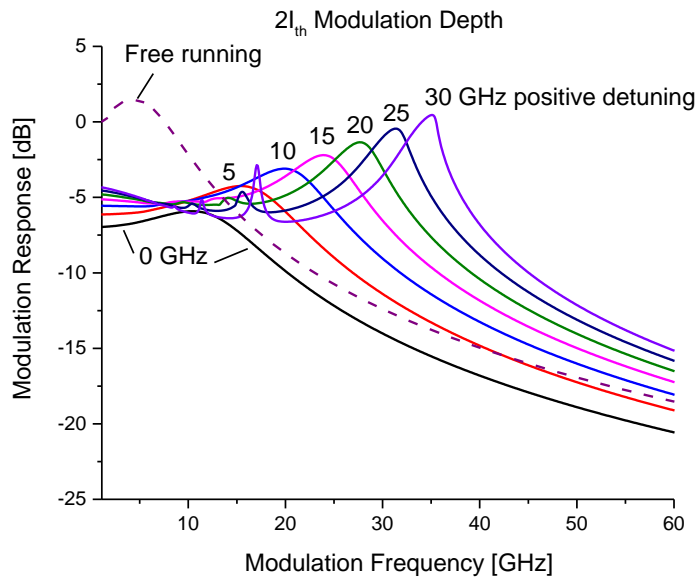
Fig. 4-25 shows the modulation response of the weak injection scheme of Fig. 4-1b when $I_{or}\delta$ is equal to twice the threshold current. When the ring laser is under positive detuning, as the modulation depth increases, the resonance frequency slightly increases and the resonance peak becomes lower due to larger damping, as illustrated in Fig. 4-26. The shift in resonant frequency be explained by Eq. (2-3), or more generally [Lau 2009]:

$$\omega_{res} = \left| \Delta\omega_{inj} - \Delta\omega(N) \right| = \left| \Delta\omega_{inj} - \frac{\alpha}{2} v_{g,eff} G_N \Delta N \right|. \quad (4-22)$$

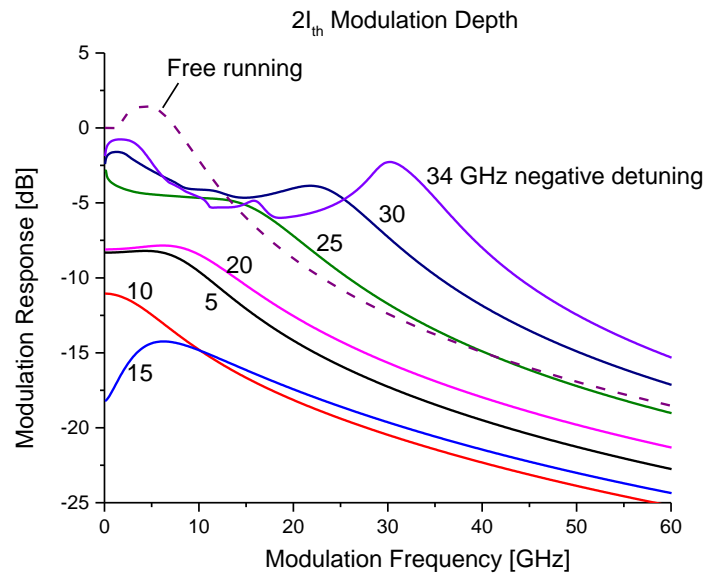
Under positive detuning, $\Delta\omega_{inj} = \omega_{inj} - \omega_0$ is positive while ΔN is negative because of the reduced carrier number from its threshold value due to optical injection. The resulting resonance frequency is then the sum of the frequency detuning and the cavity mode shift. As the modulation depth increases, the slight increase in $G_N \Delta N$ results in larger shift in cavity mode and hence the resonance frequency. On the other hand, when the ring laser is under negative detuning, $\Delta\omega_{inj}$ is negative and according to Eq. (4-22), the resonance frequency is the difference between the frequency detuning and the cavity mode shift.

Thus an increase in modulation depth will cause a lower resonance frequency, as shown in Fig. 4-27 for the case of 34 GHz negative detuning.

Another feature that becomes prominent with the increase of modulation depth is the resonance at lower frequencies. These resonances are subharmonics of the resonance frequency and occur at ω_{res}/m , where $m = 2, 3, 4 \dots$ [Wieczorek 2006], and are more pronounced as the detuning approaches the boundary of stable locking range. As an example, Fig. 4-26 shows the subharmonics for $m=3, 2$, and 1 for 30 GHz positive detuning. The waveforms of the photon number in CCW mode when the modulation frequencies are around the subharmonics are shown in Fig. 4-28a to 4-28c. At these modulation frequencies, the photon numbers deviate from sinusoidal behavior due to strong interference between the modulation frequency and the resonance frequency. Also shown are the waveforms when the modulation frequency is around the resonance frequency (Fig. 4-27d), where the waveform remains sinusoidal.



(a)



(b)

Fig. 4-25. Large signal modulation frequency response of the free-running ring laser (dashed curves) and that of the injection-locked ring laser (weak-injection scheme of Fig. 4-1b) calculated for several values of (a) positive frequency detuning and (b) negative frequency detuning. Modulation frequency response is normalized to low-frequency response of the free-running ring laser. $I_m = 12 \text{ mA}$, $I_r = 6 \text{ mA}$.

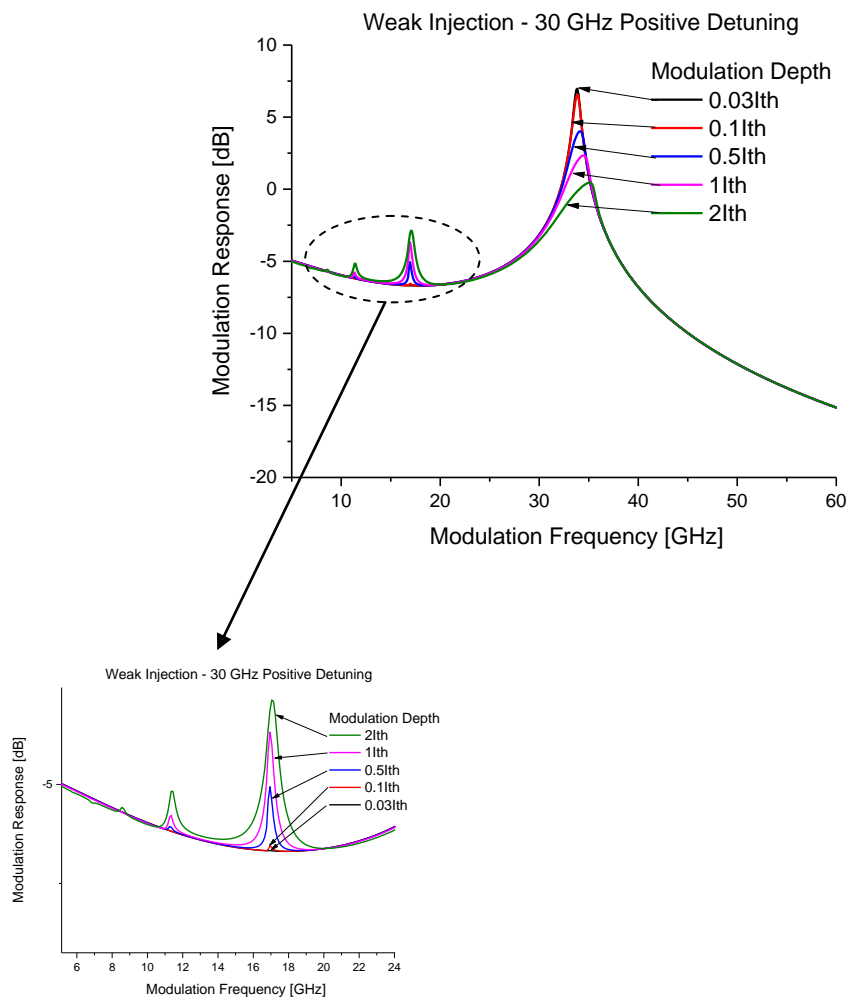


Fig. 4-26. Modulation frequency response of weak-injection scheme of Fig. 4-1b under 30 GHz positive detuning calculated for several values of modulation depth. Modulation frequency response is normalized to low-frequency response of the free-running ring laser. $I_m = 12 \text{ mA}$, $I_r = 6 \text{ mA}$.

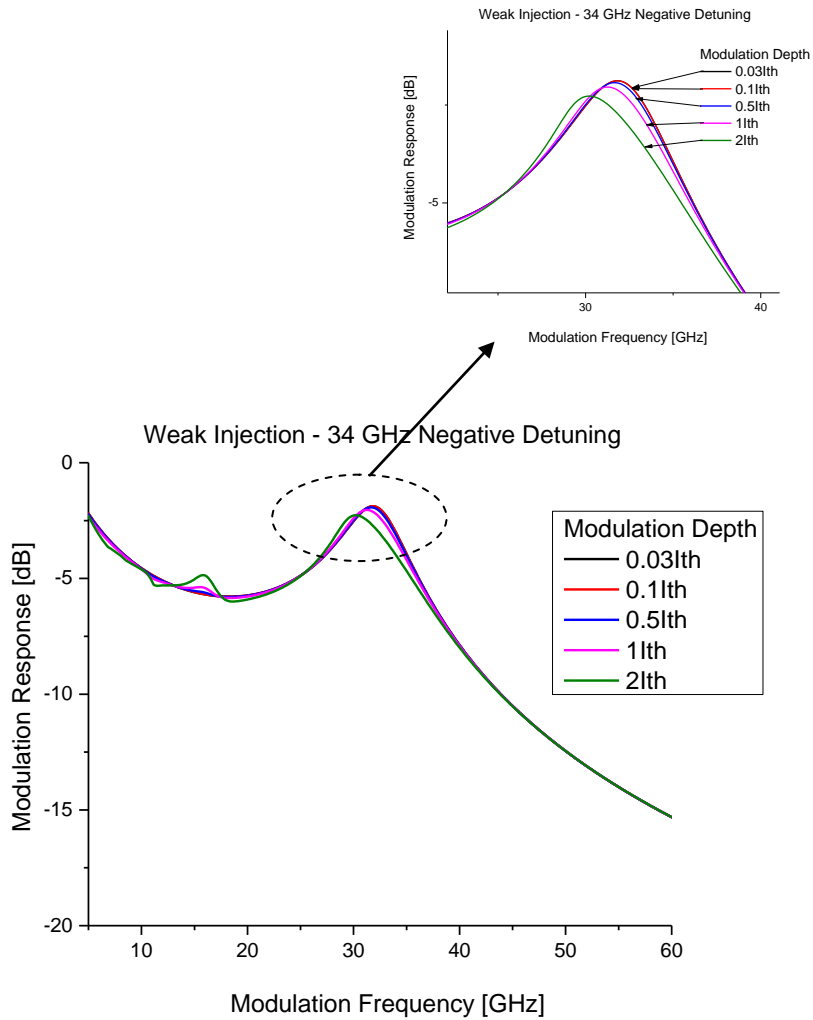
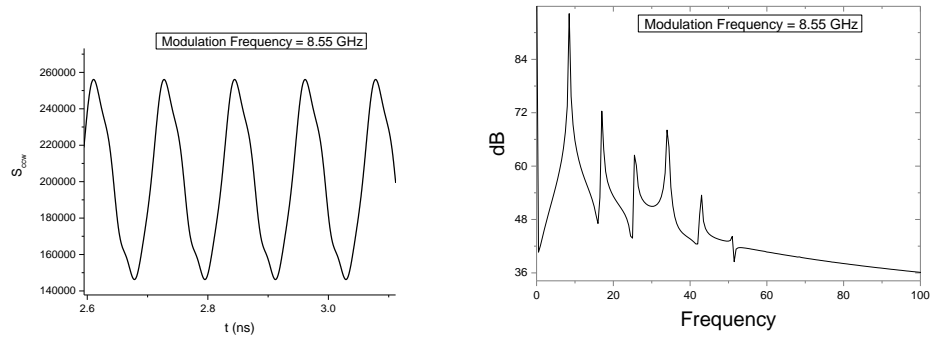
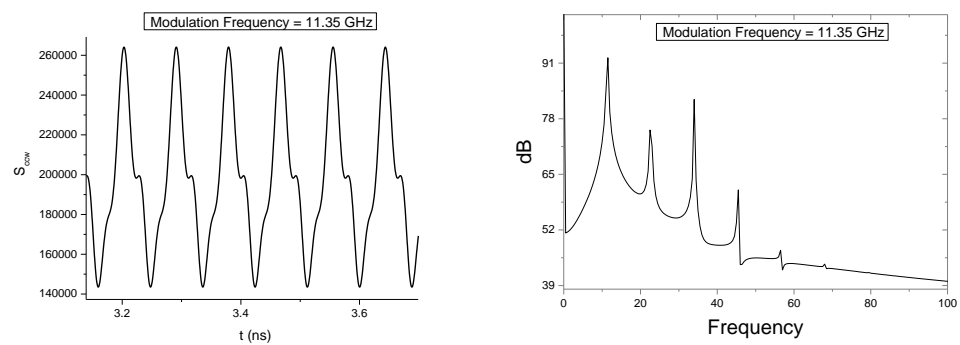


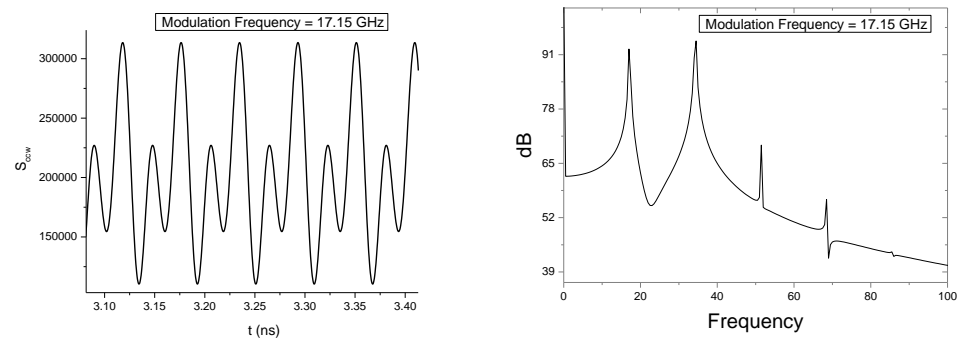
Fig. 4-27. Modulation frequency response of weak-injection scheme of Fig. 4-1b under 34 GHz negative detuning calculated for several values modulation depth. Modulation frequency response is normalized to low-frequency response of the free-running ring laser. $I_m = 12 \text{ mA}$, $I_r = 6 \text{ mA}$.



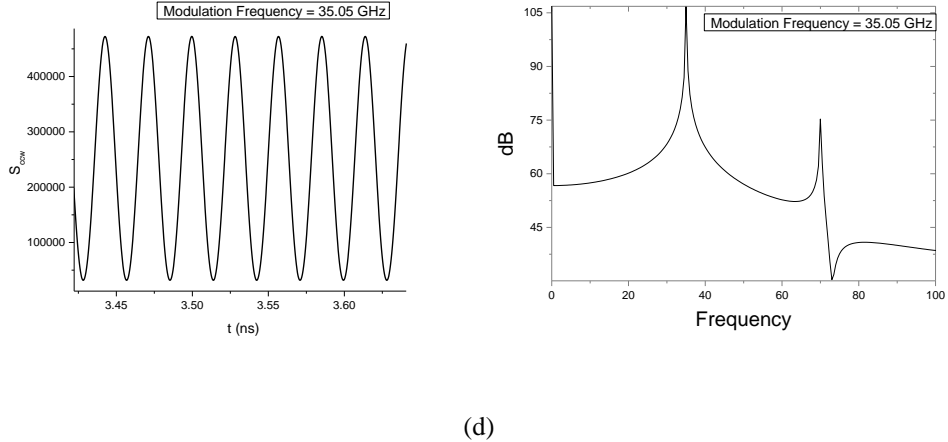
(a)



(b)



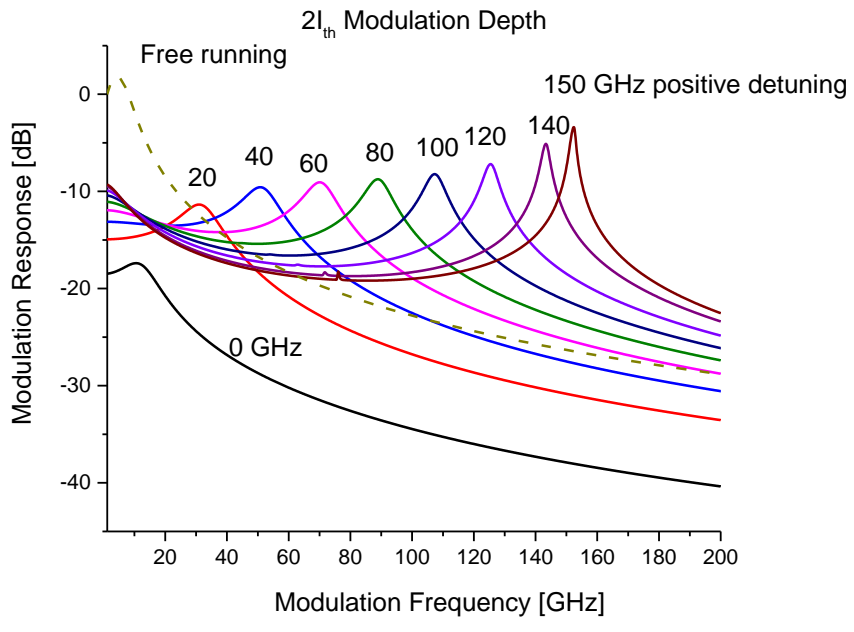
(c)



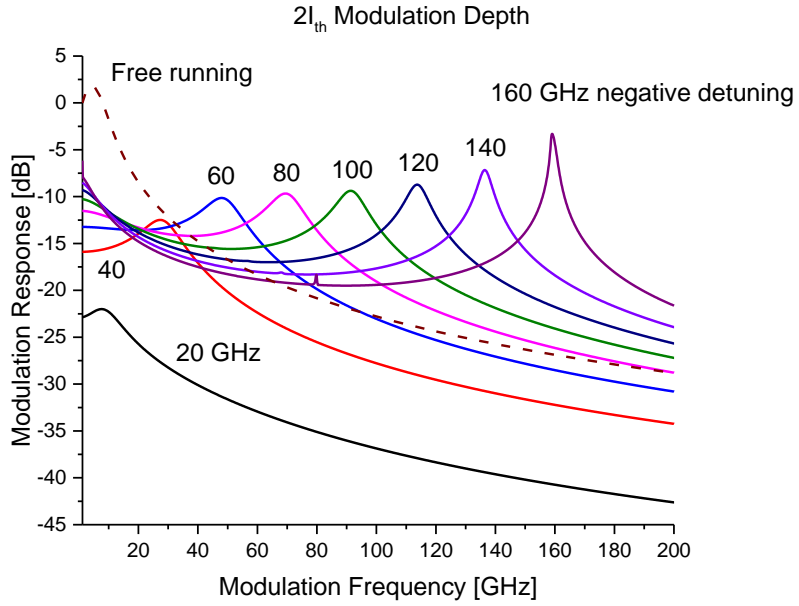
(d)

Fig. 4-28. Waveforms (left) and their fourier transforms (right) of photon number in CCW mode (S_{ccw}) of weak-injection scheme of Fig. 4-1b under 30 GHz positive detuning when the modulation frequency is around the subharmonic frequencies for (a) $m=4$, (b) $m=3$, (c) $m=2$, and when the modulation frequency is (d) near the resonance frequency.

For the strong injection scheme of Fig. 4-1a, the modulation response when $I_{or}\delta$ is equal to twice the threshold current is shown in Fig. 4-29. Similar to the weak-injection scheme, the resonance frequency increases with modulation depth under positive detuning (Fig. 4-30) and decreases under negative detuning (Fig. 4-31), and the resonance peak lowers with increasing modulation depth. Under strong injection, only the $m=2$ subharmonic stands out when the detuning approaches the boundary of stable locking range, though $m=3$ subharmonic still exists but is hardly noticeable, as illustrated in Fig. 4-30 for the case of 150 GHz positive detuning. The waveforms shown in Fig. 4-32 confirm that the interference between the modulation frequency and the resonance frequency is significant when the modulation frequency is around $m=2$ subharmonic.



(a)



(b)

Fig. 4-29. Large signal modulation frequency response of the free-running ring laser (dashed curves) and that of the injection-locked ring laser (strong-injection scheme of Fig. 4-1a) calculated for several values of (a) positive frequency detuning and (b) negative frequency detuning. Modulation frequency response is normalized to low-frequency response of the free-running ring laser. $I_m = 12 \text{ mA}$, $I_r = 6 \text{ mA}$.

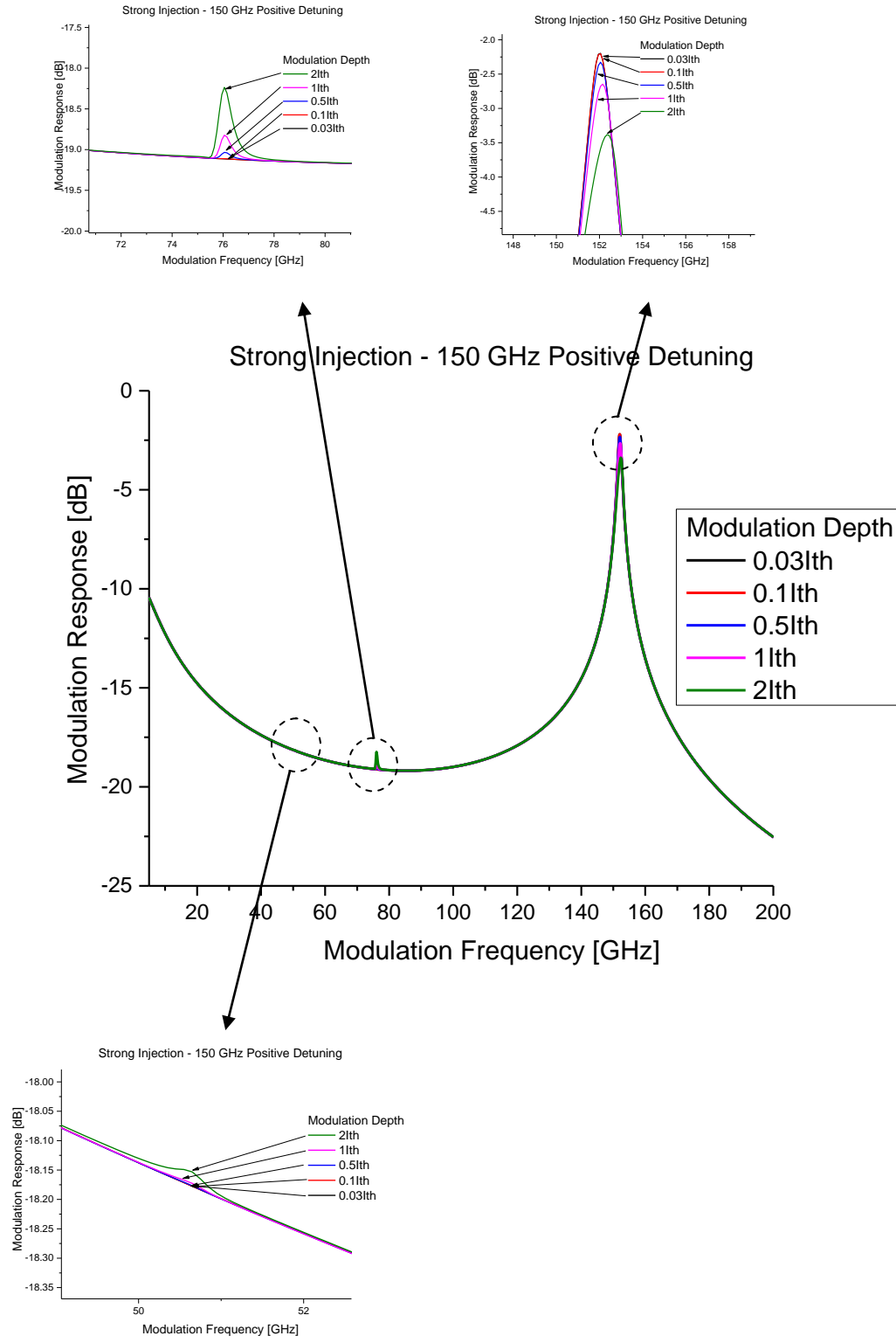


Fig. 4-30. Modulation frequency response of strong-injection scheme of Fig. 4-1a under 150 GHz positive detuning calculated for several values of modulation depth. Modulation frequency response is normalized to low-frequency response of the free-running ring laser. $I_m = 12$ mA, $I_r = 6$ mA.

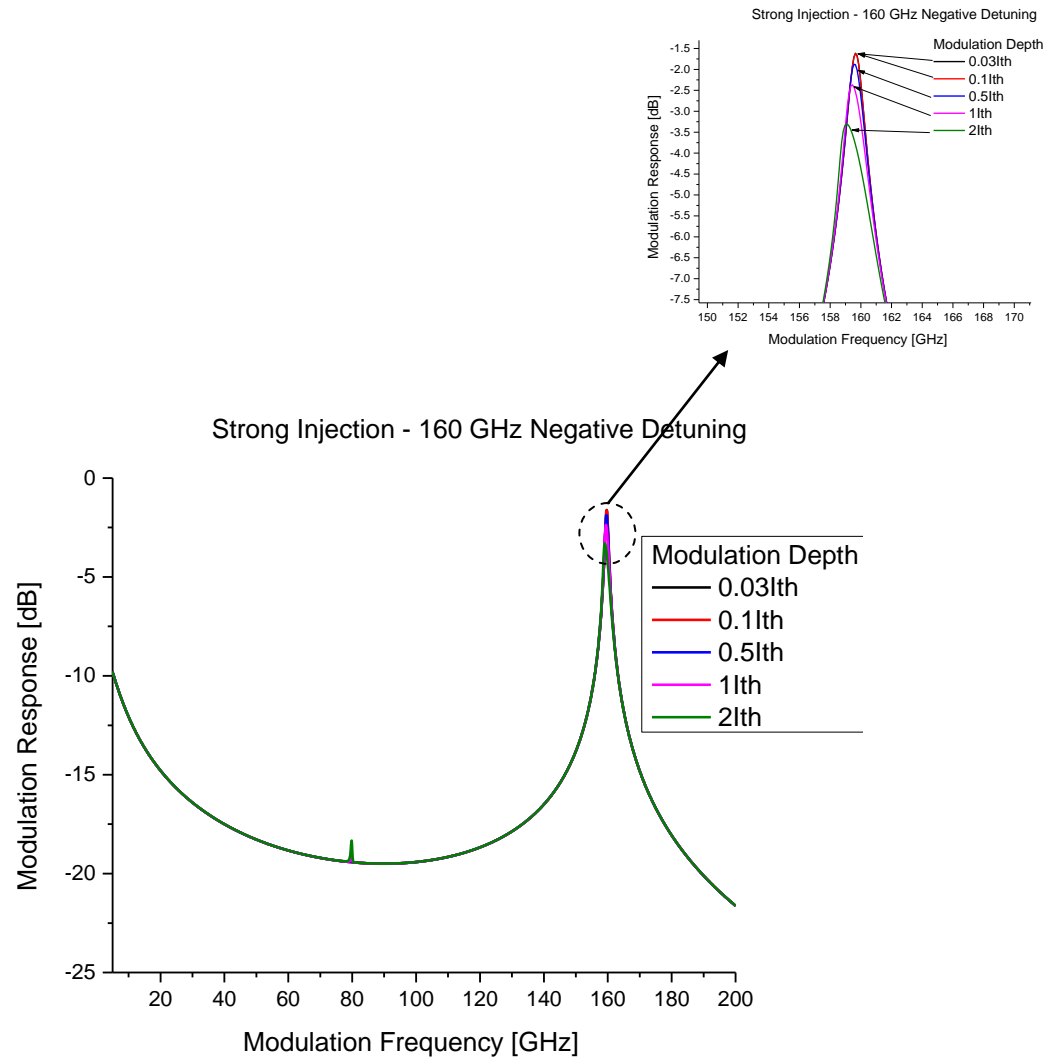
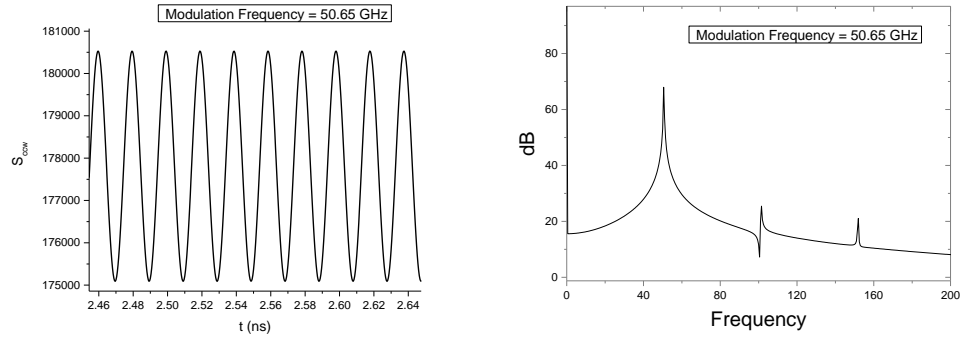
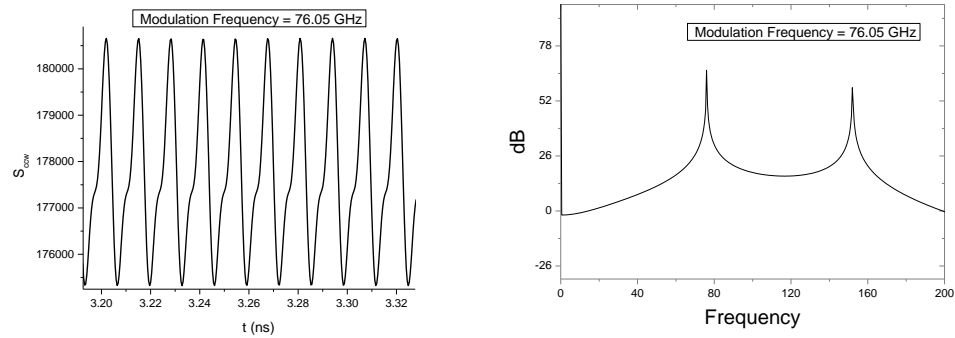


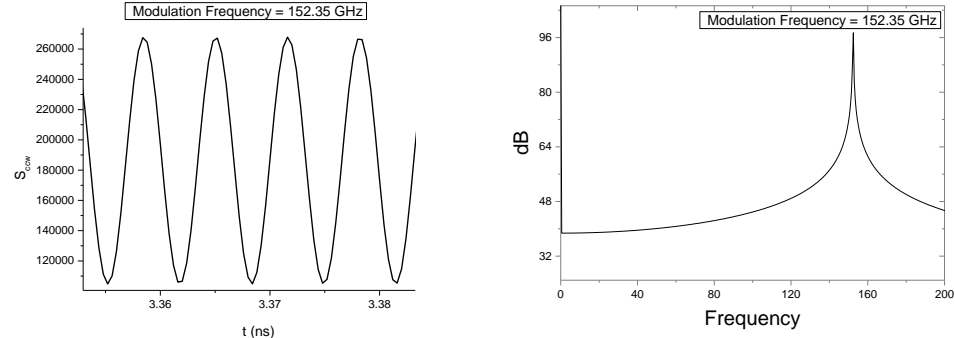
Fig. 4-31. Modulation frequency response of strong-injection scheme of Fig. 4-1a under 160 GHz negative detuning calculated for several values modulation depth. Modulation frequency response is normalized to low-frequency response of the free-running ring laser. $I_m = 12$ mA, $I_r = 6$ mA.



(a)



(b)



(c)

Fig. 4-32. Waveforms (left) and their fourier transforms (right) of photon number in CCW mode (S_{ccw}) of strong-injection scheme of Fig. 4-1a under 150 GHz positive detuning when the modulation frequency is around the subharmonic frequencies for (a) $m=3$, (b) $m=2$, and when the modulation frequency is (c) near the resonance frequency.

4.5 CONCLUSION

In conclusion, we have described a novel injection-locking scheme, involving DBR master laser monolithically integrated with a whistle-geometry microring laser for enhanced ultra-high-speed performance. The novel scheme allows for complete coupling of the master laser output into the ring laser, providing dramatically increased injection coupling rate as compared with the optical injection scheme based on a waveguide directional coupler adjacent to the ring laser. The advantage of the novel injection-locking scheme has been confirmed in numerical modeling by making direct comparison between the two schemes for optical injection under identical bias conditions. Greatly enhanced resonance frequency of up to ~ 160 GHz has been predicted in numerical calculations for the strongly injection-locked ring laser, which is almost five times the maximum resonance frequency attainable in the weak-injection scheme. Typical for all optical injection-locking schemes, the modulation response shows a very significant reduction in the modulation efficiency between low frequency and the resonance frequency, which limits the usefulness of the novel scheme to narrow-band applications. Two possible approaches to overcome the low-frequency roll-off problem and to attain tailorabile and broad modulation bandwidth will be discussed in the chapters that follow. The first is to use cascaded injection locking [Zhao 2007], which will be described in Chapter 5, and another approach, Q-modulation [Wang 2011], will be presented in Chapter 7.

Furthermore, the linear coupling between the two counterpropagating modes due to light backscattering was investigated and it has been found out that, depending on frequency detuning between the master and the ring laser, the strongly injection-locked

WRL can tolerate at least 1% or more of backscattering between the CCW and CW modes. Finally, large signal effects due to increase of the modulation depth up to twice the threshold current have been investigated.

CHAPTER 5

ANALYSIS OF HIGH-FREQUENCY MODULATION RESPONSE OF STRONGLY INJECTION-LOCKED CASCADED SEMICONDUCTOR RING LASERS

Typical for all optical injection-locking schemes, the modulation response showed a very significant reduction in the modulation efficiency between low frequency and the resonance frequency [Smolyakov 2011], which limits the usefulness of the novel scheme to narrow-band applications. One possible way to overcome the low-frequency roll-off problem and to attain tailorable and broad modulation bandwidth is to use cascaded injection locking [Zhao 2007]. Using that concept, we modified the injection-locking scheme to a cascaded system with two strongly injection-locked whistle-geometry unidirectional ring lasers (Fig. 5-1), where the modulated optical output of the first ring laser is used to injection-lock the second ring laser.

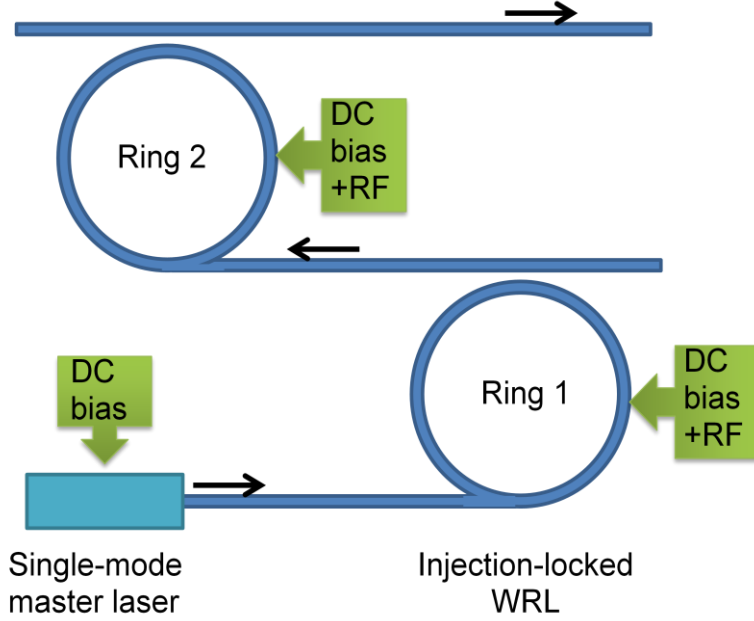


Fig. 5-1 Schematic diagram of two cascaded injection-locked whistle-geometry semiconductor ring lasers monolithically integrated with single-mode master DBR laser.

5.1 RATE EQUATIONS FOR CASCADED SCHEME

The dynamics of an optically injection-locked microring laser monolithically integrated with single-mode master DBR laser in the previous chapter was modeled by a system of rate equations written in terms of the photon numbers, phases, and total carrier numbers in the master DBR and microring slave lasers. The model can be extended for the case of cascaded injection locking (Fig. 5-1) by introducing five additional rate equations describing the dynamics of the second ring laser. Adopting subscripts 1 and 2 to refer to the first ring and the second ring lasers, respectively, we can write the following system of equations:

$$\frac{dS_m}{dt} = \left[G_{0m}(N_m - N_{0m}) - \frac{1}{\tau_p^m} \right] S_m + R_{sp} \quad (5-1)$$

$$\frac{d\theta_m}{dt} = \frac{\alpha}{2} \left[G_{0m}(N_m - N_{0m}) - \frac{1}{\tau_p^m} \right] \quad (5-2)$$

$$\frac{dN_m}{dt} = \eta_i \frac{I_m}{q} - \frac{N_m}{\tau_c} - G_{0m}(N_m - N_{0m})S_m \quad (5-3)$$

$$\frac{dS_{ccw1}}{dt} = \left[G_{ccw1} - \frac{1}{\tau_p^{ccw1}} \right] S_{ccw1} + R_{sp} + 2k_{c1} \sqrt{S_m S_{ccw1}} \cos(\theta_{ccw1} - \theta_m) \quad (5-4)$$

$$\frac{d\theta_{ccw1}}{dt} = \frac{\alpha}{2} \left[G_{ccw1} - \frac{1}{\tau_p^{ccw1}} \right] - (\omega_{01} - \omega_{th1}) - k_{c1} \sqrt{\frac{S_m}{S_{ccw1}}} \sin(\theta_{ccw1} - \theta_m) \quad (5-5)$$

$$\frac{dS_{cw1}}{dt} = \left[G_{cw1} - \frac{1}{\tau_p^{cw1}} \right] S_{cw1} + R_{sp} \quad (5-6)$$

$$\frac{d\theta_{cw1}}{dt} = \frac{\alpha}{2} \left[G_{cw1} - \frac{1}{\tau_p^{cw1}} \right] - (\omega_{01} - \omega_{th1}) \quad (5-7)$$

$$\frac{dN_{r1}}{dt} = \eta_i \frac{I_{r1}}{q} - \frac{N_{r1}}{\tau_c} - G_{cw1} S_{cw1} - G_{ccw1} S_{ccw1} \quad (5-8)$$

$$\frac{dS_{ccw2}}{dt} = \left[G_{ccw2} - \frac{1}{\tau_p^{ccw2}} \right] S_{ccw2} + R_{sp} \quad (5-9)$$

$$\frac{d\theta_{ccw2}}{dt} = \frac{\alpha}{2} \left[G_{ccw2} - \frac{1}{\tau_p^{ccw2}} \right] - (\omega_{02} - \omega_{th2}) \quad (5-10)$$

$$\frac{dS_{cw2}}{dt} = \left[G_{cw2} - \frac{1}{\tau_p^{cw2}} \right] S_{cw2} + R_{sp} + 2k_{c2} \sqrt{S_{ccw1} S_{cw2}} \cos(\theta_{cw2} - \theta_{ccw1}) \quad (5-11)$$

$$\frac{d\theta_{cw2}}{dt} = \frac{\alpha}{2} \left[G_{cw2} - \frac{1}{\tau_p^{cw2}} \right] - (\omega_{02} - \omega_{th2}) - k_{c2} \sqrt{\frac{S_{ccw1}}{S_{cw2}}} \sin(\theta_{cw2} - \theta_{ccw1}) \quad (5-12)$$

$$\frac{dN_{r2}}{dt} = \eta_i \frac{I_{r2}}{q} - \frac{N_{r2}}{\tau_c} - G_{cw2} S_{cw2} - G_{ccw2} S_{ccw2} \quad (5-13)$$

Eqs. (5-1) - (5-8) are identical (other than the subscript 1 in eqs. (5-4) - (5-8) denoting the parameters of the first ring laser) to the ones used in the previous chapter for injection locking of a single ring laser, with the same definitions for all the parameters used. Optical injection from the master laser into the CCW mode of the first ring laser and that from the CCW mode of the first ring laser into the CW mode of the second ring laser is accounted for by appropriate terms in Eqs. (5-4), (5-5), (5-11), and (5-12) that contain the injection coupling rates κ_{c1} and κ_{c2} . We again allow for unequal photon lifetimes $\tau_p^{cw1} \neq \tau_p^{ccw1}$, and $\tau_p^{cw2} \neq \tau_p^{ccw2}$ for the CW and CCW modes of the first and second ring lasers, respectively. Other parameters in Eqs. (5-4) – (5-13) are the mode frequency of the ring cavity $\omega_{01,2}$, and the free-running mode frequency of the ring cavity at threshold $\omega_{th01,2}$ for the first and second ring lasers, correspondingly. Under stable injection-locking conditions, $\omega_{01} - \omega_{th1}$ and $\omega_{02} - \omega_{th2}$ terms in Eq. (5-7) and Eq. (5-10) were set equal to zero in the calculations for the CW mode of the first ring cavity and the CCW mode of the second ring cavity that stay below threshold, whereas ω_{01} in Eq. (5-5) and ω_{02} in Eq. (5-12) are locked to the frequency of the master laser, and those terms effectively represent the angular frequency detunings $\Delta\omega_1$ and $\Delta\omega_2$ between the master

laser and the first and second ring lasers, respectively. In the calculations, $\Delta\omega_1$ and $\Delta\omega_2$ were treated as independent parameters. Ring lasers of the same diameter and active region volume $V_{r1} = V_{r2}$, as well as identical transparency carrier density for the master laser and the two ring lasers were assumed in the modeling, that is $N_{0m}/V_m = N_{0r1}/V_{r1} = N_{0r2}/V_{r2}$.

As with the simulation of injection locking of a single ring laser, all mechanisms that could possibly lead to feedback from the first ring laser to the master laser, and from the second ring laser to the first ring laser are neglected for the same reasons described in Chapter 4.

The same material parameters for 1.55- μm InGaAs/AlGaInAs/InP MQW deeply etched ridge-waveguide laser structure are assumed in the simulation. The coupling rate for injection into the second ring laser κ_{c2} was calculated as

$$\kappa_{c2} = \frac{c\sqrt{T_r}}{\pi n_{\text{eff}2} d}, \quad (5-14)$$

where d is the ring laser diameter, $n_{\text{eff}2}$ is the modal effective index, and T_r represents the power transmission coefficient at the output of the directional coupler. Assuming that 5% of the light goes from the first into the second ring laser, that is $T_r = 0.05$, we calculated the value for κ_{c2} as $\kappa_{c2} = 3.25 \times 10^{11} \text{ s}^{-1}$.

5.2 SIMULATION RESULTS

With the cascaded injection-locking scheme of Fig. 5-1 being an extension of that of Fig. 4-1b, we can rely in our simulations on the previous results of high-speed modulation analysis of strongly injection-locked single WRL that are presented in Chapter 4. For the purpose of comparison between the two injection-locking schemes, simulations of steady-state characteristics and high-frequency modulation response of the second ring laser in the cascaded injection-locking scheme of Fig. 5-1 have been carried out for the same configuration and under the same bias conditions that were assumed in Chapter 4 for the master and the ring lasers. Master laser bias of 12 mA and ring laser bias of 6 mA at $3I_{th}$ for both ring lasers were consistently chosen throughout the simulations. The results from Chapter 4 are thus fully applicable to the first ring laser in the cascaded injection-locking scheme, and no separate analysis is required for that laser. One of the most important observations in Chapter 4 was that the very high injection coupling rate in WRL configuration (κ_{cl} in present notation) results in a very wide range for stable injection locking of the ring laser. The first ring laser in the cascaded injection-locking scheme remains stably locked by the master in a very wide range of the frequency detuning $-165 \text{ GHz} < \Delta\omega_1 < 160 \text{ GHz}$. In this set of calculations the frequency detuning $\Delta\omega_1$ between the master DBR laser and the first ring laser was kept constant and positive at 100 GHz, while the frequency detuning $\Delta\omega_2$ between the master DBR laser and the second ring laser was varied.

Fig. 5-2 illustrates the effect of optical injection from the first ring laser (locked by the master at $\Delta\omega_1 = 100 \text{ GHz}$) into the second ring laser by showing evolution of the photon number in the CW mode and carrier number in the second ring laser with

increasing injection coupling rate κ_{c2} for zero frequency detuning $\Delta\omega_2$ between the master and the second ring laser. As the coupling rate κ_{c2} increases, one can see the carrier number very rapidly being depleted by the external injected light, while significant intensity builds up in the CW mode of the second injection-locked ring laser. This confirms that conditions of strong injection locking are also attainable for the second injection-locked ring laser in the cascaded injection-locking scheme.

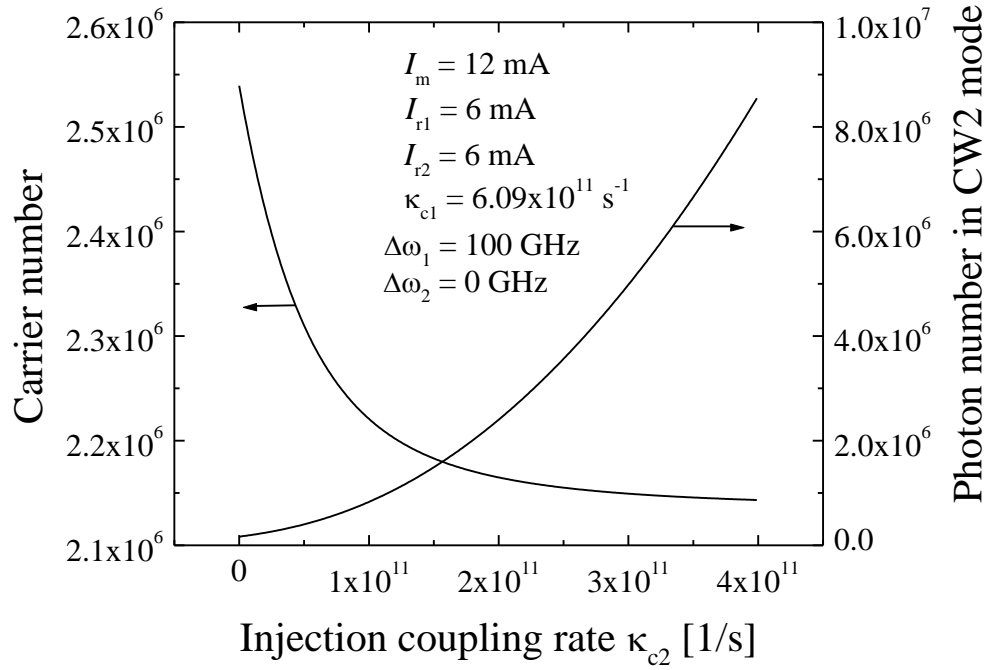


Fig. 5-2. Carrier number and photon number in the CW mode of the second injection-locked whistler ring laser as a function of injection coupling rate κ_{c2} calculated for the cascaded injection-locking scheme under steady-state conditions.

The stable injection-locking range obtained for the second ring laser is shown in Fig. 5-3 in terms of the photon number in the CW mode of the second ring laser versus the frequency detuning $\Delta\omega_2$ between the master laser and the second ring laser. The stable locking range obtained for the second ring laser in the cascaded injection-locking scheme is not as wide as that obtained for the first ring laser injection-locked directly by the master laser. On the positive detuning side, the stable continuous laser output is observed up to ~ 75.4 GHz, with onset of oscillations beyond this positive detuning edge. On the negative detuning side, the stable continuous laser output is maintained up to ~ 81.4 GHz. It is worth noting that all over the entire stable locking range the CCW mode of the second ring laser stays suppressed. The CW mode of the second ring laser stays locked even when the phase offset $\theta_{cw2} - \theta_{ccw1}$ between the CW mode of the second ring laser and the CCW mode of the first ring laser goes slightly out of $[-\pi/2; \pi/2]$ range at the edges of the stable locking range (Fig. 5-4). Both the maximum of the photon number in the CW mode of the second ring laser (Fig. 5-3) and the minimum of the carrier number (Fig. 5-5) are reached at the negative frequency detuning of $\Delta\omega_2 \sim 11.8$ GHz, which corresponds to zero phase offset $\theta_{cw2} - \theta_{ccw1}$ between the first ring laser and the second ring laser (Fig. 5-4), that is to the strongest injection-locking conditions.

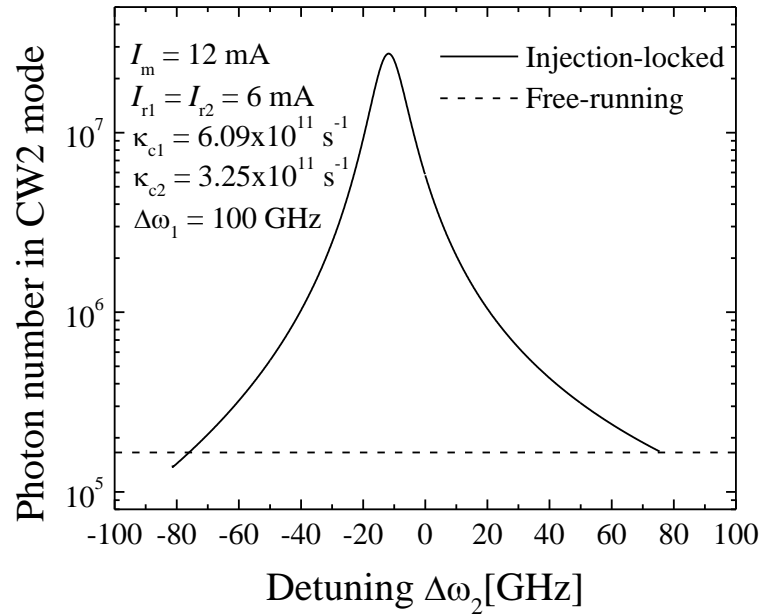


Fig. 5-3. Photon number in the CW mode of the second injection-locked WRL versus frequency detuning $\Delta\omega_2$ calculated for the cascaded injection-locking scheme under steady-state conditions.

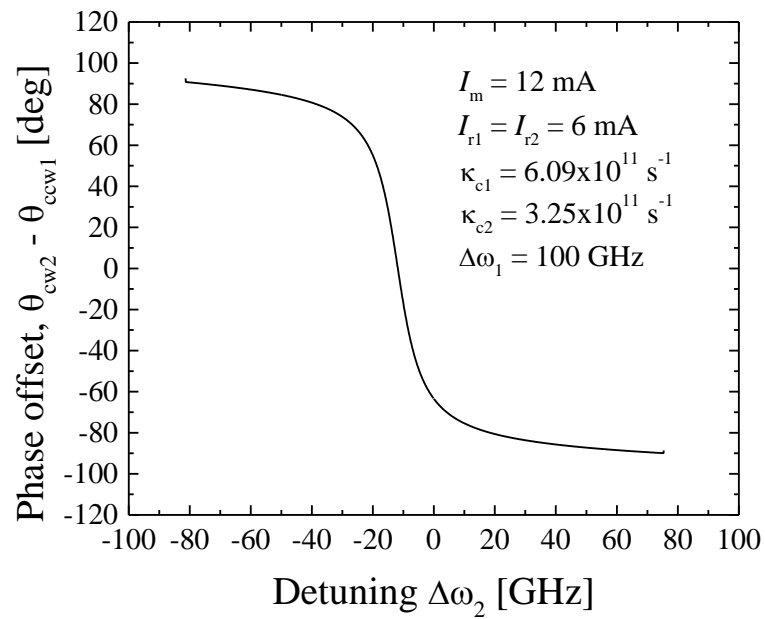


Fig. 5-4. Optical phase offset between the CW mode of the second injection-locked WRL and the CCW mode of the first injection-locked WRL versus frequency detuning $\Delta\omega_2$ calculated for the cascaded injection-locking scheme under steady-state conditions.

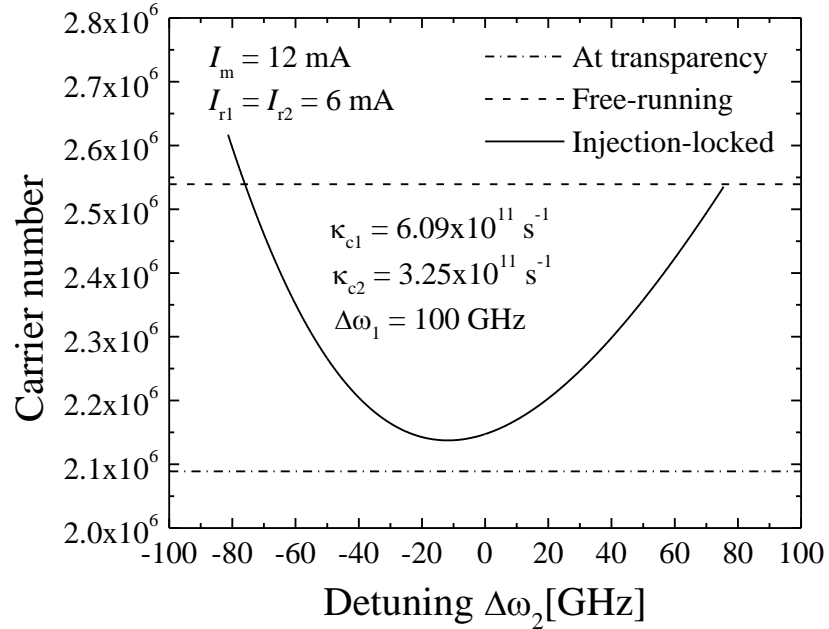


Fig. 5-5. Carrier number in the second injection-locked WRL versus frequency detuning $\Delta\omega_2$ calculated for the cascaded injection-locking scheme under steady-state conditions.

In the modulation response simulations, a small-signal modulation was applied to the first ring laser injection current I_{r1} of Eq. (5-8) in the form

$$I_{r1} = I_{0r1} [1 + \delta \sin(2\pi f t)], \quad (5-15)$$

where I_{0r1} is the injection current at a constant ring laser bias, f is the modulation frequency, and δ is the modulation depth. One percent modulation depth for the injection current ($\delta = 0.01$) was assumed throughout the simulations. With the modulation signal applied to the first ring laser, the modulated optical output is injected into the second ring laser. The calculated results for modulation response are presented in terms of the corresponding modulation depth in the photon number in the CW mode of the second ring laser versus modulation frequency.

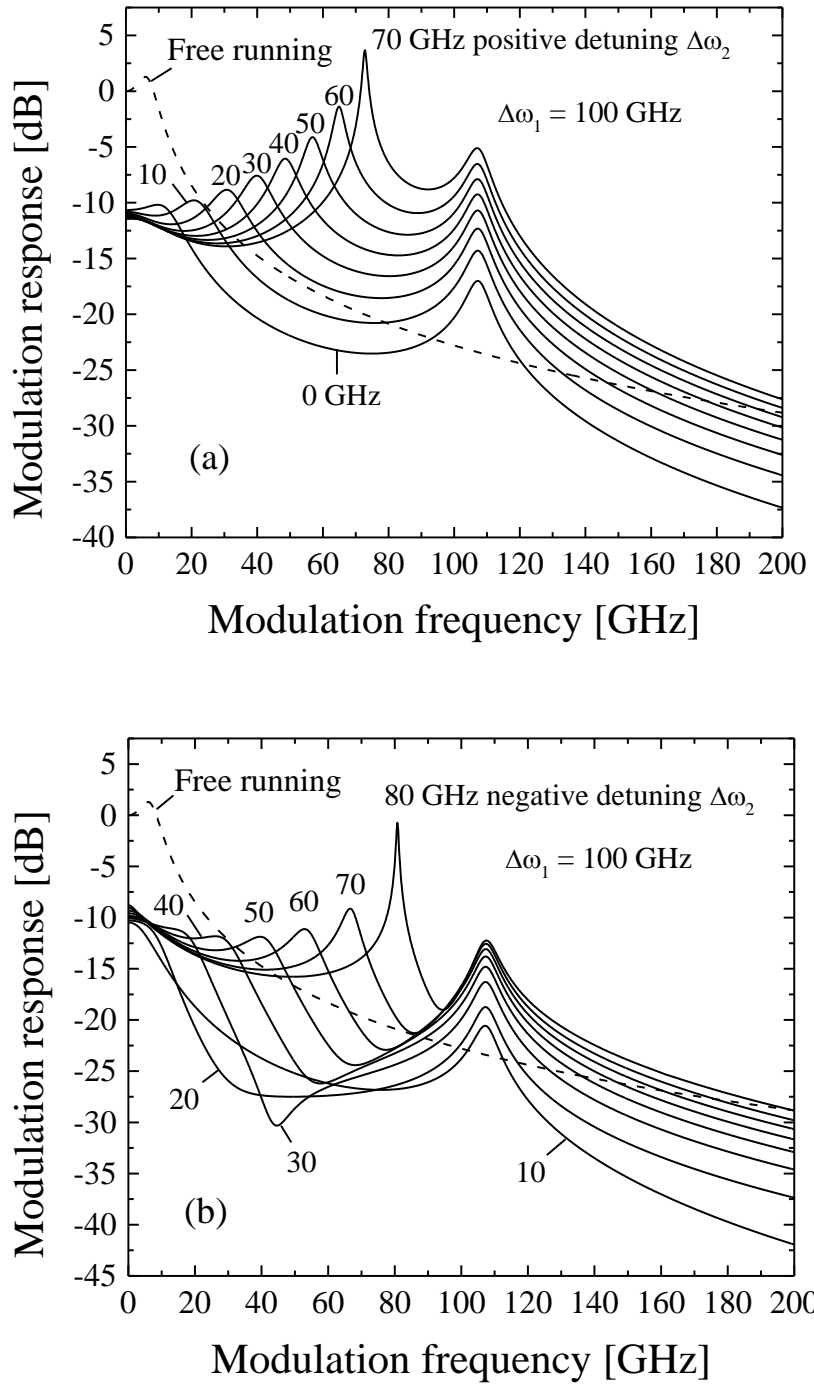


Fig. 5-6. Modulation frequency response of the free-running WRL (dashed curves) and that of the second injection-locked WRL (cascaded injection-locking scheme of Fig. 5-1) calculated for several values of (a) positive frequency detuning $\Delta\omega_2$ and (b) negative frequency detuning $\Delta\omega_2$. Modulation frequency response is normalized to low-frequency response of the free-running ring laser. $I_m = 12$ mA, $I_{rl} = I_{r2} = 6$ mA, $\Delta\omega_1 = 100$ GHz.

Fig. 5-6 shows modulation frequency response of the free-running ring laser and that of the second ring laser in the cascaded injection-locking scheme of Fig. 5-1, calculated for several positive and negative values of frequency detuning $\Delta\omega_2$. For comparison, modulation frequency response in each case is normalized to the low frequency response of the free-running laser. One can clearly see further enhancement of the modulation response as the second resonance peak occurring at a lower modulation frequency corresponding to the frequency detuning $\Delta\omega_2$ between the master and the second ring laser. Comparison between the two sets of calculated modulation response for negative and positive frequency detuning identifies positive frequency detuning $\Delta\omega_2$ as more adequate for tailoring the modulation response and getting significant enhancement of the modulation bandwidth.

In order to illustrate further improvement in the modulation response of the cascaded injection-locking scheme of Fig. 5-1 as compared to that of the injection-locking scheme of Fig. 4-1a, we show in Fig. 5-7 the modulation response calculated for the two injection-locking schemes under identical bias conditions at frequency detunings $\Delta\omega_1 = 100$ GHz and $\Delta\omega_2 = 50$ GHz between the master and the first and the second ring lasers, respectively. The modulation response in both cases is normalized to the low-frequency response of the injection-locking scheme of Fig. 4-1a. Obvious improvement is seen in the modulation response of the cascaded injection-locking scheme, showing 3-dB modulation bandwidth of ~ 117 GHz, as compared to that of ~ 17.3 GHz obtained for the injection locking with single ring laser.

As it was pointed out in [Zhao 2007], for an integrated device, the modulation signal can be applied simultaneously to all the slave lasers in the cascaded injection-locking scheme, thus providing equal distribution of the RF signal to all the devices. We tested this possibility for modulation efficiency enhancement in numerical modeling by applying injection current modulation in the form (5-15) to both the first ring laser injection current I_{r1} of Eq. (5-8) and to the second ring laser injection current I_{r2} of Eq. (5-13). As one can see in Fig. 5-8, with the second ring laser being effectively modulated both optically and through the injection current, its modulation response is further enhanced as evidenced by the more pronounced resonance peak at modulation frequency corresponding to the frequency detuning $\Delta\omega_2$ between the master and the second ring laser. Increased low-frequency modulation response is also obvious in Fig. 5-8 when compared to that of Fig. 5-6. We illustrate this improvement in the modulation response of the cascaded injection-locking scheme more clearly in Fig. 5-9 by showing the modulation response calculated for specific bias and frequency detuning conditions in two situations: (i) modulation signal is applied to the first ring laser only; (ii) modulation signal is applied to both the first and the second ring lasers. Modulation response in both cases is normalized to the low-frequency response of the free-running ring laser.

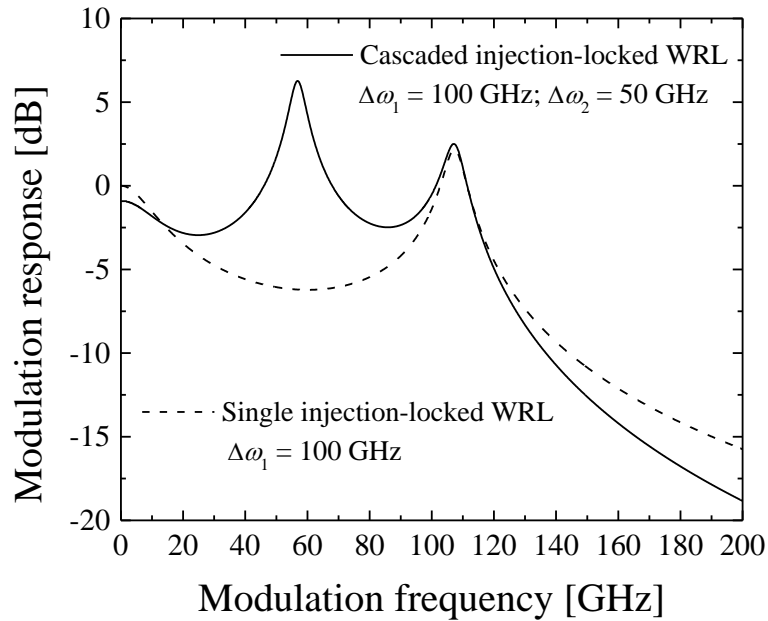


Fig. 5-7. Modulation frequency response of the second injection-locked WRL in the cascaded injection-locking scheme of Fig. 5-1 (solid curve: positive frequency detunings $\Delta\omega_1 = 100$ GHz and $\Delta\omega_2 = 50$ GHz) and that of the injection-locked WRL in the injection-locking scheme of Fig. 4-1a (dashed curve: positive frequency detuning $\Delta\omega_1 = 100$ GHz), calculated under identical bias conditions: $I_m = 12$ mA, $I_{r1} = I_{r2} = 6$ mA. Modulation frequency response is normalized to the low-frequency response of the WRL in the injection-locking scheme of Fig. 4-1a.

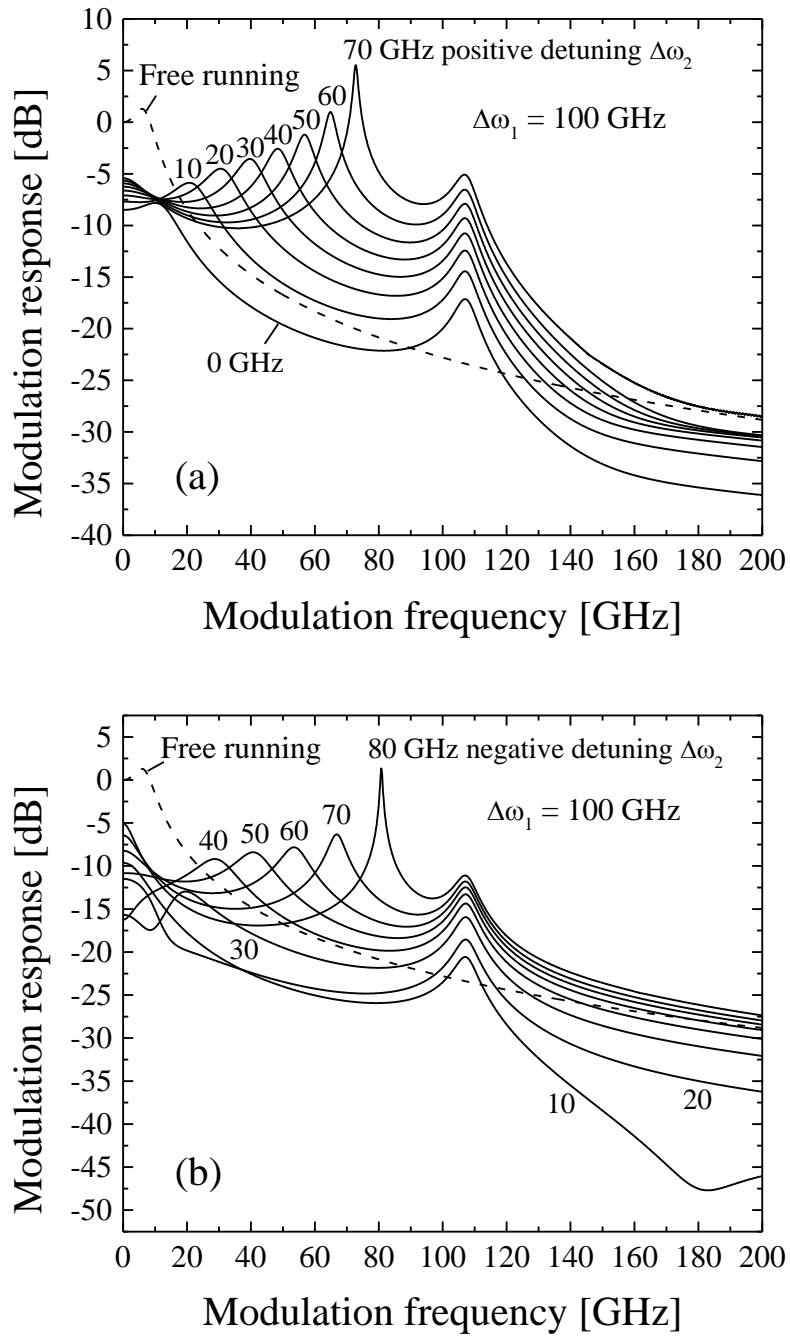


Fig. 5-8. Modulation frequency response of the free-running WRL (dashed curves) and that of the second injection-locked WRL (cascaded injection-locking scheme of Fig. 5-4) calculated for several values of (a) positive frequency detuning $\Delta\omega_2$ and (b) negative frequency detuning $\Delta\omega_2$. Modulation signal is applied to both the first and second injection-locked WRLs. Modulation frequency response is normalized to low-frequency response of the free-running ring laser. $I_m = 12$ mA, $I_{rl} = I_{r2} = 6$ mA, $\Delta\omega_1 = 100$ GHz.

Finally, we verified (Fig. 5-10) that applying injection current modulation to the second injection-locked WRL only in the cascaded injection-locking scheme of Fig. 5-1 would not result in any improvement as compared to the modulation response of the injection-locking scheme of Fig. 4-1a.

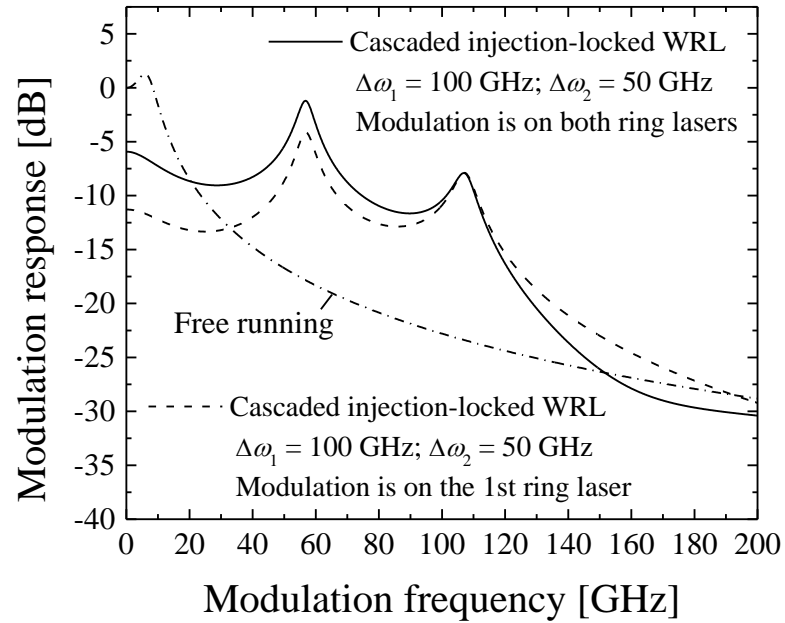


Fig. 5-9. Modulation frequency response of the second injection-locked WRL in the cascaded injection-locking scheme of Fig. 5-1, calculated for positive frequency detunings $\Delta\omega_1 = 100$ GHz and $\Delta\omega_2 = 50$ GHz under bias conditions $I_m = 12$ mA, $I_{r1} = I_{r2} = 6$ mA. Dashed curve: modulation signal is applied to the first WRL. Solid curve: modulation signal is applied to both the first and second injection-locked WRLs. Modulation frequency response is normalized to the low-frequency response of the free-running ring laser.

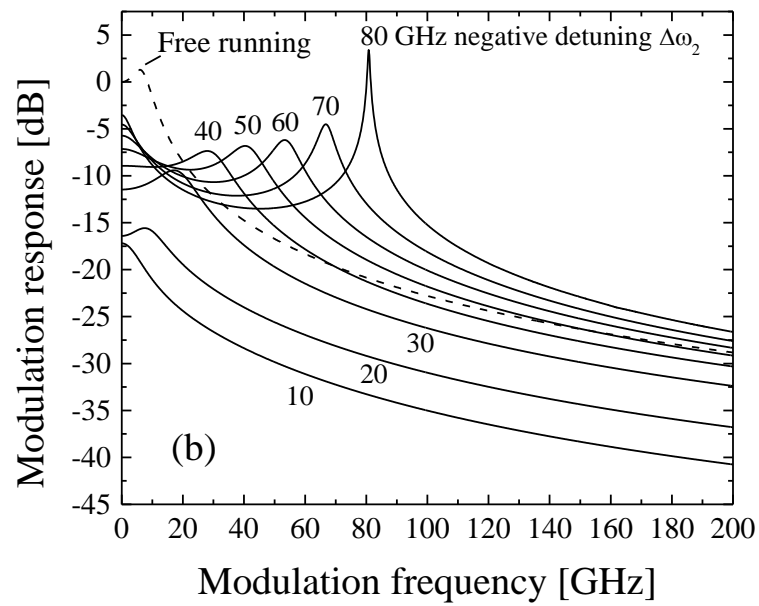
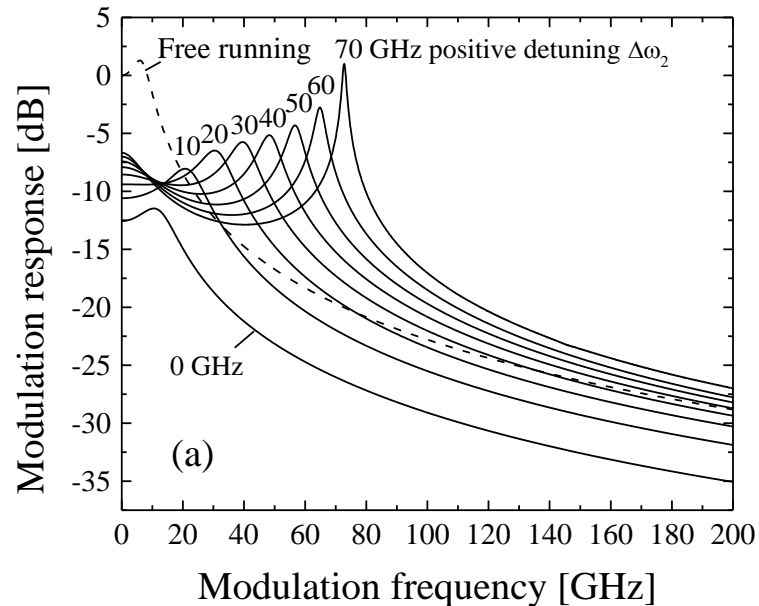


Fig. 5-10. Modulation frequency response of the free-running WRL (dashed curves) and that of the second injection-locked WRL (cascaded injection-locking scheme of Fig. 5-1) calculated for several values of (a) positive frequency detuning $\Delta\omega_2$ and (b) negative frequency detuning $\Delta\omega_2$. Modulation signal is applied to the second injection-locked WRL. Modulation frequency response is normalized to low-frequency response of the free-running ring laser. $I_m = 12$ mA, $I_{r1} = I_{r2} = 6$ mA, $\Delta\omega_1 = 100$ GHz.

5.3 CONCLUSION

A novel injection-locking scheme, involving DBR master laser monolithically integrated with a whistle-geometry microring laser for enhanced ultrahigh- speed performance was proposed in Chapter 4, which is expected to allow for strong coupling of the master laser output into the ring laser, providing dramatically increased injection coupling rate and hence a greatly enhanced resonance frequency of up to ~ 160 GHz. However, the modulation response showed a very significant reduction in the modulation efficiency between low frequency and the resonance frequency, which limits the usefulness of the novel scheme to narrow-band applications [Chrostowski 2008]. In this chapter, the possibility to overcome the low-frequency roll-off problem and to attain tailororable and broad modulation bandwidth has been demonstrated in numerical modeling of the high-frequency modulation response of the cascaded strongly injection-locked whistle-geometry semiconductor ring lasers. Further improvement is expected to come from utilizing injection-locking scheme with multiple cascaded ring lasers that should result in flat broadband modulation response.

CHAPTER 6

FREQUENCY CHIRP IN STRONGLY INJECTION-LOCKED SEMICONDUCTOR RING LASERS

The frequency chirping performance of strongly injection-locked ring lasers is investigated with rate-equation-based simulations. In the case of injection-locking a single ring, the proposed whistle-geometry for strong injection shows dramatic reduction in chirp-to-power ratio compared to the configuration of weak injection with a bus waveguide. Furthermore, when two ring lasers are cascaded, with the output of the first injection-locked ring laser injection-locking the second ring laser, the chirp-to-power ratio becomes negligible over a wide frequency range at zero frequency detuning between the second ring laser and the maser laser.

6.1 INTRODUCTION

One of the techniques to simultaneously increase the modulation bandwidth and reduce the frequency chirp is injection locking [Lau 2009], [Tartarini 2007]. In this chapter, we extend the numerical analyses of injection-locked semiconductor ring lasers from previous chapters to include the frequency chirp performance of the three schemes to verify that superior high-speed performance can be achieved with the proposed whistle-geometry ring lasers. The three configurations considered are the weak injection of ring laser through a direction coupler (Fig. 4-1b), strong injection of a ring laser (Fig.

4-1a), and strong injection of cascaded ring lasers (Fig. 5-1). In the case of injection-locking a single ring, the proposed whistle geometry for strong injection shows dramatic reduction in chirp-to-power ratio compared to the configuration of weak injection with a bus waveguide. Furthermore, when two ring lasers are cascaded, with the output of the first injection-locked ring laser injection-locking the second ring laser, the chirp-to-power ratio becomes negligible over a wide frequency range at zero frequency detuning between the two ring lasers. Together with the results presented in the previous chapters, these simulations confirm that the proposed whistle-geometry ring lasers provide, especially when modulation signal is applied to both ring lasers in the cascaded scheme, improved performance in terms of modulation response and frequency chirp, and more flexibility for the design of ultra-high speed transmitters.

6.2 FREQUENCY CHIRP OF SEMICONDUCTOR LASERS UNDER STRONG INJECTION LOCKING

The frequency chirping of a semiconductor laser is usually characterized experimentally and theoretically by the chirp-to-modulated-power ratio (CPR). Chen et al. derived a closed-form solution of CPR for the condition of strong injection-locking as [Ohtsubo 2013], [Chen 2000]:

$$CPR \approx f_m \alpha \sqrt{\frac{f_m^2 + (u - v/\alpha)^2}{f_m^2 + (u + v/\alpha)^2}}, \quad (6-1)$$

with

$$u = \frac{\kappa_c}{2\pi\tau_{rt}} \sqrt{\frac{S_m}{S_s}} \cos(\theta_s - \theta_m) \quad , \text{ and } v = \frac{\kappa_c}{2\pi\tau_{rt}} \sqrt{\frac{S_m}{S_s}} \sin(\theta_s - \theta_m), \quad (6-2)$$

where f_m is the modulation frequency, α is the linewidth enhancement factor, κ_c is the coupling coefficient, τ_{rt} is the roundtrip time inside the slave laser cavity, S_m and S_s are the photon number of the master and slave laser, and θ_m and θ_s are the phase of the master and slave laser field respectively.

Under free-running condition, CPR increases linearly with the modulation frequency [Koch 1984], and according to Eq. (6-1) can be approximated by $f_m\alpha$. With injection-locking, the phase difference ($\theta_s - \theta_m$) and the ratio of photon numbers S_m/S_s between the master and the slave lasers are functions of the detuning frequency [Smolyakov 2011], [Smolyakov 2012] and hence the dependence becomes sublinear for a single ring laser and nonlinear for the cascaded configuration as the results in the next section indicate.

6.3 NUMERICAL SIMULATION OF FREQUENCY CHIRP BASED ON RATE EQUATIONS

The sets of coupled nonlinear differential equations, the numerical values of all the parameters, and the detailed references, considerations and derivations of those parameters, as well as the results of frequency modulation response for the weak-, strong- and cascaded injection schemes, can be found in Chapter 4 and Chapter 5. With the solutions of the rate equations, the frequency chirp and CPR can be readily derived using [Shen 1986]:

$$\Delta\nu = \frac{1}{2\pi} \frac{d\theta_s}{dt}, \text{ and} \quad (6-3)$$

$$CPR = \frac{\max|d\theta_s / dt|}{\Delta p}, \text{ respectively,} \quad (6-4)$$

where, Δp is the modulated output power of the slave laser.

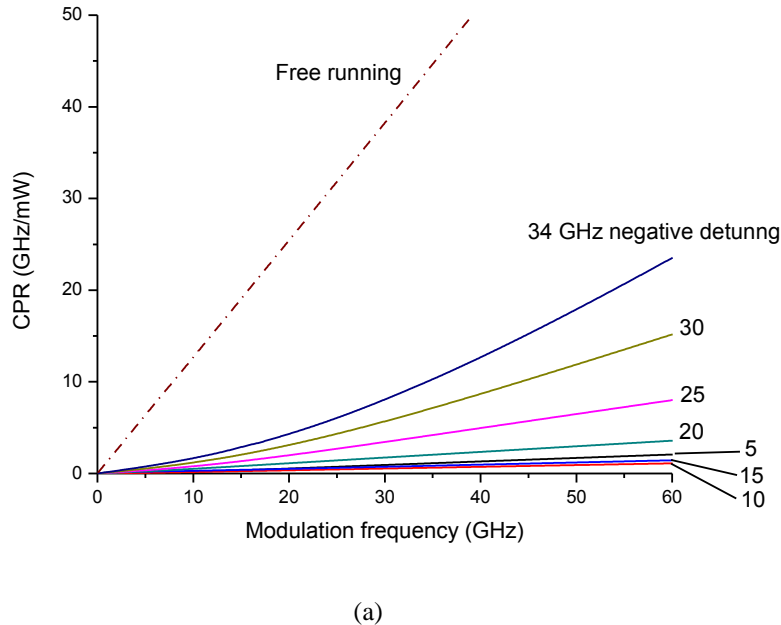
A. Weak Injection-Locking

The CPR curves calculated for the weak injection-locking configuration illustrated in Fig. 4-1b, with a stable locking range from 35 GHz negative detuning to 31.4 GHz positive detuning, are shown in Fig. 6-1 for both negative and positive detuning. Significant reduction in CPR compared to the free-running ring laser is observed, with the curves showing linear dependence on the modulation frequency for small detuning and sublinear dependence for large detuning. The 10 GHz negative detuning, which is the closest to the frequency detuning (~ 11.5 GHz) with zero optical phase offset between the master laser and the CCW mode of the ring laser, corresponds to the lowest CPR.

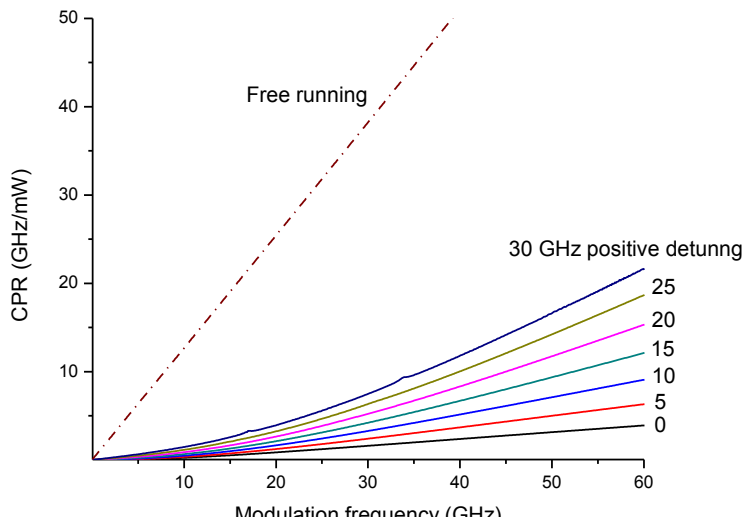
B. Strong Injection-Locking

When the ring laser is strongly injection-locked, with the proposed configuration shown in Fig. 4-1a, CPR shows further reduction and the curves remain sublinear (Fig. 6-2). For a numerical comparison, at 30 GHz of modulation frequency, the CPR is 0.54 GHz/mW at 10 GHz negative detuning in the weak-injection case and 0.08 GHz/mW at

20 GHz negative detuning in the strong-injection case. It is worth noting that lower CPR can be obtained when the negative frequency detuning approaches 11.9 GHz where the phase offset between the master and the slave lasers is close to zero.

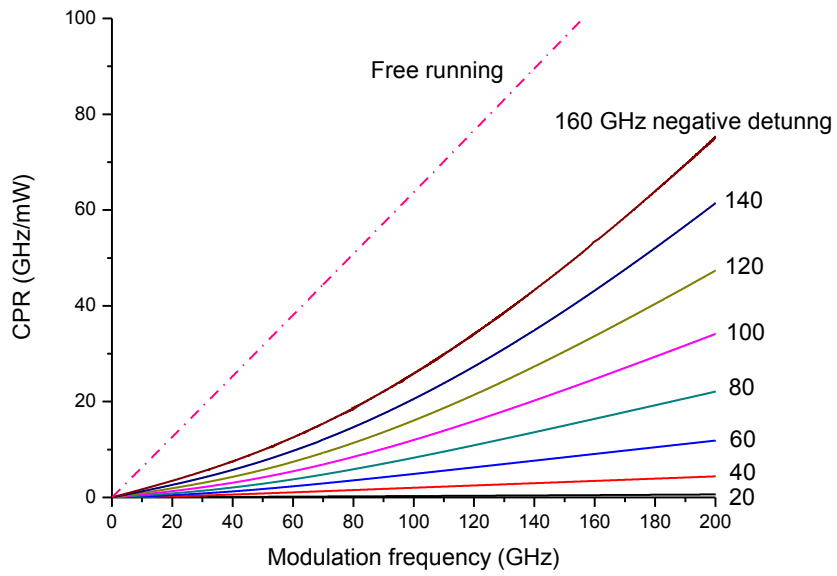


(a)

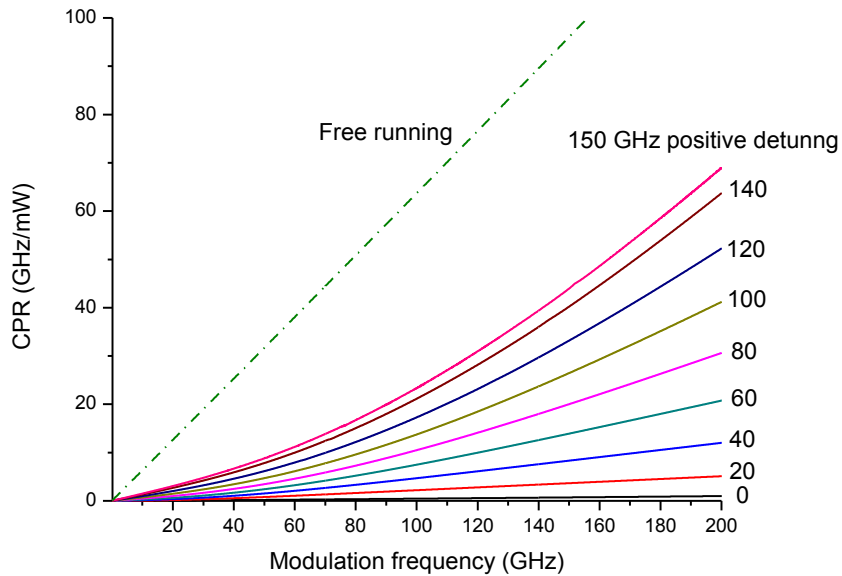


(b)

Fig. 6-1. Chirp-to-power ratio of the free-running ring laser (dashed curves) and that of the weakly injection-locked ring laser for (a) negative detuning and (b) positive detuning.



(a)



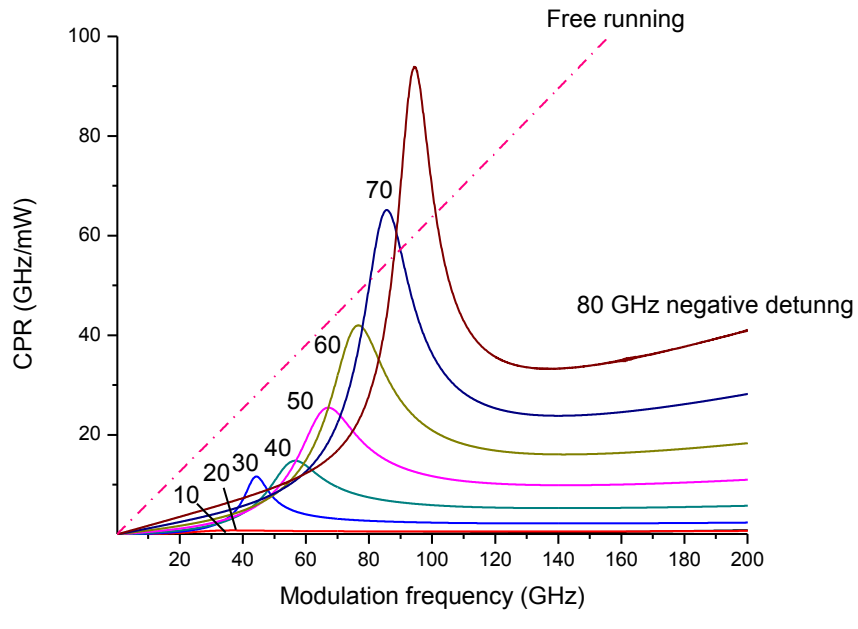
(b)

Fig. 6-2. Chirp-to-power ratio of the free-running WRL (dashed curves) and that of the strongly injection-locked WRL for (a) negative detuning and (b) positive detuning

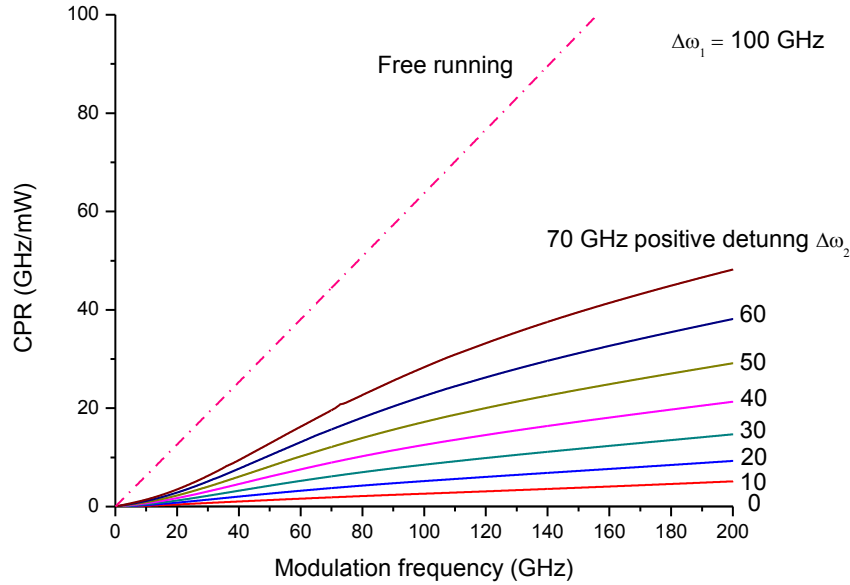
C. Cascaded Injection-Locking

In the cascaded configuration, the frequency detuning between the master DBR laser and the first ring laser $\Delta\omega_1$ is fixed at 100 GHz positive detuning in the simulations, with the stable locking range of the second ring laser calculated in terms of frequency detuning $\Delta\omega_2$ to be from 81.4 GHz negative detuning to 75.4 GHz positive detuning. Three possible scenarios are considered: modulation signal applied to the first ring laser, the second ring laser, and both ring lasers.

Fig. 6-3 shows the CPR curves when the modulation signal is applied to the first ring laser, whose output in turn modulates the second ring laser optically. For negative detuning (Fig. 6-3a), the CPR remains very small for detuning frequencies below 30 GHz. When the detuning frequency is above 30 GHz, the CPR curves first increase linearly with the modulation frequency with a moderate slope, and rise dramatically near the first resonance corresponding to the frequency detuning $\Delta\omega_2$. The peaks in the CPR curves are reached at modulation frequencies corresponding to the valley in the modulation response, indicating significant drop (close to 20 dB for all detuning frequencies) in the modulated power [Smolyakov 2011]. On the contrary, under positive detuning (Fig. 6-3b), the drop in modulation response is less than 15 dB for all frequency detunings considered [Smolyakov 2011], and the CPR curves are all well below the free-running values, with the CPR being on the order of 10^{-4} GHz/mW for zero $\Delta\omega_2$ detuning.

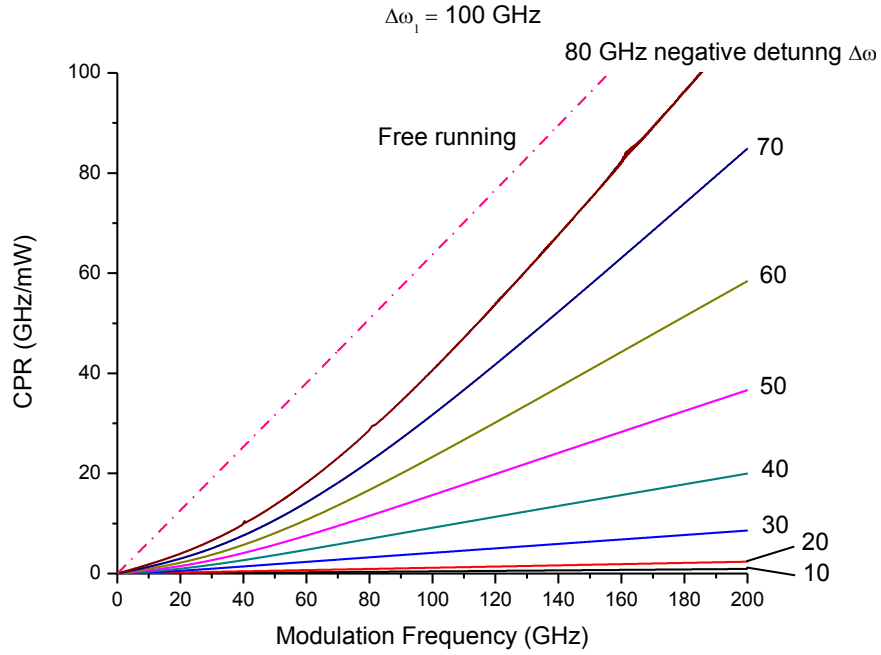


(a)

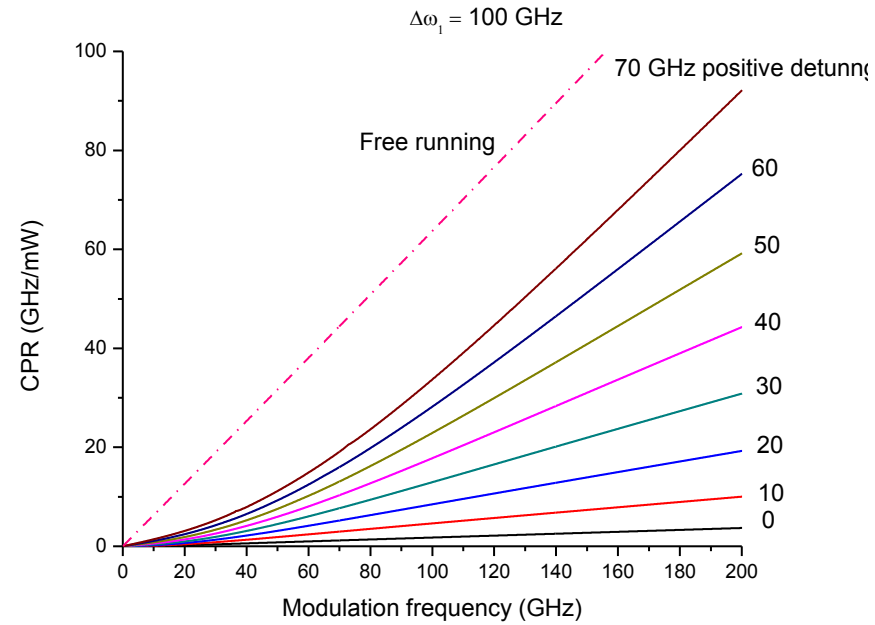


(b)

Fig. 6-3. Chirp-to-power ratio of the free-running WRL (dashed curves) and that of the second injection-locked WRL in cascaded scheme for (a) negative detuning and (b) positive detuning. Modulation signal is applied to the first WRL. $\Delta\omega_1=100$ GHz.



(a)



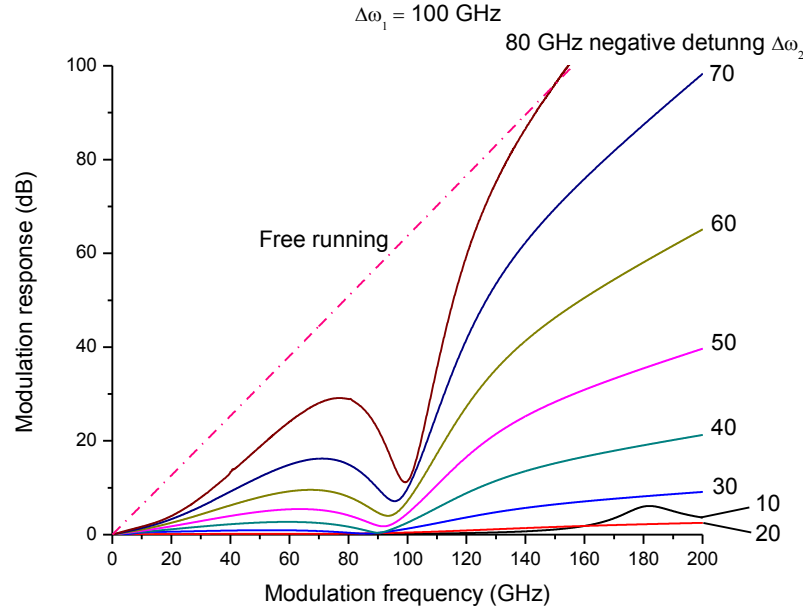
(b)

Fig. 6-4. Chirp-to-power ratio of the free-running WRL (dashed curves) and that of the second injection-locked WRL in cascaded scheme for (a) negative detuning and (b) positive detuning. Modulation signal is applied to the second WRL. $\Delta\omega_1=100 \text{ GHz}$.

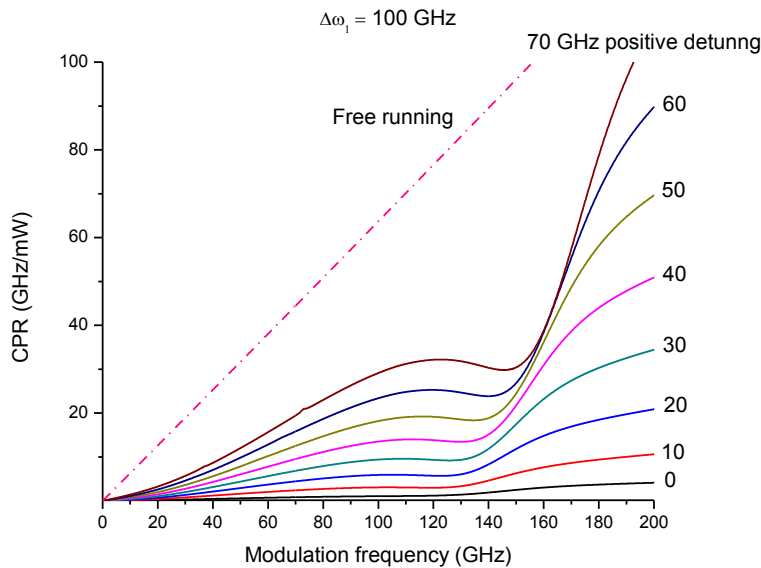
When the modulation current is applied only to the second ring laser, which is equivalent to strong injection-locking of a single ring laser with a smaller rate of optical injection from the output of the first ring laser as compared to the case described in Case B, the CPR (Fig. 6-4) shows improvement over the free-running values, though the reduction in CPR is not as significant as that shown in Fig. 6-2. The results again confirm that chirp performance can be improved with strong injection.

Finally, when the modulation current is applied to both ring lasers, the second ring laser is modulated both optically by the first ring laser and electrically by the modulation current. For negative detuning (Fig. 6-5a), the CPR curves show peaks at the first resonant frequency (corresponding to $\Delta\omega_2$), followed by local minima around 100 GHz of modulation frequency, corresponding to the frequency detuning $\Delta\omega_1$ between the master DBR laser and the first ring laser. This phenomenon is also present, though less obvious, when the second ring laser is positively detuned, as can be seen in Fig. 6-5b, where the curves reach local maxima around 100 GHz and remain flat up to 140 GHz.

For a comparison of chirp performance between different configuration and modulation schemes, Fig. 6-6 singles out the curves with lowest CPR from Fig. 6-1 to Fig. 6-5, where the improvement in CPR of strong injection is obvious. Among different modulation scenarios for the cascaded case, the lowest CPR for modulation frequency above 30 GHz is obtained when the modulation signal is applied to only the first WRL and the second WRL is at zero detuning. However, the high values of CPR at lower modulation frequencies may not be desired in some applications.



(a)



(b)

Fig. 6-5. Chirp-to-power ratio of the free-running WRL (dashed curves) and that of the second injection-locked WRL in cascaded scheme for (a) negative detuning and (b) positive detuning. Modulation signal is applied to both WRLs. $\Delta\omega_1=100 \text{ GHz}$.

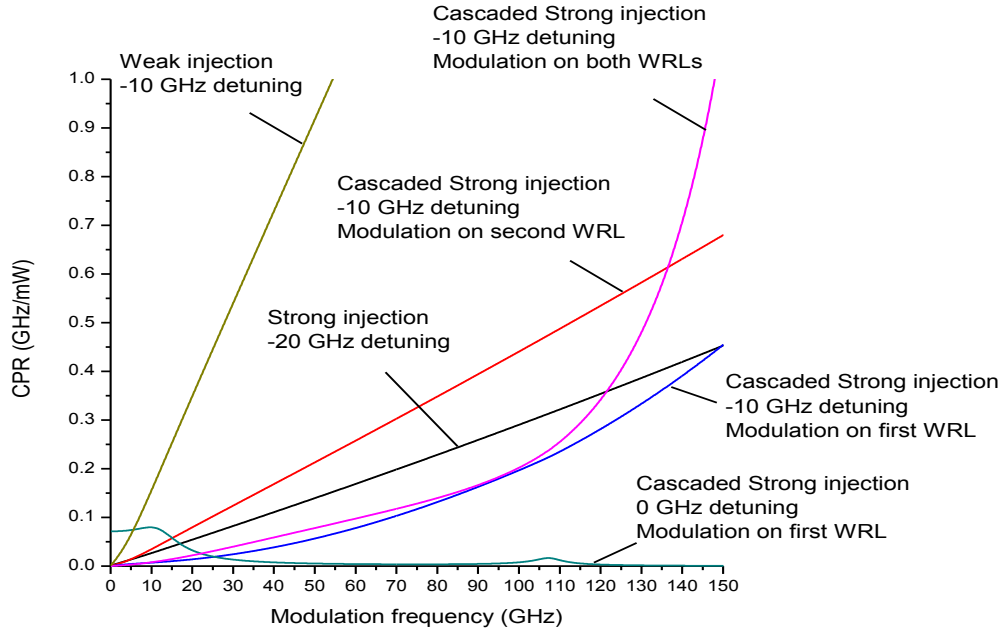


Figure 6-6. Curves corresponding to the lowest chirp-to-power ratio in Fig. 6-1 to Fig. 6-5

6.4 CONCLUSION

Chirp performance is evaluated by calculating CPR of strongly injection-locked ring lasers and compared against the conditions of free-running and weak injection-locking. Conclusions can be made from the simulation results that (i) injection locking induces sublinear and/or nonlinear behavior of CPR curves, which is approximately linear for free-running lasers; (ii) strong injection-locking greatly improves the CPR; and (iii) in the case of cascaded injection-locking, when the second ring laser is at zero detuning relative to the master laser and is only optically modulated by the output of the first WRL, CPR values on the order of 10^{-4} GHz/mW are obtained. Based on these results, combined with the enhanced modulation responses shown in previous chapters, high-speed transmitters can be designed for specific applications in long-haul fiber communication to minimize chromatic dispersion and maximize modulation frequency.

CHAPTER 7

Q-MODULATED STRONGLY-INJECTION-LOCKED WHISTLE-GEOMETRY RING LASERS

In a monolithically integrated strongly-injection-locked whistle-geometry semiconductor ring laser, modulating the photon lifetime or the optical losses in the cavity can lead to higher modulation bandwidth and complete elimination of low-frequency roll-off, which is commonly observed under direct current modulation of injection-locked semiconductor lasers. Rate equation analysis is performed to show that modulating the photon-lifetime is significantly more advantageous than the conventional injection-current modulation. Different schemes to achieve photon-lifetime or optical-loss modulation in a strongly-injection-locked whistle-geometry ring laser are proposed and discussed.

7.1 INTRODUCTION

Modulation of injection current is the most conventional method to directly modulate semiconductor lasers. However, the drawback of current modulation is that the modulation bandwidth is limited by the resonance frequency due to relaxation oscillations between carrier and photon densities in the laser cavity. Another modulation technique is the Q -factor modulation (or, equivalently, photon-lifetime modulation). In this scheme, the photon density in the laser cavity is directly affected by modulating the physical parameters impacting the cavity Q [He 2007], [Dai 2009], [Liu 2010]. In contrast, the photon density in a current-modulated laser is changed indirectly through the

relatively slow-varying carrier density via the pumping current. In a diode laser above threshold, the photon lifetime is much shorter than the carrier lifetime. Hence, photon-lifetime modulation can be potentially much faster than the conventional current modulation. The Q -modulation scheme also offers additional advantages, such as a reduced wavelength chirp as compared to current-modulated diode lasers while maintaining a stable output wavelength, high extinction ratio between the “ON” and “OFF” states, and high power efficiency [He 2007], [Dai 2009], [Liu 2010]. Owing to its numerous benefits, the Q modulation is very attractive for direct modulation among various other modulation techniques.

In this chapter, a novel injection-locked WRL is proposed, with directly modulated photon lifetime, rather than modulated injection current, as an elegant solution to the task of flattening the frequency response and achieving a broadband transmitter operating at frequencies beyond 100 GHz. We begin by brief summary of our previous work on strongly injection-locked solitary and cascaded current-modulated WRLs. We then provide numerical evidence supporting our assumption of different photon lifetimes for the counterpropagating modes in WRLs. Next, we discuss various practical schemes to achieve photon-lifetime modulation in injection-locked whistle ring lasers. In subsequent sections, we present our rate equation model and the results of analysis of the high-frequency modulation response of Q -modulated strongly injection-locked WRLs.

7.2 Q-MODULATED WRLS

Photon-lifetime (and therefore cavity Q) modulation was independently proposed theoretically in [Avrutin 1993] for edge-emitting DBR lasers and in [Dods 1994] for VCSELs, as a means of improving the high-frequency response of semiconductor lasers. Subsequently, the concept was extended to bidirectional ring lasers that were coupled to external electro-optic or electro-absorption (EA) modulators in a compound cavity [Dai 2009]. As mentioned earlier, the photon-lifetime modulation mechanism is potentially much faster than the conventional injection-current modulation, with the additional advantage of maintaining a stable output wavelength. The latter feature requires a careful anti-resonant design of Q -modulator in multi-section DFB lasers [He 2007], [Liu 2010], [Zhi 2012], [Zhu 2015], but is easily achievable in our scheme by virtue of locking to the stabilized master laser wavelength.

Employing direct cavity- Q modulation, rather than injection-current modulation, as an effective way to eliminate the low-frequency roll-off in modulation response of injection-locked semiconductor lasers has been investigated in [Wang 2011] using small-signal and numerical analyses. While the enhanced resonant frequency in Q -modulated injection-locked lasers remained the same as in current-modulated lasers, a significant enhancement in 3-dB bandwidth has been demonstrated in numerical analysis [Wang 2011] due to elimination of low frequency roll-off and due to the fact that the modulation response in Q -modulated lasers decays as $1/f$ at modulation frequencies beyond the resonance frequency [He 2007], [Liu 2010], [Avrutin 1993]. This contrasts the case of current modulation, where the modulation response above the resonance frequency decays as $1/f^2$.

Control of the photon lifetime (or the Q -factor) in semiconductor lasers with Fabry-Perot cavity (edge-emitting lasers and VCSELs) can be achieved by modulating either mirror reflectivity [He 2007], [Dai 2009], [Avrutin 1993], [Dods 1994], or distributed optical loss [Liu 2010]. In case of a microring cavity, photon-lifetime modulation can also be achieved by modifying the coupling coefficient between the ring laser and an adjacent waveguide forming a directional coupler [Liu 2010].

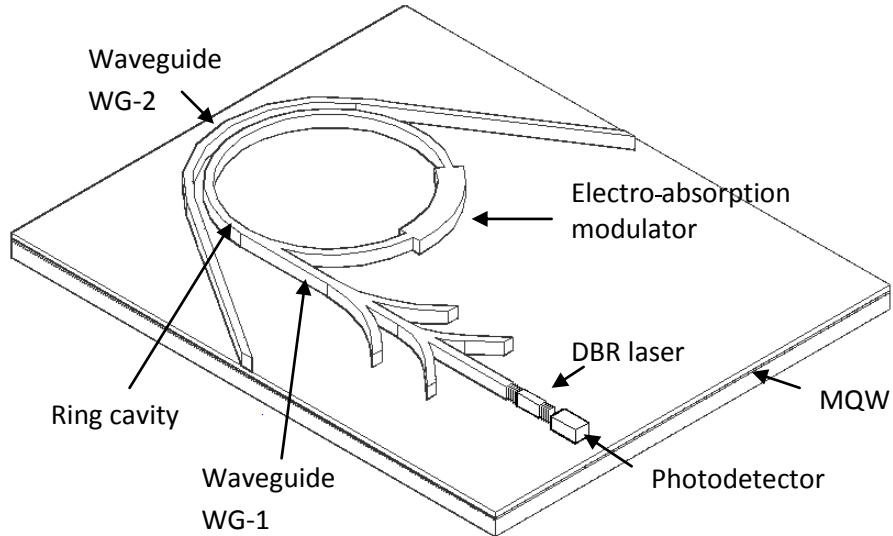


Fig. 7-1. Sketch of a DBR laser/WRL OEIC (not to scale), including a DBR laser, a ring laser, passive waveguides WG-1 and WG-2, an EA modulator section, and an integrated photodiode.

Here, we discuss two possible practical approaches to Q modulation of WRLs. First, one can insert an EA modulator section inside the microring cavity (Fig. 7-1), isolated electrically from the gain section in the ring cavity by implanting the boundaries between these two sections with protons. Proton implantation can be used to isolate the

injecting waveguide WG-1, kept at transparency, from the ring. A single-transverse-mode deep-etched ridge waveguide structure is the basis for both the 1.55- μ m InGaAs/AlGaInAs/InP multiple-quantum-well (MQW) master DBR and slave ring lasers, as well as for the waveguides WG-1 and WG-2. To maximize the output directed towards the WRL, the back DBR mirror should have a much higher reflectivity than the front mirror. It should be emphasized that the whistle geometry of the ring laser makes it unidirectional even without any external light injection, as illustrated in Section 3.2. An integrated photodetector located at the backside of the DBR laser can be used to monitor the emission from the master laser. The monolithically integrated MQW EA modulator section relies on the quantum-confined Stark effect to change the absorption coefficient of the light passing through it, and can be used to implement the Q -modulation for the light circulating in the WRL cavity. A waveguide directional coupler (see WG-2 in Fig. 7-1) can be used to collect the output of the ring laser. The same waveguide can also be used to collect the output of the DBR laser when the ring laser is kept at transparency, and to monitor any counterpropagating waves at the opposite end of WG-2. In order to minimize optical reflections, both output facets of the waveguide WG-2 can be at Brewster's angle with respect to chip edges. Several curved waveguide sections that branch off the "injecting" waveguide WG-1 can be used to suppress possible optical feedback from the WRL to the master laser.

There is a possibility, however, that the EA modulator may become saturated by the high photon density circulating inside a strongly injection-locked WRL, therefore we consider an alternative concept that could be used to bypass this problem.

Fig. 7-2 shows schematically an alternative design, again comprising a high-power DBR master laser monolithically integrated with a unidirectional WRL slave, but with an additional feedback line for the latter, which incorporates an EA modulator section inside a compound-cavity double-ring WRL. A waveguide directional coupler (see WG-2 in Fig. 7-2) together with a Y splitter can be used to collect the output of the ring laser as well as to implement the feedback line for the WRL. When dc reverse-biased and RF modulated, the MQW-EA section will be used for intensity and phase modulation of the light coupled back into the WRL, thus implementing Q modulation for the light circulating in the favored (clockwise in this case) WRL mode. It should be emphasized, however, that the analysis presented in the following sections does not apply to the design of Fig. 7-2, as the latter would require development of an appropriate model for Q -modulated compound-cavity WRL.

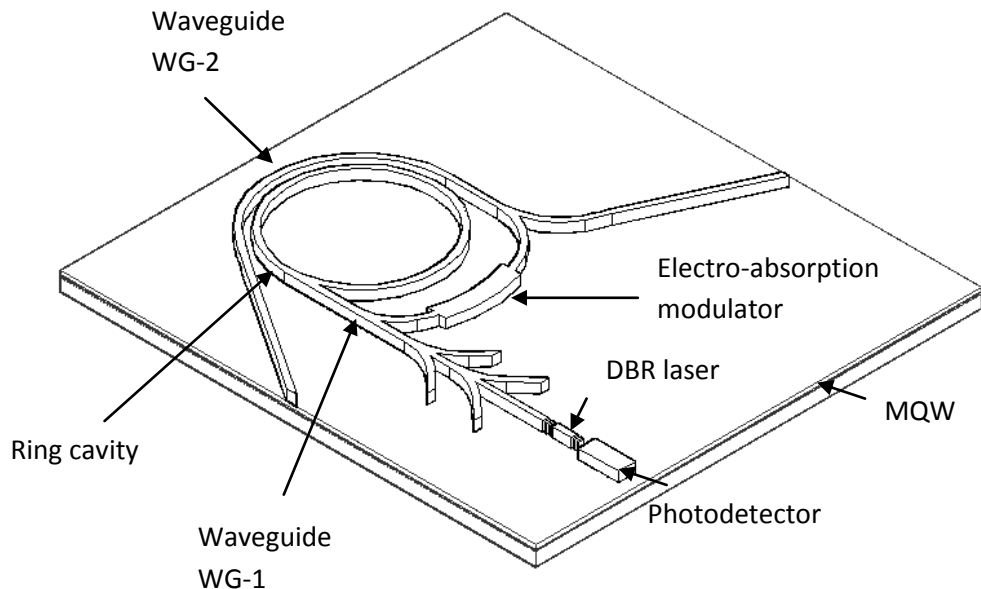


Fig. 7-2. Sketch of an alternative OEIC configuration, with a Y- splitter and a branched-off EA modulator section.

7.3 SIMULATION RESULTS

In Chapter 4, we have analyzed the potential of strongly injection-locked WRL scheme for ultrahigh frequency performance. The analysis has been done conventionally by modulating the injection current through the WRL. Here, we analyze the potential of Q -modulation mechanism by modulating the optical loss term $1/\tau_p^{ccw}$ in Eqs. (4-5), (4-6) in the form:

$$1/\tau_p^{ccw} = [I + \delta \sin(2\pi f t)] / (\tau_p^{ccw})_0 , \quad (7-1)$$

where f is the modulation frequency and δ is the modulation depth. 1% modulation depth for the optical loss ($\delta = 0.01$) was assumed in the simulations.

Similar to injection-current modulation, the calculated results for modulation response obtained through photon-lifetime modulation mechanism are presented in terms of the modulation depth in photon number in the CCW mode of ring laser versus modulation frequency.

To compare the two mechanisms for direct modulation of the strongly injection-locked WRL (Fig. 4-1a), simulations were carried out for the same configuration and under the same bias conditions that were assumed in Chapter 4 [Smolyakov 2011] for the master and the ring lasers. Master laser bias of 12 mA and ring laser bias of 6 mA at $3I_{th}$ for the ring laser were consistently chosen throughout the simulations. The results of steady-state analysis presented in Chapter 4 are thus fully applicable to the strongly injection-locked WRL modulated through photon lifetime, and no separate analysis is required.

Fig. 7-3 shows the comparison of modulation response of a free-running WRL for current modulation and photon-lifetime (optical loss) modulation cases. The modulation response for free-running ring laser was obtained by solving Eqs. (4-5) - (4-9) with $Sm = 0$. It is clearly seen that much slower decay of the modulation response was obtained for the laser modulated through optical loss.

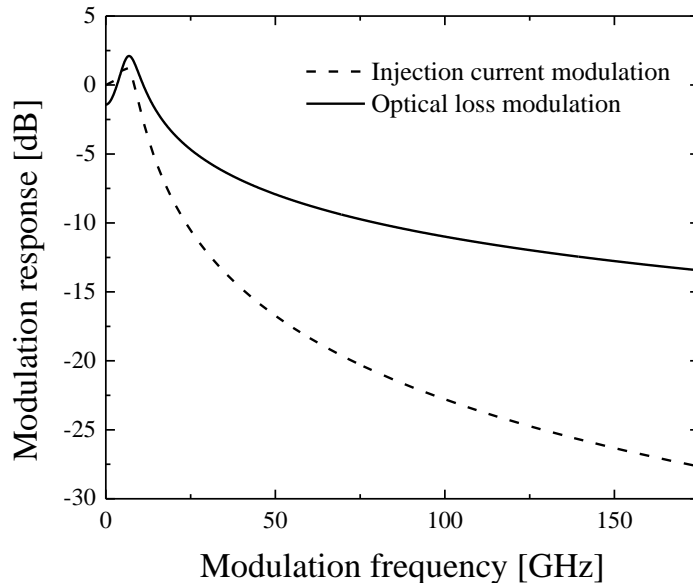


Fig. 7-3. Modulation frequency response of the free-running WRL modulated through injection current (dashed curve) compared to that of the free-running WRL modulated through optical loss (solid curve). Modulation frequency re-sponse is normalized to low-frequency response of the free-running ring laser modulated through injection current. $I_r = 6$ mA.

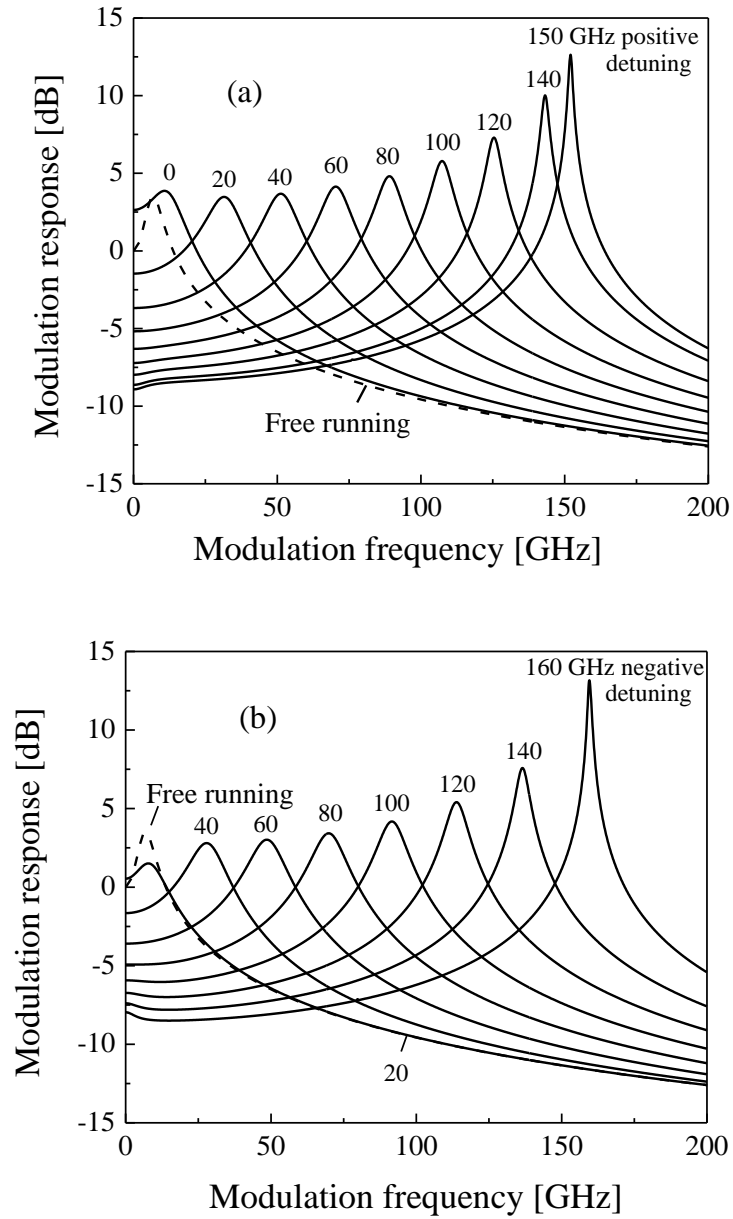


Fig. 7-4. Q -modulation frequency response of the free-running WRL (dashed curves) and that of the strongly injection-locked WRL calculated for several values of (a) positive frequency detuning and (b) negative frequency detuning between the master DBR laser and the ring laser. Modulation frequency response is normalized to low-frequency response of the free-running ring laser. $I_m = 12$ mA, $I_r = 6$ mA.

Fig. 7-4 shows modulation frequency response of the photon-lifetime-modulated strongly injection-locked WRL calculated for several positive and negative values of frequency detuning between the master laser and the ring laser. For comparison, modulation frequency response in each case is normalized to the low frequency response of the free-running laser.

As can be seen from Fig. 7-4, although there is no further enhancement of resonance frequency for the photon-lifetime modulated strongly injection-locked WRL, compared to otherwise identical current-modulated configuration (Fig. 4-12), complete elimination of low frequency roll-off and 3-dB modulation bandwidth up to 200 GHz are observed. Hence, our numerical simulation results clearly illustrate the advantage of the modulation scheme that combines Q modulation and strong optical injection locking of WRL.

7.4 CONCLUSION

In conclusion, Q modulation of a strongly injection-locked WRL has been analyzed. The potential for overcoming the low-frequency roll-off problem and attaining a tailororable and broad modulation bandwidth has been demonstrated in numerical modeling by solving rate equations with a modulated photon lifetime. Although no further enhancement of resonance frequency has been observed for the photon-lifetime modulated strongly injection-locked whistle-geometry semiconductor ring laser, a significant enhancement in 3-dB bandwidth has been demonstrated in numerical analysis due to elimination of low frequency roll-off.

CHAPTER 8

SUMMARY AND FUTURE WORK

8.1 SUMMARY

Injection-locking has been utilized to increase the modulation bandwidth of directly-modulated semiconductor lasers in optical communication systems and rf photonic links [Lau 2009], [Tartarini 2007], and it has been demonstrated, both theoretically and experimentally, to increase the modulation bandwidth and, at the same time, reduce the frequency chirp of directly modulated lasers. With injection locking, the increase in modulation bandwidth is proportional to the frequency detuning between the master and the slave laser, and the tuning range is, in turn, proportional to the coupling rate from the master to the slave laser, thus strong coupling is desired. Nevertheless, with typical semiconductor lasers, including vertical-cavity surface-emitting lasers (VCSELs) and edge-emitting lasers, injection locking cannot be achieved monolithically and requires complex optical path design to eliminate back reflection, and therefore they are not practical in real world applications.

Injection locking of semiconductor lasers with the master and the slave monolithically integrated on the same substrate can be conveniently achieved with the whistle geometry ring laser (WRL) proposed, which ensures strong injection by its small round trip time and low reflectivity, and unidirectional propagation by the non-identical photon lifetime for the two counterpropagating modes. Enhancement of high-speed modulation response was demonstrated numerically for strongly injection-locked WRL in

Chapter 4, showing a bandwidth enhancement up to as much as 160 GHz, while for weak injection locking it is only 35 GHz.

Typical for all optical injection-locking schemes, however, the modulation response showed a very significant reduction in the modulation efficiency between low frequency and the resonance frequency, which limits the usefulness of the novel scheme to narrow-band applications. One possible way to overcome the low-frequency roll-off problem and to attain tailorable and broad modulation bandwidth is to use cascaded injection locking. Using that concept, the injection-locking scheme was modified in Chapter 5 to a cascaded system with two strongly injection-locked whistle-geometry unidirectional ring lasers, where the modulated optical output of the first ring laser is used to injection-lock the second ring laser.

Other than limited modulation bandwidth under free-running condition, directly modulated lasers also suffer from frequency chirp, i.e. frequency shift due to the modulation of injection current, which results in pulse broadening over long optical fibers and limits the bitrate-distance product [Agrawal 2010]. Numerical simulations of frequency chirp were performed for injection-locked WRLs. The frequency chirp is evaluated using chirp-to-modulated-power ratio as the figure of merit. The case of weak injection with directional coupler is also presented, and comparisons between strong and weak injection are made with a conclusion that the strong injection scheme provides lower CPR. Strong injection locking of cascaded WRLs is also considered and their CPR curves show nonlinear behavior. When the second WRL is under zero detuning and is only optically modulated by the output of the first WRL, CPR with values on the order of 10-4 GHz/mW are obtained. Along with the information on modulation responses

presented in the previous chapters, the high-speed performance can be tailored according to the requirement of specific applications. In addition, further enhancement of both the modulation bandwidth and frequency chirp may be achieved by cascading several WRLs.

Finally, an alternative approach to improve the low frequency roll-off is proposed, which involves Q modulation of a strongly injection-locked WRL. The potential for overcoming the low-frequency roll-off problem and attaining a tailorabile and broad modulation bandwidth has been demonstrated in numerical modeling by solving rate equations with a modulated photon lifetime. Although no further enhancement of resonance frequency has been observed for the photon-lifetime modulated strongly injection-locked whistle-geometry semiconductor ring laser, a significant enhancement in 3-dB bandwidth has been demonstrated in numerical analysis due to elimination of low frequency roll-off.

8.2 FUTURE WORK

Several aspects of the research can be improved and/or extended, including optimization of the straight-to-ring junction design for larger photon lifetime mismatch between the CW and CCW mode, and simulation of the whistle-geometry ring laser under high speed digital modulation as compared to the sinusoidal modulation presented in this work. Also, further improvement of modulation response may be achieved, for example, by master laser modulation where it has been shown to improve the low-frequency roll-off with injection-locked distributed feedback semiconductor laser [Lau 2008c], [Memon 2009]. Finally and most importantly, the proposed optoelectronic integrated circuit (OEIC) needs to be fabricated for experimental verification.

REFERENCES

- [Agrawal 2010] G. P. Agrawal, *Fiber-Optic Communication Systems*, 4th ed., Hoboken, NJ, John Wiley & Sons Inc. 2010, ch. 3.
- [Akram 2004] M. N. Akram, C. Silfvenius, O. Kjebon, and R. Schatz, “Design optimization of InGaAsP–InGaAlAs 1.55 μm strain-compensated MQW lasers for direct modulation applications,” *Semicond. Sci. and Technol.*, 19 (#5), pp. 615-625 (2004).
- [Avrutin 1993] E. A. Avrutin, V. B. Gorfinkel, S. Luryi, and K. A. Shore, “Control of surface-emitting laser diodes by modulating the distributed Bragg mirror reflectivity: Small-signal analysis,” *Appl. Phys. Lett.*, vol. 63, no. 18, pp. 2460–2462, Nov. 1993.
- [Brown De Colstoun 1994] F. Brown De Colstoun, G. Khitrova, A. V. Fedorov, T. R. Nelson, C. Lowry, T. M. Brennan, B. G. Hammons, and P. D. Maker, “Transverse modes, vortices and vertical-cavity surface-emitting lasers,” *Chaos, Solitons & Fractals*, vol. 4, no. 8–9, pp. 1575–1596, Aug./Sep. 1994.
- [Brown 2005] D. H. Brown, M. B. Flynn, L. O'Faolain, and T. F. Krauss, “Low tuning current semiconductor coupled-cavity lasers incorporating Bragg reflectors,” *IEEE Photon. Technol. Lett.*, 17 (#11), pp. 2262-2264 (2005).
- [Celebi 2006] F. V. Celebi, I. Dalkiran, and K. Danisman, “Injection level dependence of the gain, refractive index variation, and alpha (α) parameter in broad-area InGaAs deep quantum-well lasers,” *Optik*, vol. 117, no. 11, pp. 511-515, 2006.
- [Chang 2002] W. S. C. Chang, Ed., *RF Photonic Technology in Optical Fiber Links*, Chs. 4-7, Cambridge Univ. Press, Cambridge, UK, 2002.
- [Chang 2003] C. H. Chang, L. Chrostowski, and C. J. Chang-Hasnain, “Injection locking of VCSELs,” *IEEE J. Sel. Topics Quantum Electron.*, vol. 9, no. 5, pp. 1386-1393, Sept.-Oct. 2003.
- [Chen 2000] H. F. Chen, J. M. Liu, and T. B. Simpson, “Response characteristics of direct current modulation on a bandwidth-enhanced semiconductor laser under strong injection locking,” *Opt. Commun.*, vol. 173, no. 1–6, pp. 349–355, Jan. 1, 2000.
- [Chrostowski 2002] L. Chrostowski, C. H. Chang, and C. J. Chang-Hasnain, ”Injection-locked 1.55 μm VCSELs with enhanced spur-free dynamic range,” *Electron. Lett.*, vol. 38, no. 17, pp. 965-967, Aug. 2002.

- [Chrostowski 2003] L. Chrostowski, C. H. Chang, and C. J. Chang-Hasnain, "Enhancement of dynamic range in 1.55- μ m VCSELs using injection locking," *IEEE Photon. Technol. Lett.*, vol. 15, no. 4, pp. 498-500, April 2003.
- [Chrostowski 2006a] L. Chrostowski, X. Zhao, C. J. Chang-Hasnain, R. Shau, A. Ortsiefer, and M. C. Amann, "50-GHz optically injection-locked 1.55- μ m VCSELs," *IEEE Photon. Technol. Lett.*, vol. 18, no. 1-4, pp. 367-369, Jan.-Feb. 2006.
- [Chrostowski 2006b] L. Chrostowski, X. X. Zhao, and C. J. Chang-Hasnain, "Microwave performance of optically injection-locked VCSELs," *IEEE Trans. Microw. Theory Tech.*, vol. 54, no. 2, pt. 2, pp. 788-796, Feb. 2006.
- [Chrostowski 2008] L. Chrostowski and W. Shi, "Monolithic injection-locked high-speed semiconductor ring lasers," *J. Lightw. Technol.*, vol. 26, no. 19, pp. 3355-3362, Oct. 2008.
- [Chung 1991] H. Y. Chung, W. S. C. Chang, and E. L. Adler, "Modeling and optimization of traveling-wave LiNbO₃ interferometric modulators," *IEEE J. Quantum Electron.*, vol. 27, no. 3, pp. 608-617, Mar. 1991.
- [Covega 2008] Covega Products & Services Catalog, Covega Corporation, Jessup, MD: 2008. [Online]. Available: <http://www.covega.com/Products/?catID=7>.
- [Cox 2006] C. H. Cox III, E. I. Ackerman, G. E. Betts, and J. L. Prince, "Limits on the performance of RF-over-fiber links and their impact on device design," *IEEE Trans. Microw. Theory Tech.*, vol. 54, no. 2, pt. 2, pp. 906-920, Feb. 2006.
- [Dai 2009] D. X. Dai, A. Fang, and J. E. Bowers, "Hybrid silicon lasers for optical interconnects," *New J. Phys.*, vol. 11, Art. 125016 (17 pp.), Dec. 2009.
- [Dods 1994] S. Dods and M. Ogura, "Q-modulation of a surface emitting laser and an integrated detuned cavity," *IEEE J. Quantum Electron.*, vol. 30, no. 5, pp. 1204–1211, May 1994.
- [Espana-Boquera 1996] M. C. España-Boquera and A. Puerta-Notario, "Noise effects in injection locked laser simulation: Phase jumps and associated spectral components," *Electron. Lett.*, vol. 32, no. 9, pp. 818–819, 25 Apr. 1996.
- [Goldberg 1985] L. Goldberg, A. M. Yurek, H. F. Taylor, and J. F. Weller, "35 GHz microwave signal generation with an injection-locked laser diode," *Electron. Lett.*, vol. 21, no. 18, pp. 814–815, 29 Aug. 1985.
- [Gopalakrishnan 1994] G. K. Gopalakrishnan and W. K. Burns, "Performance and modeling of resonantly enhanced LiNbO₃ modulators for low-loss analog fiberoptic links," *IEEE Trans. Microw. Theory Tech.*, vol. 42, no. 12, pt. 2, pp. 2650-2656, Dec. 1994.

- [Han 1992] H. Han, M.E. Favaro, D.V. Forbes, and J.J. Coleman, “In_xGa_{1-x}As- Al_yGa_{1-y}As-GaAs strained-layer quantum-well heterostructure circular ring lasers,” *IEEE Photon. Technol. Lett.*, v 4, n 8, p 817-819, Aug 1992.
- [He 2007] J.-J. He, “Proposal for Q-modulated semiconductor laser,” *IEEE Photon. Technol. Lett.*, vol. 19, no. 5, pp. 285–287, 1 Mar. 2007.
- [Henry 1985] C. H. Henry, N. A. Olsson, and N. K. Dutta, “Locking range and stability of injection locked 1.54 μm InGaAsP semiconductor lasers,” *IEEE J. Quantum Electron.*, vol. QE-21, no. 8, pp. 1152–1156, Aug. 1985.
- [Höfling 1999] E. Höfling, F. Schafer, J. P. Reithmaier, and A. Forchel, “Edge-emitting GaInAs-AlGaAs microlasers,” *IEEE Photon. Technol. Lett.* 11 (#8), pp. 943-945, 1999.
- [Hohimer 1992a] J.P. Hohimer, G.A. Vawter, D.C. Craft, and G.R. Hadley, “Interferometric ring diode lasers,” *Applied Physics Letters*, v 61, n 12, p 1375-1377, Sep 21 1992.
- [Hohimer 1992b] J. P. Hohimer, G. A. Vawter, and D. C. Craft “Unidirectional operation in a semiconductor ring diode laser,” *Applied Physics Letters*, v 62, n 11, p 1185-1187, Mar 15 1993.
- [Hwang 2004] S. K. Hwang, J. M. Liu, and J. K. White, “35-GHz intrinsic bandwidth for direct modulation in 1.3-μm semiconductor lasers subject to strong injection locking,” *IEEE Photon. Technol. Lett.*, vol. 16, no. 4, pp. 972-974, Apr. 2004.
- [Ivanov 2007] A. V. Ivanov, V. D. Kurnosov, K. V. Kurnosov, A. A. Marmalyuk, V. I. Romantsevich, Yu. L. Ryaboshtan, and R. V. Chernov, “Refractive indices of solid AlGaInAs solutions,” *Quantum Electron.* 37 (#6), pp. 545-548, 2007.
- [Iwashita 1982] K. Iwashita and K. Nakagawa, “Suppression of mode partition noise by laser diode light injection,” *IEEE J. Quantum Electron.*, vol. QE-18, no. 10, pp. 1669–1674, Oct. 1982.
- [Jambunathan 1997] R. Jambunathan and J. Singh, “Design studies for distributed Bragg reflectors for short-cavity edge-emitting lasers,” *IEEE J. Quantum Electron.*, 33 (#7), pp. 1180-1189, 1997.
- [Jin 2006] X. M. Jin and S. L. Chuang, “Bandwidth enhancement of Fabry-Perot quantum-well lasers by injection-locking,” *Solid-State Electron.*, 50 (#6), pp. 1141-1149, June 2006.
- [Jones 2000] R. J. Jones, P. S. Spencer, and K. A. Shore, “Influence of detuned injection locking on the relaxation oscillation frequency of a multimode semiconductor laser,” *J. Mod. Opt.*, vol. 47, no. 11, pp. 1977–1986, Sep. 2000.

- [Kawaguchi 1994] H. Kawaguchi, *Bistabilities and Nonlinearities in Laser Diodes*, Artech House, Norwood, MA 1994, p. 151.
- [Kasunic 2000] K. J. Kasunic, "Design equations for the reflectivity of deep-etch distributed Bragg reflector gratings," *J. Lightw. Technol.*, 18(#3), pp. 425-429, 2000.
- [Kim 2003] H.-C. Kim, H. Kanjo, T. Hasegawa, S. Tamura, and S. Arai, "1.5- μ m wavelength narrow stripe distributed reflector lasers for high-performance operation," *IEEE J. Sel. Topics Quantum Electron.*, 9 (#5), pp. 1146-1152, 2003.
- [Kjebon 1997] O. Kjebon, R. Schatz, S. Lourdudoss, S. Nilsson, B. Stalnacke, and L. Backbom, "30 GHz direct modulation bandwidth in detuned loaded InGaAsP DBR lasers at 1.55 μ m wavelength," *Electron. Lett.*, vol. 33, no. 6, pp. 488–489, Mar. 1997.
- [Kobayashi 1976] K. Kobayashi and R. Lang, "Suppression of the relaxation oscillation in the modulated output of semiconductor lasers," *IEEE J. Quantum Electron.*, vol. 12, no. 3, pp. 194-199, Mar. 1976.
- [Kobayashi 1982] S. Kobayashi and T. Kimura, "Optical phase modulation in an injection locked AlGaAs semiconductor laser," *IEEE J. Quantum Electron.*, vol. QE-18, no. 10, pp. 1662–1657, Oct. 1982.
- [Koch 1984] T. L. Koch and J. E. Bowers, "Nature of Wavelength Chirping in Directly Modulated Semiconductor lasers," *Electron. Lett.*, vol. 20, no. 25/26, pp. 1038-1040, Dec. 1984
- [Krauss 1995] T.F. Krauss, R.M. De La Rue, and P.J.R. Laybourn, "Impact of output coupler configuration on operating characteristics of semiconductor ring lasers," *Journal of Lightwave Technology*, v 13, n 7, p 1500-1506, July 1995.
- [Lau 1985] K. Y. Lau and A. Yariv, "Ultra-high speed semiconductor lasers," *IEEE J. Quantum Electron.*, vol. 21, no. 2, pp. 121-138, Feb. 1985.
- [Lau 2007] E. K. Lau, H.-K. Sung, and M. C. Wu, "Scaling of resonance frequency for strong injection-locked lasers," *Opt. Lett.*, vol. 32, no. 23, pp. 3373–3375, Dec. 2007.
- [Lau 2008a] E. K. Lau, H.-K. Sung, and M. C. Wu, "Frequency response enhancement of optical injection-locked lasers," *IEEE J. Quantum Electron.*, vol. 44, no. 1, pp. 90–99, Jan. 2008.
- [Lau 2008b] E. K. Lau, X. X. Zhao, H.-K. Sung, D. Parekh, C. Chang-Hasnain, and M. C. Wu, "Strong optical injection-locked semiconductor lasers demonstrating > 100-GHz resonance frequencies and 80-GHz intrinsic bandwidths," *Opt. Express*, vol. 16, no. 9, pp. 6609–6618, Apr. 2008.

- [Lau 2008c] E. K. Lau, L. J. Wong, X. Zhao, Y.-K. Chen, C.J. Chang-Hasnain, and M. C. Wu, “Bandwidth enhancement by master modulation of optical injection-locked lasers,” *J. Lightwave Technol.*, v 26, n 15, p 2584-2593, 2008.
- [Lau 2009] E. K. Lau, L. J. Wong, and M. C. Wu, “Enhanced modulation characteristics of optical injection-locked lasers: A tutorial,” *IEEE J. Sel. Topics Quantum Electron.* 15 (#3), pp. 618-633, 2009.
- [Lang 1976] R. Lang and K. Kobayashi, “Suppression of the relaxation oscillation in the modulated output of semiconductor lasers,” *IEEE J. Quantum Electron.*, vol. QE-12, no. 3, pp.194–199, Mar. 1976.
- [Lee 2002] M. Lee, H. E. Katz, C. Erben, D. M. Gill, P. Gopalan, J. D. Heber, and D. J. McGee, “Broadband modulation of light by using an electro-optic polymer,” *Science*, vol. 298, no. 5597, pp. 1401-1403, Nov. 2002.
- [Li 1996] H. Li, T. L. Lucas, J. G. McInerney, M. W. Wright, and R. A. Morgan, “Injection locking dynamics of vertical cavity semiconductor lasers under conventional and phase conjugate injection,” *IEEE J. Quantum Electron.*, vol. 32, no. 2, pp. 227-235, Feb. 1996.
- [Lin 1984] C. Lin and F. Mengel, “Reduction of frequency chirping and dynamic linewidth in high-speed directly modulated semiconductor lasers by injection locking,” *Electron. Lett.*, vol. 20, no. 25–26, pp. 1073–1075, 6 Dec. 1984.
- [Liu 1997] J. M. Liu, H. F. Chen, X. J. Meng, and T. B. Simpson, “Modulation bandwidth, noise, and stability of a semiconductor laser subject to strong injection locking,” *IEEE Photon. Technol. Lett.*, vol. 9, no. 10, pp. 1325–1327, Oct. 1997.
- [Liu 2010] D. K. Liu, L. Wang, and J.-J. He, “Rate equation analysis of high speed Q -modulated semiconductor laser”, *J. Lightwave Technol.*, vol. 28, no. 21, pp. 3128–3135, Nov. 2010.
- [Luo 1991] J. M. Luo and M. Osiński, Side-mode injection locking characteristics of semiconductor lasers: Multimode analysis,” in *Proc. 1st International Workshop on Photonic Networks, Components and Applications* (J. Chrostowski and J. Terry, Eds.), Montebello, Quebec, Canada, 11-13 Oct., 1990, Series in Optics and Photonics Vol. 2, World Scientific, Singapore 1991, pp. 195–199.
- [Luo 1992a] J.-M. Luo and M. Osiński, “Side-mode injection locking characteristics of semiconductor lasers: Frequency and field noise spectra,” in *Proc. 2nd IEEE International Workshop on Photonic Networks, Components and Applications* (J. Chrostowski and J. Terry, Eds.), Montebello, Québec, Canada, 9-11 Mar., 1992, OCRI Publications, pp. 3.1.1–3.1.6.

- [Luo 1992b] J.-M. Luo and M. Osiński, “Multimode small-signal analysis of side-mode injection-locked semiconductor lasers,” *Jpn. J. Appl. Phys. Pt. 2 (Lett.)*, vol. 31, pp. L685–L688, Jun. 1992.
- [Matsui 1997] Y. Matsui, H. Murai, S. Arahira, S. Kutsuzawa, and Y. Ogawa, “30-GHz bandwidth 1.55- μm strain-compensated InGaAlAs—InGaAsP laser,” *IEEE Photon. Technol. Lett.*, vol. 9, no. 1, pp. 25–27, Jan. 1997.
- [Maximov 2002] M. V. Maximov, E. M. Ramushina, V. L. Skopina, E. M. Tanklevskaya, V. A. Solov'Ev, Y. M. Shernyakov, I. N. Kaiander, M. A. Kaliteevski, S. A. Gurevich, N. N. Ledentsov, V. M. Ustinov, Z. I. Alferov, C. M. Sotomayor Torres, and D. Bimberg, “Edge-emitting InGaAs/GaAs lasers with deeply etched semiconductor/air distributed Bragg reflector mirrors,” *Semicond. Sci. and Technol.* 17 (#11), pp. L69-L71, 2002.
- [Memon 2009] M. I. Memon, B. Li, G. Mezosi, Z. Wang, M. Sorel, S. Yu, “Frequency response enhancement in optical injection locked semiconductor ring laser using master laser modulation,” *35th European Conference on Optical Communication, ECOC 2009 - Proceedings*, 2009.
- [Meng 1998a] X. J. Meng, T. Chau, and M. C. Wu, “Experimental demonstration of modulation bandwidth enhancement in distributed feedback lasers with external light injection,” *Electron. Lett.*, vol. 34, no. 21, pp. 2031–2032, 15 Oct. 1998.
- [Meng 1998b] X. J. Meng, T. Chau, D. T. K. Tong, and M. C. Wu, “Suppression of second harmonic distortion in directly modulated distributed feedback lasers by external light injection,” *Electron. Lett.*, vol. 34, no. 21, pp. 2040–2041, Oct. 1998.
- [Meng 1999] X. J. Meng, T. Chau, and M. C. Wu, “Improved intrinsic dynamic distortions in directly modulated semiconductor lasers by optical injection locking,” *IEEE Trans. Microw. Theory Tech.*, vol. 47, no. 7, pt. 2, pp. 1172–1176, Jul. 1999.
- [Mezosi 2014] G. Mezosi and M. Sorel, "Semiconductor Micro-Ring Lasers," *Compact Semiconductor Lasers*, ed., R.M. De La Rue, J.-M. Lourtioz, S. Yu, Ch. 6, Wiley-VCH 2014.
- [Mohrdiek 1994] S. Mohrdiek, H. Burkhard, and H. Walter, “Chirp reduction of directly modulated semiconductor lasers at 10 Gb/s by strong CW light injection,” *J. Lightwave Technol.*, vol. 12, no. 3, pp. 418–424, Mar. 1994.
- [Murakami 2003] A. Murakami, K. Kawashima, and K. Atsuki, “Cavity resonance shift and bandwidth enhancement in semiconductor lasers with strong light injection,” *IEEE J. Quantum Electron.*, vol. 39, no. 10, pp. 1196–1204, Oct. 2003.

- [Nizette 2002] M. Nizette, T. Erneux, A. Gavrielides, and V. Kovanis, “Averaged equations for injection locked semiconductor lasers,” *Phys. D*, vol. 161, nos. 3–4, pp. 220–236, Jan. 2002.
- [Nizette 2001] M. Nizette, T. Erneux, A. Gavrielides, and V. Kovanis, “Stability and bifurcations of periodically modulated, optically injected laser diodes,” *Phys. Rev. E*, vol. 63, no. 2, p. 026212, Feb. 2001.
- [Noguchi 1998] K. Noguchi, O. Mitomi, and H. Miyazawa, “Millimeter-wave Ti:LiNbO₃ optical modulators,” *J. Lightwave Technol.*, vol. 16, no. 4, pp. 615-619, Apr. 1998.
- [Ohtsubo 2013] J. Ohtsubo, *Semiconductor Lasers - Stability, Instability and Chaos*, 3rd ed., Springer 2013, ch. 3.
- [Okajima 2003] Y. Okajima, S. K. Hwang, and J. M. Liu, “Experimental observation of chirp reduction in bandwidth-enhanced semiconductor lasers subject to strong optical injection,” *Opt. Commun.*, vol. 219, no. 1-6, pp. 357-364, April 2003.
- [Oku 1999a] S. Oku, S. Kondo, Y. Noguchi, T. Hirono, M. Nakao, and T. Tamamura, “Surface-grating distributed Bragg reflector lasers with deeply etched grooves formed by reactive beam etching,” *Jpn. J. Appl. Phys. Pt. 1* 38 (#2B), pp. 1256-1260, 1999.
- [Oku 1999b] S. Oku, T. Ishii, R. Iga, and T. Hirono, “Fabrication and performance of AlGaAs-GaAs distributed Bragg reflector lasers and distributed feedback lasers utilizing first-order diffraction gratings formed by a periodic groove structure,” *IEEE J. Sel. Topics Quantum Electron.*, 5 (#3), pp. 682-687, 1999.
- [Olsson 1985] N. A. Olsson, H. Temkin, R. A. Logan, L. F. Johnson, G. J. Dolan, J. P. van der Ziel, and J. C. Campbell, “Chirp-free transmission over 82.5 km of single mode fibers at 2 Gbit/s with injection locked DFB semiconductor lasers,” *J. Lightwave Technol.*, vol. LT-3, no. 1, pp. 63–67, Jan. 1985.
- [Park 2005] S. Park, S. S. Kim, L. W. Wang, and S. T. Ho, “InGaAsP-InP nanoscale waveguide-coupled microring lasers with submilliampere threshold current using Cl₂-N₂-based high-density plasma etching,” *IEEE J. Quantum Electron.* 41 (#3), pp. 351-356, 2005.
- [Peral 2000] E. Peral, and A. Yariv, “Large-signal theory of the effect of dispersive propagation on the intensity modulation response of semiconductor lasers,” *J. Lightwave Technol.*, v 18, n 1, p 84-89, January 2000.
- [Piazzolla 1986] S. Piazzolla, P. Spano, and M. Tamburini, "Small Signal Analysis of Frequency Chirping in Injection-Locked Semiconductor Lasers," *IEEE J. Quantum Electron.*, vol. QE-22, no. 12, pp. 2219-2223, Dec. 1986.

- [Raj 1998] M. M. Raj, K. Numata, S Toyoshima, and S. Arai, “GaInAsP/InP multiple short cavity laser with $\lambda/4$ -air gap/semiconductor Bragg reflectors,” *Jpn. J. Appl. Phys. Pt. 2* 37 (#12A), pp. L1461-L1464, 1998.
- [Raj 1999] M. M. Raj, S. Toyoshima, and S. Arai, “Multiple micro-cavity laser with benzocyclobutene/ semiconductor high reflective mirrors fabricated by CH₄/H₂-reactive ion etching,” *Jpn. J. Appl. Phys. Pt. 2* 38 (#7B), pp. L811-L814, 1999.
- [Raj 2000] M. M. Raj, J. Wiedmann, Y. Saka, K. Ebihara, and S. Arai, “Highly uniform 1.5 μm wavelength deeply etched semiconductor/benzocyclobutene distributed Bragg reflector lasers,” *Jpn. J. Appl. Phys.* 39 (#12B), pp. L1297-L1299, 2000.
- [Raj 2001] M. M. Raj, J. Wiedmann, S. Toyoshima, Y. Saka, K. Ebihara, and S. Arai, “High-reflectivity semiconductor/benzocyclobutene Bragg reflector mirrors for GaInAsP/InP lasers,” *Jpn. J. Appl. Phys. Pt. 1* 40 (#4A), pp. 2269-2277, 2001.
- [Schunk 1986] N. Schunk and K. Petermann, “Noise analysis of injection-locked semiconductor injection lasers,” *IEEE J. Quantum Electron.*, vol. QE-22, no. 5, pp. 642–650, May 1986.
- [Seeds 1988] A. J. Seeds, I. D. Blanchflower, N. J. Gomes, G. King, and S. J. Flynn, “New developments in optical control techniques for phased array radar,” in 1988 *IEEE MTT International Microwave Symposium Digest* (Cat.No.88CH2489-3). IEEE. 1988, pp. 905–908, vol. 2. New York, NY, USA, 1988.
- [Shen 1986] T. M. Shen, and G. P. Agrawal, “Pulse-Shape Effects on Frequency Chirping in Single-Frequency Semiconductor Lasers Under Current Modulation,” *J. Lightwave Technol.*, vol. LT-4, no. 5, May 1986.
- [Sung 2004] H.-K. Sung, T. Jung, M. C. Wu, D. Tishinin, T. Tanbun-Ek, K. Y. Liou, and W. T. Tsang, “Modulation bandwidth enhancement and nonlinear distortion suppression in directly modulated monolithic injection-locked DFB lasers,” in *MWP 2003 Proc. International Topical Meeting on Microwave Photonics*, pp. 27-30, 2004.
- [Simpson 1995] T. B. Simpson, J. M. Liu, and A. Gavrielides, “Bandwidth enhancement and broadband noise reduction in injection-locked semiconductor lasers,” *IEEE Photon. Technol. Lett.*, vol. 7, no. 7, pp. 709–711, Jul. 1995.
- [Simpson 1996] T. B. Simpson, J. M. Liu, and A. Gavrielides, “Small-signal analysis of modulation characteristics in a semiconductor laser subject to strong optical injection,” *IEEE J. Quantum Electron.*, vol. 32, no. 8, pp. 1456–1468, Aug. 1996.

- [Simpson 1997] T. B. Simpson and J. M. Liu, “Enhanced modulation bandwidth in injection-locked semiconductor lasers,” *IEEE Photon. Technol. Lett.*, vol. 9, no. 10, pp. 1322–1324, Oct. 1997.
- [Smolyakov 2011a] G. A. Smolyakov and M. Osiński, “Rate equation analysis of dynamic response in strongly injection-locked semiconductor microring lasers,” *Physics and Simulation of Optoelectronic Devices XIX* (B. Witzigmann, F. Henneberger, Y. Arakawa, and A. Freundlich, Eds.), SPIE International Symp. on Integrated Optoelectronic Devices OPTO 2011, San Francisco, CA, 24-27 Jan. 2011, *Proc. SPIE*, vol. 7933, Paper 79330D (12 pp.).
- [Smolyakov 2011b] G. A. Smolyakov and M. Osiński, “High-speed modulation analysis of strongly injection-locked semiconductor ring lasers,” *IEEE J. Quantum Electron.*, vol. 47, no. 11, pp. 1463–1471, Nov. 2011.
- [Smolyakov 2012] G. A. Smolyakov, Y. Fichou, and M. Osiński, “Analysis of high-frequency modulation response of strongly injection-locked cascaded semiconductor ring lasers,” *IEEE J. Quantum Electron.*, vol. 48, no. 12, pp. 1568–1577, Dec. 2012.
- [Sung 2007] H.-K. Sung, E. K. Lau, and M. C. Wu, “Optical single sideband modulation using strong optical injection-locked semiconductor lasers,” *IEEE Photon. Technol. Lett.*, vol. 19, no. 13, pp. 1005–1007, 1 Jul. 2007.
- [Sung 2004] H.-K. Sung, T. Jung, M. C. Wu, D. Tishinin, T. Tanbun-Ek, K. Y. Liou, and W. T. Tsang, “Modulation bandwidth enhancement and nonlinear distortion suppression in directly modulated monolithic injection-locked DFB lasers,” in *MWP 2003 Proc. International Topical Meeting on Microwave Photonics*, pp. 27-30, 2004.
- [Sung 2008] H.-K. Sung and M. C. Wu, “Amplitude modulation response and linearity improvement of directly modulated lasers using ultra-strong injection-locked gain-lever distributed Bragg reflector lasers,” *J. Opt. Soc. Korea*, vol. 12, no. 4, pp. 303–308, Dec. 2008.
- [Tartarini 2007] G. Tartarini, A. Lena, D. Passaro, L. Rosa, S. Selleri, P. Faccin, and E. M. Fabbri, “Harmonic and intermodulation distortion modeling in IM-DD multi-band radio over fiber links exploiting injection locked lasers,” *Opt. and Quant. Electron.*, vol. 38, no. 9-11, pp. 869-876, Jul. 2006.
- [Toba 1984] H. Toba, Y. Kobayashi, K. Yanagimoto, H. Nagai, and M. Nakahara, “Injection-locking technique applied to a 170 km transmission experiment at 445.8 Mbit/s,” *Electron. Lett.*, vol. 20, no. 9, pp. 370–371, 26 Apr. 1984.

- [Wang 1995] J. Wang, M. K. Haldar, and F. V. C. Mendis “Large-signal modulation characteristics of laser diodes with weak coherent optical feedback,” *Microwave and Opt. Technol. Lett.*, vol. 9, no. 6, pp. 343-345, Aug 20 1995
- [Wang 1996] J. Wang, M. K. Haldar, L. Li, and F. V. C. Mendis, “Enhancement of modulation bandwidth of laser diodes by injection locking,” *IEEE Photon. Technol. Lett.* 8 (#1), pp. 34-36, 1996.
- [Wang 2008] Z. Wang, G. Yuan, G. Verschaffelt, J. Danckaert, and S. Yu, “Injection locking and switching operations of a novel retro-reflector-cavity-based semiconductor micro-ring laser,” *IEEE Photon. Technol. Lett.*, v 20, n 20, p 1673-1675, October 15, 2008.
- [Wang 2011] X. Wang and L. Chrostowski, “High-speed Q-modulation of injectionlocked semiconductor lasers,” *IEEE Photon. J.*, vol. 3, no. 5, pp. 936–945, Oct. 2011.
- [Wieczorek 2006] S. Wieczorek, W. W. Chow, L. Chrostowski, and C. J. Chang-Hasnain, “Improved semiconductor-laser dynamics from induced population pulsation,” *IEEE J. Quantum Electron.*, vol. 42, no. 5–6, pp. 552–562, May/Jun. 2006.
- [Wiedmann 2001a] J. Wiedmann, M. Madhan, K. Ebihara, K. Matsui, S. Tamura, and S. Arai, “Deeply etched semiconductor/benzocyclobutene distributed Bragg reflector laser combined with multiple cavities for 1.5- μm -wavelength single-mode operation,” *Jpn. J. Appl. Phys. Pt. 1* 40 (#6A), pp. 4031-4037, 2001.
- [Wiedmann 2001b] J. Wiedmann, H.-C. Kim, K. Ebihara, B. Chen, M. Ohta, S. Tamura, J.-I. Shim, and S. Arai, “GaInAsP/InP distributed reflector lasers consisting of deeply etched vertical gratings,” *Jpn. J. Appl. Phys. Pt. 1* 40 (#12), pp. 6845-6851, 2001.
- [Wong 2005] H. Y. Wong, M. Sorel, A. C. Bryce, J. H. Marsh, and J. M. Arnold, “Monolithically integrated InGaAs-AlGaInAs Mach-Zehnder interferometer optical switch using quantum-well intermixing,” *IEEE Photon. Technol. Lett.*, 17 (#4), pp. 783-785, 2005.
- [Wong 2006] E. Wong, X. X. Zhao, C. J. Chang-Hasnain, W. Hofmann, and M. C. Amann, “Optically injection-locked 1.55- μm VCSELs as upstream transmitters in WDM-PONs,” *IEEE Photon. Technol. Lett.*, vol. 18, no. 21-24, pp. 2371-2373, Nov.-Dec. 2006.

- [Yabre 2000] G. Yabre, H. De Waardt, H. P. A. van den Boom, and G. D. Khoe, “Noise characteristics of single-mode semiconductor lasers under external light injection,” *IEEE J. Quantum Electron.*, vol. 36, no. 3, pp. 385–393, Mar. 2000.
- [Yamashita 2000] S. Yamashita and D. Matsumoto, “Waveform reshaping based on injection locking of a distributed-feedback semiconductor laser,” *IEEE Photon. Technol. Lett.*, vol. 12, no. 10, pp. 1388–1390, Oct. 2000.
- [Yu 2009] Z. F. Yu and S. H. Fan, “Complete optical isolation created by indirect interband photonic transitions,” *Nature Photon.*, vol. 3, no. 2, pp. 91–94, Feb. 2009.
- [Yu 2010] Z. F. Yu and S. H. Fan, “Integrated nonmagnetic optical isolators based on photonic transitions,” *IEEE J. Sel. Topics Quantum Electron.*, vol. 16, no. 2, pp. 459–466, Mar./Apr. 2010.
- [Yuan 2007] G. Yuan and S. Yu, “Analysis of dynamic switching behavior of bistable semiconductor ring lasers triggered by resonant optical pulse injection,” *IEEE J. Sel. Topics Quantum Electron.*, vol. 13, no. 5, pt. 1, pp. 1227–1234, Sep./Oct. 2007.
- [Yuan 2008a] G. Yuan, Z. Wang, B. Li, M. I. Memon, Muhammad, and S. Yu, “Theoretical and experimental studies on bistability in semiconductor ring lasers with two optical injections,” *IEEE J. Sel. Topics Quantum Electron.*, v 14, n 3, p 903-910, May/June 2008.
- [Yuan 2008b] G. Yuan and S. Yu, “Bistability and switching properties of semiconductor ring lasers with external optical injection,” *IEEE J. Quantum Electron.*, v 44, n 1, p 41-48, January 2008.
- [Zhao 2004] X. Zhao, M. Moewe, L. Chrostowski, C. H. Chang, R. Shau, M. Ortsiefer, M. C. Amann, and C. Chang-Hasnain, “28 GHz optical injection-locked 1.55 μ m VCSELs,” *Electron. Lett.*, vol. 40, no. 8, pp. 476-478, Apr. 2004.
- [Zhao 2006] X. X. Zhao, D. Parekh, E. K. Lau, H.-K. Sung, M. C. Wu, and C. J. Chang-Hasnain, “High extinction ratio of injection-locked 1.55- μ m VCSELs,” *IEEE Photon. Technol. Lett.*, vol. 18, no. 1-4, pp. 166-168, Jan.-Feb. 2006.
- [Zhao 2007] X. Zhao, D. Parekh, E. K. Lau, H. K. Sung, M. C. Wu, W. Hofmann, M. C. Amann, and C. J. Chang-Hasnain, “Novel cascaded injection-locked 1.55- μ m VCSELs with 66 GHz modulation bandwidth,” *Opt. Express*, vol. 15, no. 22, pp.14810-14816, Oct. 2007.
- [Zhi 2012] J. K. Zhi, H. L. Zhu, D. K. Liu, L. Wang, and J.-J. He, “Travelling wave analysis on high-speed performance of Q -modulated distributed feedback laser,” *Opt. Express*, vol. 20, no. 3, pp. 2277–2289, Jan. 30, 2012.

[Zhu 2015] H. L. Zhu, Y. M. Xin, and J.-J. He, “Pattern dependence in high-speed Q -modulated distributed feedback laser,” *Opt. Express*, vol. 23, no. 9, pp. 11887–11897, 4 May 2015.

LIST OF PUBLICATIONS

1. M. Osiński, G. A. Smolyakov, F.-H. Chu, H. S. Kalagara, and E. Mercado-Sotelo, “Strongly injection-locked semiconductor ring lasers for ultrafast transmitters (Invited Paper)”, *Technical Digest, International Photonics Conference*, 8-10 Dec. 2011, Tainan, Taiwan.
2. F.-H. Chu, L. Naznin, H. Kalagara, G. A. Smolyakov, and M. Osiński, “Bending losses and modal properties of serpentine and bent waveguides”, *Physics and Simulation of Optoelectronic Devices XX* (B. Witzigmann, M. Osiński, F. Henneberger, and Y. Arakawa, Eds.), SPIE International Symposium on Integrated Optoelectronic Devices OPTO 2012, San Francisco, CA, 23-26 Jan. 2012, *Proceedings of SPIE*, Vol. 8255, Paper 825511 (9 pp.).
3. M. Osiński, G. A. Smolyakov, F.-H. Chu, and F. Grillot, “Strongly injection-locked cascaded microring lasers for optical communications at 100 GHz and beyond (Invited Paper)”, *Technical Digest, International Symposium on Physics and Applications of Laser Dynamics 2013* (IS-PALD 2013), 29-31 Oct. 2013, Paris, France, pp. 8-10.
4. F.-H. Chu, G. A. Smolyakov, and M. Osiński, “Numerical analysis of frequency chirp in strongly injection-locked semiconductor ring lasers”, *Physics and Simulation of Optoelectronic Devices XXII* (B. Witzigmann, M. Osiński, F. Henneberger, and Y. Arakawa, Eds.), SPIE International Symposium on Integrated Optoelectronic Devices OPTO 2014, San Francisco, CA, 3-6 Feb. 2014, *Proceedings of SPIE*, Vol. 8980, Paper 898018 (9 pp.).
5. F.-H. Chu, H. Kalagara, G. A. Smolyakov, and M. Osiński, “Reciprocity principle and nonequivalence of counterpropagating modes in whistle-geometry ring lasers”, accepted for *Physics and Simulation of Optoelectronic Devices XXIV* (B. Witzigmann, M. Osiński, and Y. Arakawa, Eds.), SPIE International Symposium on Integrated Optoelectronic Devices OPTO 2016, San Francisco, CA, 15-18 Feb. 2016.
6. M. Osiński, F.-H. Chu, G. A. Smolyakov, and F. Grillot, “Rate equation analysis of frequency chirp in strongly injection-locked cascaded semiconductor ring lasers”, accepted for *Semiconductor Lasers and Laser Dynamics*, SPIE Photonics Europe, Brussels, Belgium, 4-7 April 2016.
7. F.-H. Chu, G. A. Smolyakov, and M. Osiński, “Frequency chirp simulation of strongly injection-locked whistle-geometry ring lasers”, submitted to *Journal of Lightwave Technology*.